Dissertations, Master's Theses and Master's Reports

2020

Numerical Investigation Of Spray Characterization Of Heater-GDI System

Ashwin Karthik Purushothaman
Michigan Technological University, purushot@mtu.edu

NUMERICAL INVESTIGATION OF SPRAY CHARACTERIZATION OF HEATER-
GDI SYSTEM

By

Ashwin Karthik Purushothaman

A THESIS

Submitted in partial fulfillment of the requirements for the degree of

MASTER OF SCIENCE

In Mechanical Engineering

MICHIGAN TECHNOLOGICAL UNIVERSITY

2020

© Ashwin Karthik Purushothaman

This thesis has been approved in partial fulfillment of the requirements for the Degree of MASTER OF SCIENCE in Mechanical Engineering.

Department of Mechanical Engineering – Engineering Mechanics

Thesis Advisor: *Dr. Youngchul Ra*

Committee Member: *Dr. Chunpei Cai*

Committee Member: *Dr. Sajjad Bigham*

Department Chair: *Dr. William Predebon*

Table of Contents

iv

List of figures

List of tables

Acknowledgement

List of abbreviations

DISI	Direct Injected Spark Ignition
GDI	Gasoline Direct Injection
UHC	Unburnt Hydrocarbons
NO_x	Nitrogen Oxides
CAFE	Corporate Average Fuel Economy
FTP	Federal Test Procedure
ASTM	American Society for Testing and Materials
CVCC	Constant Volume Combustion Chamber
KH	Kelvin Helmholtz
RT	Rayleigh Taylor
ROI	Rate of Injection
ASOI	After the Start of Injection
E10	Ethanol 10% by volume with gasoline
E85	Ethanol 85% by volume with gasoline
CFD	Computational Fluid Dynamics

Abstract

Gasoline engines require fuel enrichment at low temperature cranking (cold start) conditions for efficient engine operation. Since the amount of fuel injected is high at cold start to compensate low fuel evaporation, fuel sprays tend to impinge on the cold surfaces of the piston and cylinder walls leading to the formation of excessive unburned hydrocarbons. One of the ways to ensure reliable cold start performance and to reduce UHC emissions is to have the fuel subjected to preheating. The objective of this study is to investigate the effects of fuel preheating on Gasoline Direct Injection sprays to improve the mixture preparation during the cold start conditions. Injection of fuel sprays of neat gasoline and gasoline-ethanol blends (E10 and E85) from the heater-injector into a constant volume combustion chamber was studied. Computational Fluid Dynamics (CFD) simulations of the fuel flow through the injector were performed to understand the impact of the heater in improving the mixture preparation quality. The gasoline was modelled with 14 component surrogate fuel model to capture its physical properties and distillation characteristics. Fuel spray processes in the Constant Volume Combustion Chamber (CVCC) were simulated using an in-house CFD code, MTU-KIVA. Parametric simulations were performed at different injection pressures and at a wide range of fuel temperature ranging from -6°C to 250°C. The simulation of injector internal flow could improve the spray simulations in the CVCC by providing accurate velocity and temperature distributions of fuel sprays at the exit of individual nozzles. The results show that the injector with the preheating system performs reliably at cold start conditions to increase the fuel temperature from -6°C to 75°C in less than a second. The spray were in good agreement between the measurements and predictions. For the given operating range, the spray changes from normal evaporation to flash boiling regime. The model captures the spray collapsing behaviour for the flash boiling conditions. However, the model tends to over-predict the spray penetration for fuel temperatures in the higher range of boiling/flash boiling, regardless of the injection pressure variation.

1. Introduction

1.1. Background and Motivation

The depleting oil resources and climate changes has forced nations to use clean fuels. In recent years chemical composition of the fuel is being altered to reduce emission. Chemical contents like olefins, aromatics, sulphur are being modified to alter the distillation properties of gasoline. Besides this, oxygenated fuels are added to gasoline because of its higher-octane rating, which enables to achieve higher compression ratio. The most commonly used oxygenated fuels are ethanol and dimethyl ether. Ethanol produced from sugarcane or corn is blended with gasoline to form oxygenated fuel such as E10, E85. In Brazil, a large group of Light duty vehicles are designed to operate with 25% ethanol and even in US Light Duty vehicles are deigned to operate with 10% ethanol [1, 2]. The higher heat of vaporization of ethanol can maximize the charge cooling effect thereby enabling ethanol to be injected directly into the combustion chamber improving volumetric efficiency. Also because of this property ethanol is hard to vaporize than gasoline. Engine downsizing has developed the adaptation of Direct Injection system in gasoline engines. Recent study shows that there has been a rapid increase in employing DI on Spark Ignition engines from very limited application to over 46% [3] to achieve Corporate Average Fuel Economy (CAFE) standards. Direct injection system provides various advantages such as fuel efficiency, power output, emission performance, alternate fuel accommodation over the conventional port fuel injection system.

One of the major technical challenges encountered when injecting cold fuel with DISI engine system is its performance under Cold Start Condition. When an engine operates at its intake / wall / coolant temperatures less than 20°C then the condition can be termed as Cold start. At 20°C, a minimum of approximately 1% gasoline (0.8% for octane and 1.2% for heptane) or 4% ethanol [4] vapour fraction in air must be present in the vicinity of a spark plug to produce a combustible mixture. However, during cold start conditions, the engine, fuel, lubrication oil and the ambient temperature are very low and making fuel less volatile. It has been estimated that to reach warm up condition the lubrication oil takes about 10 minutes in summer and 14 minutes in winter and coolant water takes about 5 minutes in summer and 9 minutes in winter after cold start [5]. Thus, SI engine operations under cold conditions produces very high levels of emission than when operated under fully warmed up conditions. This is because at this low temperature in DISI system the time available for the fuel to mix and vaporize is minimal and the fuel becomes less volatile. Besides at cold condition fuel condensation occurs, leading to the formation of fuel film on the cold walls of the combustion chamber. Also, injectors used in gasoline engines are designed to operate low pressure whereas injectors used in diesel engines are designed to operate at high pressure thereby producing larger droplets comparing to diesel. Due to this the first 20 seconds in engine cold start operation is important as 80% of the Unburned Hydrocarbons of the total engine operation as measured by US FTP emission drive cycle is produced during this period [6,7]. Figure 1.1 shows the cause and effects of

cold start operation. It is observed that the low ambient temperature makes the engine body and the fuel cold. Engine operation requires rich in-cylinder condition to combust the fuel during the cold condition. The fuel economy is very low and as the temperature decreases the amount of injected fuel to form a combustible mixture increases. Since the in-cylinder temperature is very low, fuel evaporation and other conditions required to form combustible mixture is inefficient leading to poor combustion efficiency, which directly affects the environment.
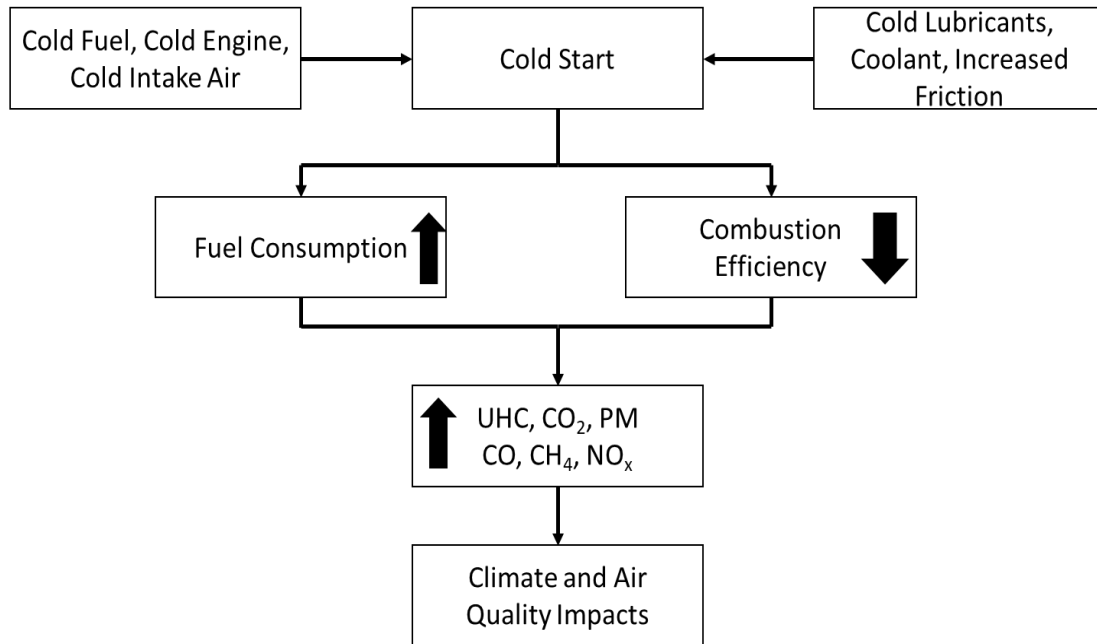
Figure 1.1 Cause and Effects of Cold Start

The advantages of GDI injectors has gained popularity among engine manufacturers and it is being widely used. In GDI engines spray atomization is the key process in the mixture formation. The development of multi-hole nozzle injectors for spray application provides flexibility in controlling the jet targeting and fuel distribution as injector holes can be oriented asymmetrically to direct each plume independently. One of the major drawbacks in using multi-hole injectors is its longer penetration profile resulting from a high velocity jets issuing from individual nozzle. Increasing the number of holes can reduce the penetration however there is limitation to the nozzle diameter. This is because over a period the carbon deposits settle on the nozzle holes blocking off the fluid pathway resulting in the degradation of the injector [8, 9].

Spray optimization is a challenging task as there are large number of parameters that must be taken into consideration. Though there are well equipped experimental facility available, performing spray characterization becomes time consuming and expensive [10]. Thus, CFD modelling is the best approach to complement experiments. Enormous amount of

2

work has been done in the past 20 years to model fuel sprays. Fuel sprays emerging from the nozzle undergoes atomization and then vaporizes. There are several approaches and models developed to characterize fuel break up and evaporation process. The most widely used spray breakup models are KH-RT wave model, TAB model, Sheet Atomization model.

Gasoline is a multicomponent fuel, but in order to avoid the complexity it was modelled as a single component fuel which is represented by iso-octane, as it resembles it physical behaviour. But with the advancement in computational capability multicomponent fuel studies are becoming largely popular. Ra and Reitz developed a robust discrete multicomponent fuel evaporation models which showed significant improvement in prediction. This is important because lighter components evaporates in the early stages of spray and that helps in forming combustible mixture during cold start which is not observed in single component evaporation [11].

1.2. Objectives

One of the ways to avoid cold start issues, is to preheat the fuel before injecting it into the combustion chamber. This work focuses on understanding the impact of fuel pre-heating in the injection system and its effect on the formation of fuel sprays, since fuel spray characterization is important to improve engine design and operation. A multicomponent surrogate model was used to model and capture the distillation properties of gasoline(E0), ethanol 10% and 85% fuel. Computational Fluid Dynamics (CFD) simulation adapting the properties of multicomponent fuel to study the fuel flow through the Heater-Gasoline Direct Injection System was studied. Non-reacting fuel sprays issued from a 6-hole GDI injector are simulated in a constant volume combustion chamber for different injection pressures with the effect of fuel temperature. The numerical data is validated against the experiments to ensure the predictive capabilities of the computational method.

1.3. Thesis Formulation

This thesis comprises of the following chapters

Chapter 1 gives a brief introduction about the background, motivation and objective of this work.

Chapter 2 discuses about the previous works which were done to improve cold start performance. Also, this chapter discusses about the importance of nozzle flows in spray formation process along with the previous efforts that has been done to couple the nozzle flows for sprays.

Chapter 3 introduces the methods that are available to model real transportation fuel. It describes the advantages and effects of using multicomponent fuel for spray analysis. This chapter also discusses about the distillation characteristics of different fuel such as gasoline, ethanol 10 and 85%. This chapter also talks about how multicomponent fuel improves preferential vaporization thereby giving the characteristics of real-world fuel. It

3

describes about the other fuel properties such as density, surface tension, specific heat, viscosity that were used as input for other calculations.

Chapter 4 explains the approach that was used to simulate the fluid flow in the heater and the injector. It includes the information about the geometry, grid generation process, boundary and input condition and the models that were used for the performance analysis of the heater.

Chapter 5 investigates the spray characteristics in a constant volume combustion chamber. It includes the information about the approach, physical models, tools used to describe the spray characteristics. This chapter also discusses the effect of injection parameters such as injection pressure, fuel temperature and fuel on spray formation process. In addition, this chapter describes the results of two different methods that were considered for CVCC spray analysis.

Chapter 6 summarises the conclusion of this work and describes about the recommendation for the future works in Chapter7.

2. Literature Review

Changing climatic patterns due to global warming has made the emission norms stricter and hence automobile manufacturers are forced to reduce the emission level from their vehicles [12, 13, 14]. There are lot of sources that can be the cause for emission in an Internal Combustion Engines and one among them is the cold start operation. Many parts of the world like Europe, North America and China where the automobile volume is high have cold climatic conditions. US FTP states that 80% of the UHC comes from the IC Engine due to cold start operation. Thus, cold start becomes an important issue to address. In the past two decades several efforts has been made by automobile manufacturers and researchers to improve the cold start performance in SI engines as well as diesel engines. During this period, several new technologies and design changes has been applied to the engine and still design optimization are being done to improve the performance by reducing emissions.

2.1. Approaches to reduce Cold Start Emission

Cylinder wall wetting is a common phenomenon that happens during the cold condition as the fuel condenses on to the wall and it is one of the major sources for the of formation of raw pollutants. To avoid the wall film formation, Gerd Grünefeld and et al [15] came up with the idea of injecting a fraction of the intake air into the combustion chamber. Since the air was injected during the compression stroke, it improved the thermal conditions of the cylinder wall and also enhanced turbulence thereby improving the fuel air mixing. This enables the engine to be operated in stoichiometric or lean mixture condition. However, this system requires an additional reservoir that needs be maintained at a higher pressure than the cylinder pressure to inject air. Besides the experiment was performed at engine body temperature of 20°C and at 950 rpm, which is not the normal cranking speed during cold start conditions.

During cold conditions the rate of fuel vaporization is very low. To improve combustion efficiency Kristine Drobot Isherwood and et al [16] incorporated on-board fuel reforming by partial oxidation. The purpose of the fuel reformers is to convert the liquid fuels into gaseous fuel. This system involved in using a small combustion chamber where the liquid fuel is partially oxidized to form gaseous fuel species. This improved fuel economy by reducing the over fuelling that is required during cold start conditions and reduced emissions.

Three Way Catalytic converter systems are commonly used devices in engine after treatment. These catalytic converters efficiently converts harmful pollutants CO, NO_x and HC into CO_2, N_2 and H_2O. However, these TWC are less efficient when operated under its light off temperature time which occurs when the efficiency of the converter reaches 50% [17]. It is true that during cold start the entire system temperature is less than 20°C and an additional heating system is required to rise the TWC temperature.

Besides the above discussed technologies, works were also carried out in preheating the fuel [18, 19]. Injector manufacturers worked on designing electrically heated injectors to raise the temperature of the fuel. Apart from this glow plugs and resistive coil heating was also used to preheat the fuel. William Fedor and et al [20] showed that electrically heated and injected fuel rail improve the cold start performance. This system improves fuel vaporization and it is most suitable for ethanol blended fuel cold start operation.

Although each technology has its own merits for cold start application, fuel preheating is the most preferred modern technology as it makes the fuel immediately available for vaporization. Apart from this, pre-crank fuel preheating can also be done with the application of preheating devices even before the engine is turned on, which is not applicable for the other cold start technologies available.

2.2. Nozzle Flows and Sprays

Fuel injectors are the vital component of the fuel injection system. With the advancement in control strategy precise fuel delivery into the combustion chamber is achieved. The key factor that governs the performance of the fuel injector is its ability to form desired spray patterns, generating finer droplets for vaporization, liquid penetration and in-cylinder mixture forming capability. These factors decides the pollutant formation [21]. For gasoline direct injection applications multi-hole injector are being widely used. The diameter of these nozzle holes is of few hundred microns. The pressure drop and the flow velocity across the nozzles are very high. Besides with the improvements in injector designs modern fuel injectors are manufactured with counter bore or stepped holes. These counter bored nozzles creates back flow of ambient gas and causes breakup in the near nozzle exit [22].

The downstream of the nozzle region leads to the development of spray process. The multi component liquid fuel ensues from the nozzle holes as liquid jets and due to the effects of perturbations caused by the nozzle or under the influence of aerodynamic forces, the liquid jets breaks down into ligaments or droplets which undergoes further breakup until a stable size of the drop is reached [23]. The fuel spray formation involves various process such as primary and secondary atomization, collision, coalescence, evaporation etc.

In a Direct Injection Spark Ignition (DISI) engine, fuel atomization influences the mixture formation around the spark plug that in turn affects the combustion efficiency. Over the past few decades, researchers have worked on developing experimental setups to understand the breakup processes and also, a lot of mathematical models have been developed to describe the breakup process.

When a liquid fuel is injected into a gaseous medium, the aerodynamic force, inertia force, surface tension and viscosity acts on the liquid jet resulting in the formation of liquid blobs, ligaments and droplets. Depending on the exit velocity, liquid Reynolds number and Ohnesorge number the breakup regimes are classified into Rayleigh Breakup regime, First-

6

f

www.manaraa.com

Wind Induced Breakup regime, Second-Wind Induced Breakup regime and Atomization regime. In fuel sprays the liquid fuel is injected at high velocity. The liquid jet disintegrates spontaneously as a result fine drops are seen along with the liquid core. This kind of phenomenon occurs with the atomization regime and usually the breakup process in fuel sprays are modelled with atomization regime [24].

In fuel sprays two modes of atomization breakup takes place namely primary atomization and secondary atomization. Primary atomization occurs due to the following phenomena aerodynamic drag, cavitation in the nozzle, turbulence in the nozzle and due to pressure oscillation. The droplets produced as a result of primary atomization undergoes further breakup due to the aerodynamic force leading to secondary atomization. The excess drop surface deforms and breaks into smaller droplets until a stable size of the droplet is reached. This is because at higher relative velocity the drop tends to deform and exceeds the critical weber number leading to breakup [25].

Engine CFD code uses the models that solves the above described processes. Researchers have contributed a lot in developing and applying these models in the CFD codes and as a result there are various model available that describes the atomization and breakup process. The models that are used in the simulation studies are discussed.

2.2.1. Blob Injection Model

The blob injection model was developed by Reitz and Diwakar [26]. In the model the liquid fuel is continuously injected in the gas phase medium as large drops. The size of the drops corresponds to the effective diameter of the nozzle. The fuel injection rate determines the rate at which new drops are to be injected in the chamber. The aerodynamic instabilities are induced on the parent drop based on the KH model which leads to the formation of smaller droplets from the parent droplets.

2.2.2. Kelvin Helmholtz Wave Model

The KH wave breakup model was developed by Reitz and Diwakar [26,27]. This model considers a cylindrical liquid jet entering into a quiescent gas chamber. The interactions between the liquid jet and the ambient gas creates a number of infinitesimal perturbations on the surface of the liquid jet. The droplets are sheared off from the liquid surface due to the aerodynamic instabilities caused be the relative velocity between gas and liquid phase. The breakup time and the new drop size is based on the Kelvin Helmholtz instabilities, which is derived from gas jet theory.

2.2.3. Rayleigh-Taylor Model

The Rayleigh-Taylor model is based on the instability theories proposed by Rayleigh and Taylor [28]. This model considers the effects that occurs at the interface of two different fluids of different densities. RT instabilities tends to develop when the fluid acceleration or deceleration has an opposite direction (normal) to the density gradient. The size of the newly formed drop is calculated based on the RT wavelength and the breakup process takes

place only if the wavelength is lesser than the size of the parent drop. This model produces numerous drops of uniform size and hence it is combined with KH model for secondary atomization process.

2.2.4. KH-RT Secondary Breakup Model

The KH-RT model combines the effect of KH wave driven by aerodynamic forces with RT instabilities caused due to the acceleration of shed drops in free stream. In this model a competition between the KH and RT takes place and the drop break up is decided on the model that has shorter breakup time [29].

Figure 2.1 shows the illustration of primary and secondary atomization based on the above discussed model which shows the breakup of parent droplet into large number of smaller droplet due to the instabilities.
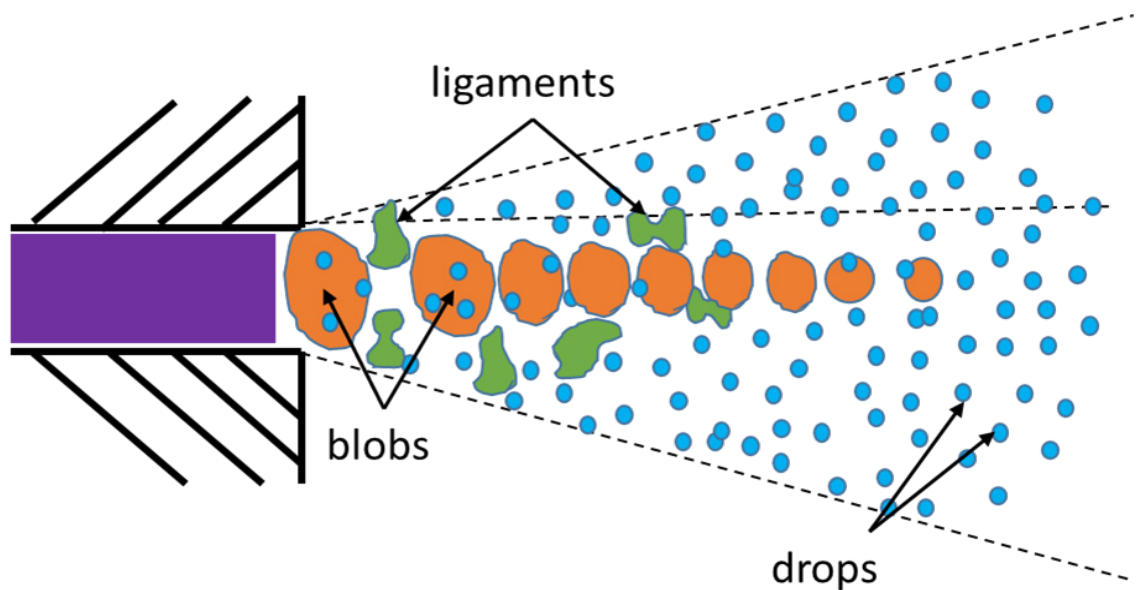
Figure 2.1 Illustration of Blob injection Spray Breakup Model

The nozzle flow is transient in nature and the fuel injection process is a multiphase event with few millisecond orders. The Reynolds number of the flow is of the order 50000 showing the nozzle flow is highly turbulent in nature [24]. Besides GDI injectors have a narrow included angle which results in plume to plume interaction and formation of dense spray near the nozzle exit making it is really hard to capture the behaviour with experimental measurement and CFD approaches should be developed to explain the internal nozzle flow with the available data [23].

The spray formation process is itself a very complex process and adding nozzle flow makes it even more complex. Conventionally fuel spray problem is approached through Discrete

www.manaraa.com

Drop Modelling and initiated by injecting liquid droplets of the size of effective nozzle diameter into the chamber and solving for breakup, collision, coalescence, evaporation. This widely applied approach is based on Eulerian-Lagrangian method, in which the liquid droplets are tracked based on Lagrangian method and the gas phase along with the fuel vapour are treated as continuum and modelled in Eulerian frame. The spray through this approach is initiated by the rate of injection. This approach is one of the best approach that computationally efficient as well as it accurately predicts the spray process but, one of major drawbacks of this approach is that it does not considers the effects of internal process that happens inside the nozzle such as cavitation for the spray formation [30].

Various research groups have proposed different methodologies for coupling internal nozzle flows and spray process. These approaches includes from solving the near nozzle spray through Direct Numerical Simulation to Reynolds Averaged Navier-Stokes model. In DNS method the details of turbulent flow fields of liquid, gas and their interfaces are solved directly through Navier-Stokes equation. This requires very fine spatial and temporal resolution to capture very small length scales. The other approach uses Large Eddy Simulation method where the turbulent flows of large eddies are computed directly and the small scales (sub-grid scales) motions are modelled. The nozzle flow involves multiphase and thus interface must be computed properly. There were various numerical strategy developed to track the interface such as Volume of Fluids method (Gueyffier et al., 1999), Level Set method (Sussman et al., 1994) and Front Tracking Method (Unverdi and Tryggvason, 1992). With the available turbulence and multiphase models pure Eulerian approach and Eulerian-Lagrangian approach are being used to describe the nozzle flow and sprays [23].

Ménard T, Tanguy S and et al. [31] carried out DNS simulation of atomization with VOF, level set and ghost fluid method. This developed method was robust but however there were no clear validation provided to explain the capability of the model. Hermann et al. [32] performed coupling between Eulerian and Lagrangian to develop primary and secondary atomization. The model switches to Lagrangian framework when a certain threshold hold value of the liquid blob is reached. The switching from Eulerian to Lagrangian occurred when the drop size of few 10-micron order. This requires very fine grid and the computation cost would be expensive. Cavitation models have also been implemented along with the Eulerian sprays to understand the dynamics of internal nozzle flow on fuel sprays.

In the above-mentioned works coupled domain was used to model internal nozzle flow and sprays. Modellers also worked on two step method i.e., solving internal nozzle flow in a separate domain and spray simulation in a separate domain. In the works of Michele Battistoni and et al. [33] the internal nozzle flow is solved in Eulerian Framework and the exit conditions are used as the boundary and input conditions for the Lagrangian Spray approach [34, 35, 36]. The nozzle exit conditions includes velocity, temperature, liquid-vapour fractions and turbulent kinetic energy are used as input for the spray calculation.

This method is however is computationally expensive and the exit conditions which are used as input are averaged properties. Moreover, the nozzle flow simulation time scales are usually around $10^{-8} - 10^{-9}$ s, while the spray calculation time scales are of the order $10^{-5} - 10^{-6}$ s and hence some interpolation must be made.

Though the two-step method is computationally expensive, this work incorporates similar kind of approach. ANSYS Fluent is used to calculate the internal nozzle flow process along with the smart heater. The nozzle exit properties such as velocity and temperature are used as input for spray simulation in MTU-KIVA-Chemkin code. The main objective of the work is to find to find the performance of the heater and its impact on improving the quality of the fuel at the nozzle exit for cold start application. Thus, temperature and velocity at the nozzle exit becomes the important property. This method is based on the assumption that there is no phase change phenomena occurring inside the fuel injector and hence multiphase equation is not solved thereby ignoring cavitation phenomenon. One of the main reasons for ignoring the phase change is that the simulation has to be performed until a steady temperature is reached. This could take up to few seconds to attain the steady temperature at the nozzle exit. In two-step simulation method the simulation is usually carried out for the injection duration period. Injection is a few millisecond order event and the proposed work is of few seconds order and this would make the computation very expensive. This work includes the spray analysis using both the conventional approach and the two-step approach using nozzle exit condition.

3. Fuel Modelling

Over the past two decades combustion models for Internal Combustion Engine application was developed with single component fuel. Pure substance such as n-heptane and iso-octane was used as the primary reference fuel for representing gasoline. In general, commercial fuels such as gasoline, diesel contains thousands of hydrocarbons. Despite the single component fuel representation predictive capability, it cannot be used to represent the physical and chemical properties of modern fuels. As the emission norms becomes stringent fuel properties are being altered and other chemical classes of hydrocarbons like aromatics, alkynes are added in various concentration to modify the fuel distillation behaviour. With the availability of advanced combustion technologies like low temperature combustion, single component fuel cannot predict the combustion behaviour as the preferential vaporization is not observed with single component fuel model [37].

Multicomponent surrogate fuel modelling approach can be classified into two groups namely Continuous Multicomponent model and Discrete Multicomponent model. The continuous multicomponent model is based on the continuous probability distribution function based on molecular weight. Other properties such as boiling point and carbon number are also calculated from this function. In Discrete Multicomponent model the fuel is treated as a discrete species whose properties are calculated based on the chemical libraries and also allows coupling reaction kinetics of individual components. One of the major drawbacks of using continuous modelling approach is the consumption of individual fuel species as the evaporation is based on a distribution function [38]. Thus, taking the advantages of discrete multicomponent approach surrogate fuel is modelled to represent the actual fuel.
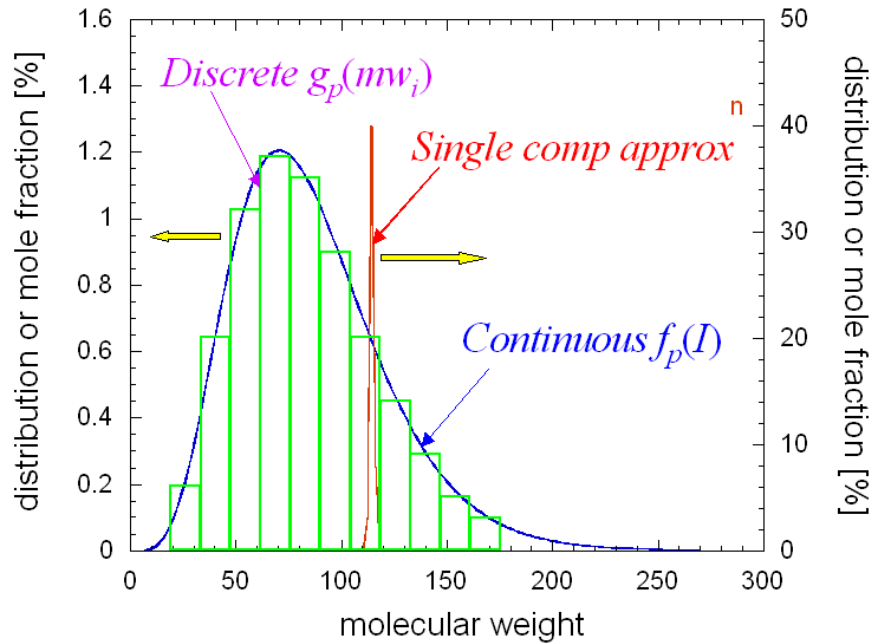
Figure 3.1 Representation of Single and Multicomponent Fuel Model [11]

Figure 3.1 describes the differences between the modelling approach using single and multi (CMC and DMC) component. It is observed that representing fuel model with single component has many disadvantages although it is computationally effective.

The performance of an Internal Combustion Engine majorly depends on the quality of the fuel. Automotive fuel is a mixture of several hundred hydrocarbon molecule with unique stoichiometric ratio, volatility and burn characteristics and this complexity makes the multicomponent approach a robust methodology to predict the fuel characteristics. A multicomponent surrogate fuel must accurately capture the physical and chemical properties of the real fuel. The physical properties includes density, viscosity, surface tension, diffusion coefficients and the chemical properties includes chemical class composition, ignition behaviour, hydrogen/carbon (H/C) ratio.

Despite all this the fuel distillation curve is important property to capture that describes the volatility of the fuel along the boiling range. Thus, volatility determines the fuel evaporation and it is because of this property the distillation of warm and winter weather fuels are different. Fuels are designed to be less evaporative in warm conditions to avoid engine vapour lock, hot fuel handling and evaporative losses that contributes to air pollution while the winter fuels are designed to be more volatile at low temperatures to promote charge preparation for cold start applications.

ASTM D86 procedure is used to determine the distillation profile of the fuel which is the plot of evaporated volume against the boiling temperature. Usually distillation is characterized at three different point T10, T50 and T90 which corresponds to the

12

temperatures of 10%, 50% and 90% evaporated volume. The front-end volatility determines the ease of engine starting, engine warming, evaporative emissions and vapour lock. The mid-range volatility determines the rapid warm-up, smooth running, power and acceleration of the engine. The tail end volatility determines the fuel economy, combustion deposits and fuel dilution.

In order to accurately capture the properties several fuel components must be selected. A 14-component gasoline surrogate fuel composition was chosen. The above described properties and distillation calculations were performed using a multidimensional CFD in-house MTU-KIVA 3V R2-Chemkin code. It works on the principle of vaporizing the DMC fuel. When a multicomponent fuel is injected at a higher temperature than the saturation temperature corresponding to the ambient pressure it undergoes boiling. Each component has different boiling point and it vaporizes at different temperatures.

The boiling process must be modelled to capture the distillation (phase change) behaviour with the selected 14 component fuel species. The current MTU-KIVA-Chemkin code can handle the boiling situation. The code uses the model described by Ra and Reitz [11], for vaporizing the multicomponent fuel under boiling and normal evaporation. Processes like droplet distortion, micro explosion which is normally observed in boiling situation are neglected. The drop surface is assumed to be at the boiling temperature and the surface mass fraction is unity [11].

The 14-component fuel that were chosen are described in Table 3.1

Table 3.1 Description of 14 component Surrogate Fuel

Species	Formula	MW	Mass Fraction	Boiling point (K)
Iso-octane	ic8h18	114.233	0.125	371.90
Ethanol	c2h5oh	46	0	351.12
Iso-pentane	ic5h12	72.151	0.08	300.59
1-Pentene	c5h10	70.135	0.002	302.71
Iso-hexane	ic6h14	86.178	0.09	333.03
n-hexane	nc6h14	86.178	0.075	341.46
n-heptane	nc7h16	100.206	0.005	371.09
Methyl cyclohexane	c7h14	98.19	0.11	373.40
Toluene	c7h8	92.142	0.15	383.6
1-Octene	c8h16	112.216	0.05	393.15

13

Iso-propylbenzene	ic9h12	120.196	0.075	425.05
Iso-decane	ic10h22	142.287	0.075	432.92
Tetralin	c10h12	132.207	0.083	481.09
Butane	c4h10	58	0.08	272.27

The Table 3.1 shows that the properties and chemical composition information of the 14 components used. It can be seen that to capture the properties of the current commercial fuel a mixture of alkanes, olefins, aromatics are required and hence single component representation would either under predict or over predict the evaporation behaviour.
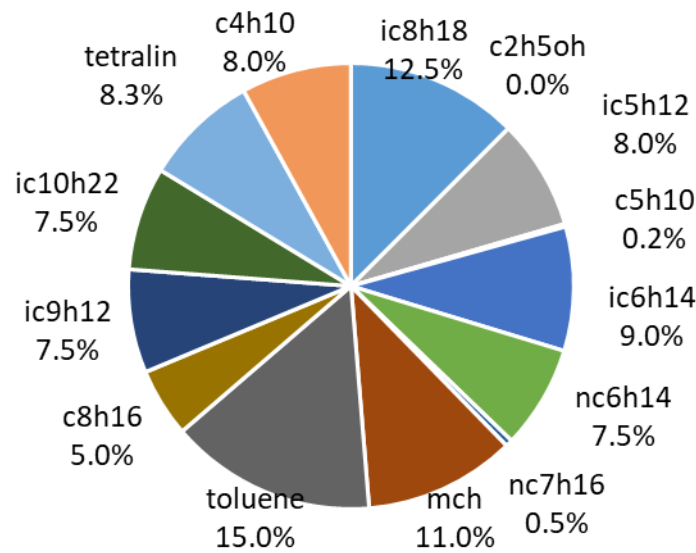
Figure 3.2 Composition of 14 components fuel that represents Gasoline

The distillation process is simulated using in-house MTU-KIVA-CHEMKIN code. The numerical simulation conditions are described in the Table 3.2. A single stagnant spherical liquid droplet of diameter 100μm at 1 atmospheric pressure is modelled with assumptions of uniform distribution of all the 14 fuel components at the drop interior with its composition indicated in the Figure 3.2. The vaporized fuel components are assumed to mix instantaneously and perfectly with the surrounding ambient gases; thus, no mass-transport phenomenon in the gas phase around the droplet is involved in the distillation process.

Table 3.2 Description of the Computational Conditions

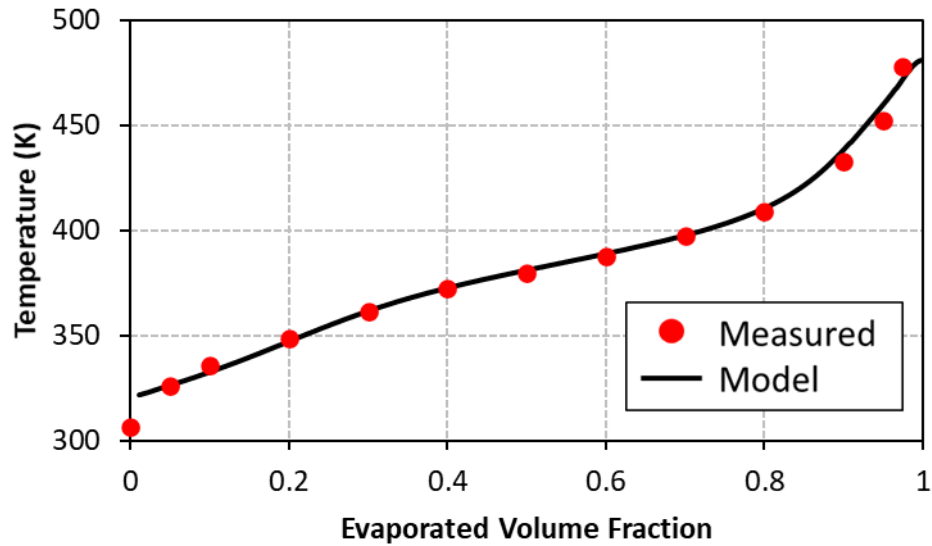| Fuel	Gasoline (multi component)
Initial Droplet Diameter	100µm
Initial Droplet Temperature	298 K
Ambient Temperature	301.15 K
Ambient Pressure	1 atm
Simulation Tool	MTU-KIVA-Chemkin

Figure 3.3 Distillation Profile of modelled and measured for Gasoline fuel

Figure 3.3 represents the distillation profile for the 14-component gasoline fuel. It is observed that the boiling range of the measured and modelled gasoline fuel ranges from 40°C to 200°C. The model over predicts the initial 5% of the evaporation, however the later stages are well captured. The discrepancy in the prediction can be due to (i) the marginal loss of evaporated fuel in the flow from evaporation to the recovered point in the distillation measurement; (ii) there is a temperature lag in the experiment because the measuring point is not the liquid/vapor surface, while the calculated boiling temperature is at the interface, which is given by the composition and ambient pressure only [38].

Besides the phase diagram, other information such as chemical classes (alkanes, olefins, aromatics) proportion, carbon/hydrogen weight percentage and octane rating of the fuel

were compared with the numerical data. The modelled data were in good agreement with the measurements which is shown in Table 3.3.

Table 3.3 Fuel Properties

Elemental Analysis	Measured	Model
Carbon (wt %)	86.25	86.115
Hydrogen (wt %)	13.75	13.885
Density	**Measured**	**Model**
(kg/m^3) @ 15.56ºC	740.4	737.39
Chemical Classes	**Measured (%v/v)**	**Model (%v/v)**
Avg % Vol of Saturates Zones	69.8	69.40
Avg % Vol of Olefins Zones	5.2	5.34
Avg % Vol of Aromatics Zones	25.1	25.24
Octane	**Measured**	**Model**
Research Octane Number	93.4	88.20
Motor Octane Number	85.3	79.39
AKI Calculation	89.4	83.79
Sensitivity	8.1	8.81

The Table 3.3 shows the experimentally measured fuel properties of base gasoline(E0) is within 1% error range. However, the octane rating of measured and modelled fuel are slightly off. The major focus is on non-reacting fuel spray and hence the fuel physical properties were given more importance. The base gasoline fuel is mixed with ethanol in volume proportion to get E10 and E85 fuel.
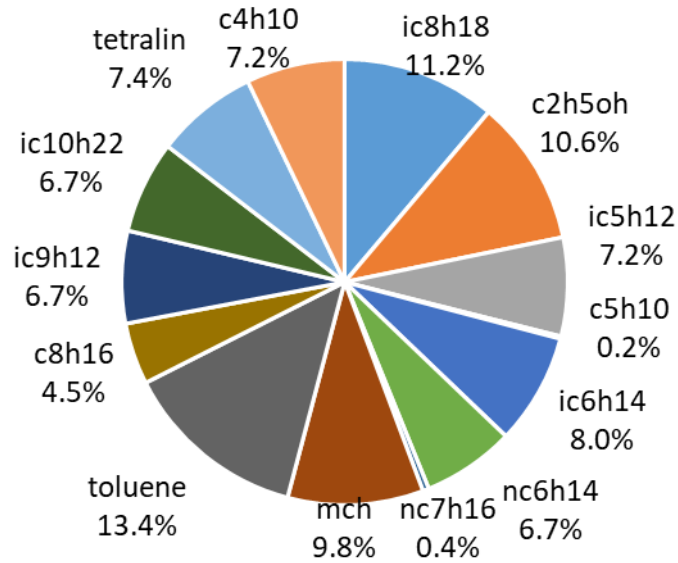
Figure 3.4 Composition of 14 component Ethanol 10% fuel
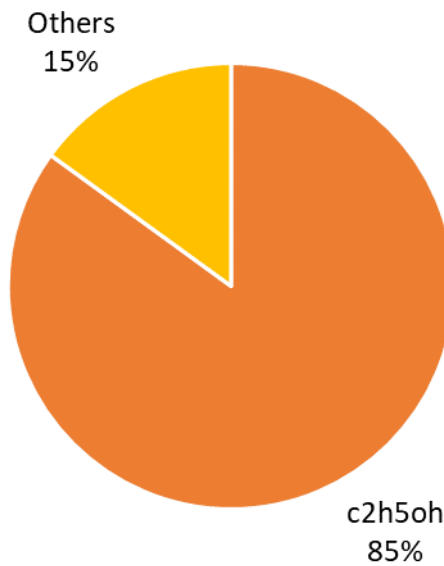
Figure 3.5 Composition of 14 component Ethanol 85% fuel

Figure 3.4 and Figure 3.5 shows the composition of fuel used in the property calculation for ethanol 10% and 85% fuel.

The vapour pressure determines the evaporation rate. For a multi component surrogate fuel the vapour pressure is determined based on Raoult's law, which states the total vapour pressure of a mixture is equal to the weighted sum of its individual vapour pressure in its pure form. This is only true if the mixture is ideal and also the intermolecular forces between the unlike molecule is considered to be equal. However, this is not valid for non-

17

ideal mixtures as it fails to consider the intermolecular forces and azeotropic behaviour of the mixture. These behaviours must be considered because they change the vapour pressure of the mixtures. Azeotrope is a mixture of two or more components which is formed as a result of intermolecular interactions whose pure form cannot be obtained with simple distillation. At this state the boiling point can be either above or below the individual boiling point and thus classified into positive and negative azeotrope.

Commercial fuels contains polar compounds, for example ethanol, benzene. These polar compounds are electronegative and tends to attract molecules and hence the interactions between these molecules must be considered. Because these intermolecular forces determines the vapour pressure and evaporation rate of the fuel. However Ra, Reitz and et al [39] developed a non-ideal mixture model (UNIFAC) that considers the effect of intermolecular forces and azeotropic behaviour. The UNIFAC model determines the activity coefficient. The vapour-liquid phase equilibrium is corrected based on the activity coefficient. This model is well validated for ethanol fuels.

The current MTU-KIVA-Chemkin code considers the effects of the above mentioned behaviour. With the UNIFAC model turned and with the fuel composition as shown in Figure 3.4 and Figure 3.5 properties were calculated similar to the base gasoline case.

Figure 3.6 represents the distillation profile for E0, E10 and E85 fuel which utilises the UNIFAC model.
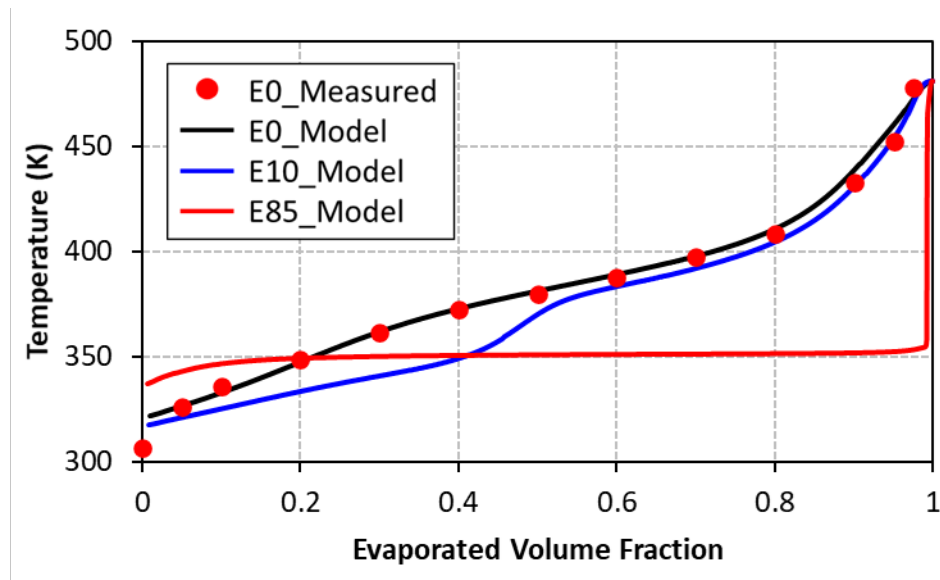
Figure 3.6 Distillation Profile for the modelled Gasoline and Ethanol (10% & 85%) fuel

In the Figure 3.6 the black line represents the base gasoline case with ethanol 0%. The blue line indicates 10% ethanol mixed with the gasoline by volume percentage and the red line indicating 85% ethanol mixed with gasoline by volume percentage. It can be seen from

Figure 3.6 adding ethanol to the gasoline fuel reduces the boiling temperature. Addition of 10% ethanol to the gasoline fuel has significant impact on the front end of the distillation, however in the mid and tail end of the distillation the low volatile gasoline components tends to push the distillation behaviour similar to gasoline. The phase diagram of E85 fuel shows the preferential vaporization of low boiling point components in the initial stage and tends to flattens throughout. The constant boiling temperature for E85 fuel corresponds to the azeotropic behaviour of ethanol blends as it suppresses the effect of low volatile gasoline components. The sudden rise in the trend in the later stage represents vaporization of less volatile components that has high boiling point. This shows that E85 fuel can vaporize at a much lower temperature than the E10 and the base gasoline fuel.

Other properties such as density, liquid specific heat, surface tension, viscosity were also calculated as a function of temperature. A polynomial correlation is made as a function of temperature with the above calculated KIVA based properties. This data is used to simulate the fuel flow for the Heater-Injector using ANSYS Fluent.

In Figure 3.7 the solid line indicates the density values and the dashed lines indicates the Liquid Specific Heat values. It is well known that density of ethanol is greater than the density of gasoline. The trend here shows the same pattern. As the volume percentage of ethanol increases the density values increases for the same temperature. Similarly, the fuel with higher ethanol content has higher specific heat values because of the presence of OH group in ethanol.
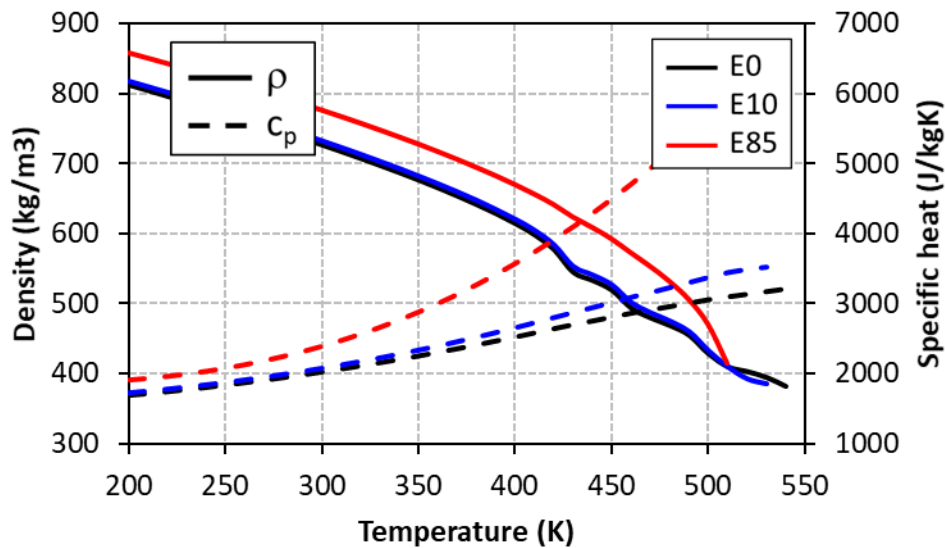
Figure 3.7 Density and Specific Properties of Gasoline and Ethanol Blended (10% & 85%) Fuel

In Figure 3.8 the solid line represents surface tension and the dashed lines represents viscosity. Both viscosity and surface tension decreases as a function of temperature. These

properties play a crucial role in spray development process such as drop breakup, drop collision, drop deformation etc
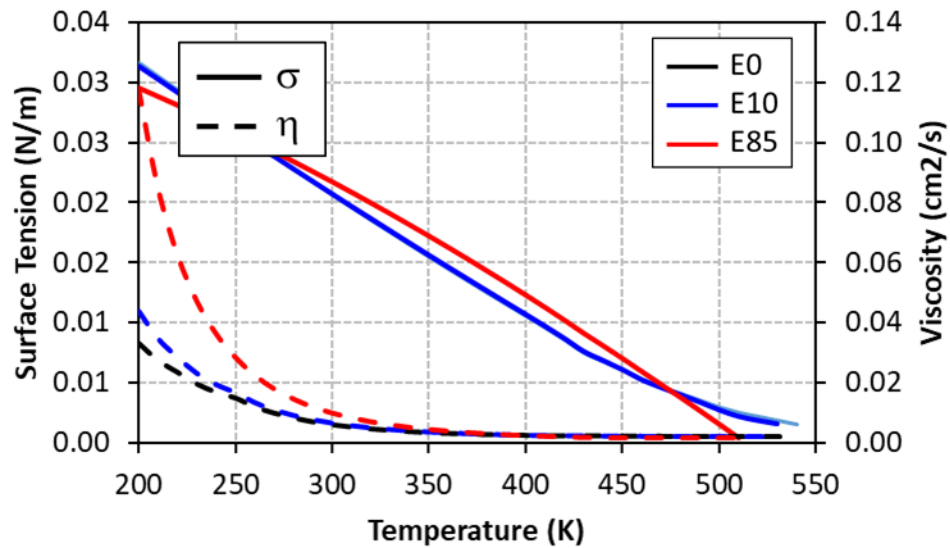
Figure 3.8 Surface Tension and Viscosity property of Gasoline and Ethanol (10% & 85%) fuel
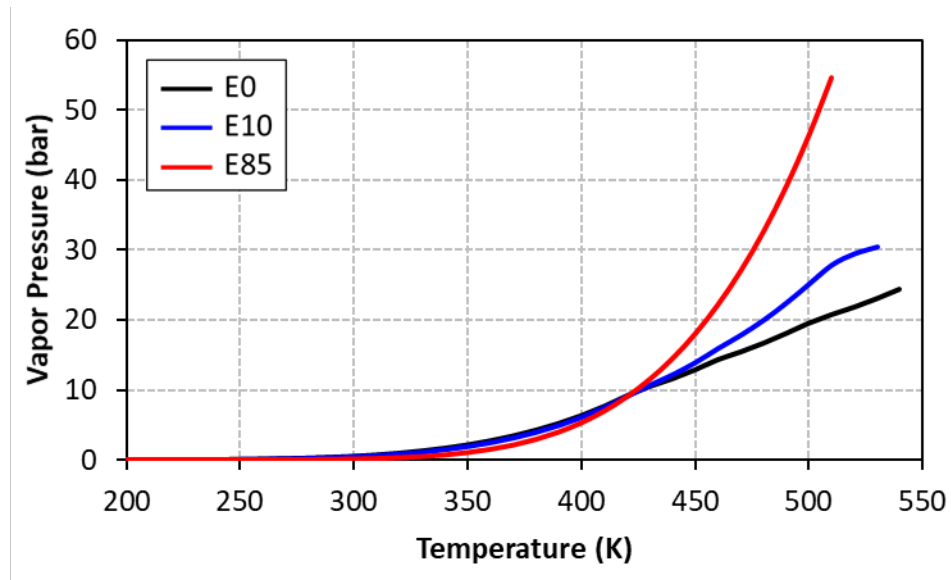

Figure 3.9 Vapour Pressure Property of Gasoline and Ethanol 10% and 85%

Figure 3.9 shows the vapour pressure relation of gasoline, ethanol 10% and 85% fuel. It is observed from the figure that the vapour pressure of E85 fuel is less than the base gasoline and E10 fuel initially, however it tends to increase as the temperature increases. This shows

20

that E85 fuel vaporises easily at higher temperature corresponding the E0 and E10 fuel. Vapour Pressure is an important property that determines the degree of superheat which is crucial in high temperature spray formation. If the momentary chamber pressure is less than the vapour pressure of the fuel it undergoes boiling and flashing resulting in improved vaporization, fuel mixing, reduced drop size.

4. Heater Injector Simulation

One of the main objectives of this work is to understand the performance of the Heater and GDI injector for cold start applications. The heater is coupled with the GDI fuel injector to improve the quality of the fuel at the nozzle exit for improved vaporization and mixture formation. The heated fuel from the heater flows through the fuel injector. There are various kinds of fuel heating system available in the market and most of them are highly energy demanding. One of the key aim of this heater system for fuel heating is to achieve energy consumption less than 120 W/heater as described by WLTP/RDE cycle. The heater heats up the fuel through the PTC (positive temperature coefficient) material. One of the key feature of using this PTC in heating system is that it has very short heating time and power consumption is very low. The designed PTC could reach up to 250°C. However the heater is a prototype and extensive Computational Fluid Dynamics analysis must be carried out to understand the performance of the heater on fuel heating.

4.1. Geometry

The geometry of the real heater coupled with the injector was used for this simulation. Fewer modifications were made to the geometry to avoid the complexities in the simulation. Solid domains were also considered for this simulation. However the entire injector mechanism were assumed to be a single solid body and the details such as needle springs or the components involving the lift mechanism were avoided. Similarly the entire path of the fluid flow from the fuel rail into the heater was not considered, however a location where the fluid just enters into the heater was modelled. ICEM CFD was used for geometry preparation.
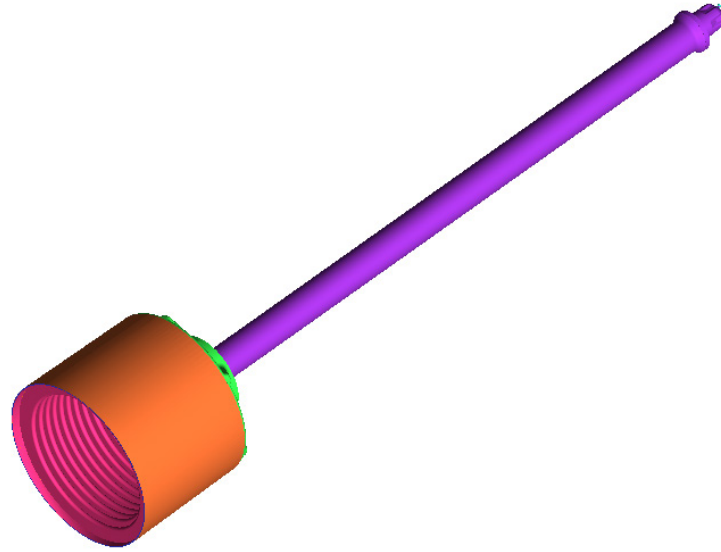
Figure 4.1 Isometric View of the Coupled GDI Smart Heater Injector

Figure 4.1 shows the isometric view of the Heater and Injector geometry for which the mesh is generated. Figure 4.2 shows the front view of the Smart Heater Injector. It includes the solid portion. As described the needle mechanism was eliminated and it was modelled as a single solid portion around which the fuel flows.
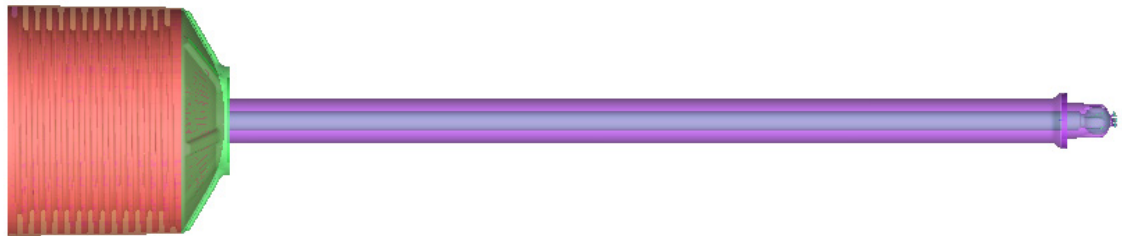
Figure 4.2 Front View of the Coupled GDI Smart Heater Injector
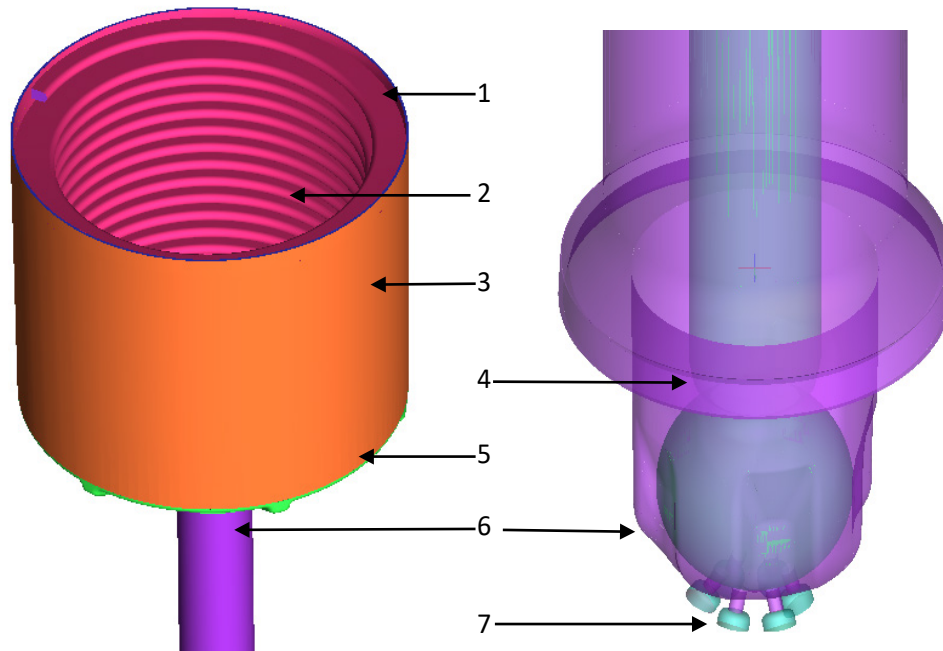
Figure 4.3 Split view of Heater and Injector

Figure 4.3 shows the detailed view of the heater and the injector near nozzle. The heater consists of spiral coil through which the fuel flows. The bottom part acts a fuel collector which eliminates the swirling motion that is created because of the spiral heater.

The injector consists of 5 dimples and 6 holes which are asymmetric whose diameter is around 200 μm and the counter bore diameter is 500 μm. Since the holes are not exactly placed below the dimple and are asymmetric full 3D section of the injector is considered for simulation.

The Table 4.1 provides information about the parts that are present in the Smart Heater GDI Injector.

Table 4.1 Parts of the Smart Heater GDI Injector

Number	Parts
1	Inlet
2	Heater Surface
3	Heater Outer Wall
4	Pintle / Needle (Fuel Injector)

24

5	Fuel Guideway to Injector
6	Outer Wall
7	Nozzle Exit

4.2. Grid Generation

One of the critical step involved in solving problem through CFD approach is the generation of appropriate meshes. This is because proper mesh leads to accurate results and faster convergence. In mesh generation technique there are three kinds grid types namely structured, unstructured and hybrid (structured and unstructured). In the modern CFD simulations unstructured meshes are being widely used. However they are computationally expensive, difficult to achieve high quality and control on the number cells is hard to achieve and hence for this reason structured meshes were preferred. Block were created for the geometry to generate hexahedral meshes.
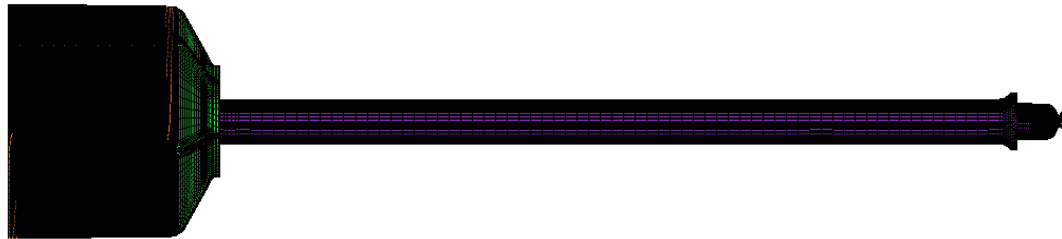
Figure 4.4 Front View of the Full Computational Domain

Figure 4.4 shows the computational grid for the full model. The total number of cells in the full model is around 900K. At the maximum needle lift location of 80μm from the fully closed position a non-moving mesh was created for the geometry as shown in Figure 4.2 using ANSYS ICEM CFD. Due to the limitation in the total number of cells and computational resource available the computational domain was broken into two parts containing heater and injector. The heater exit conditions were used as the inlet conditions for the injector.
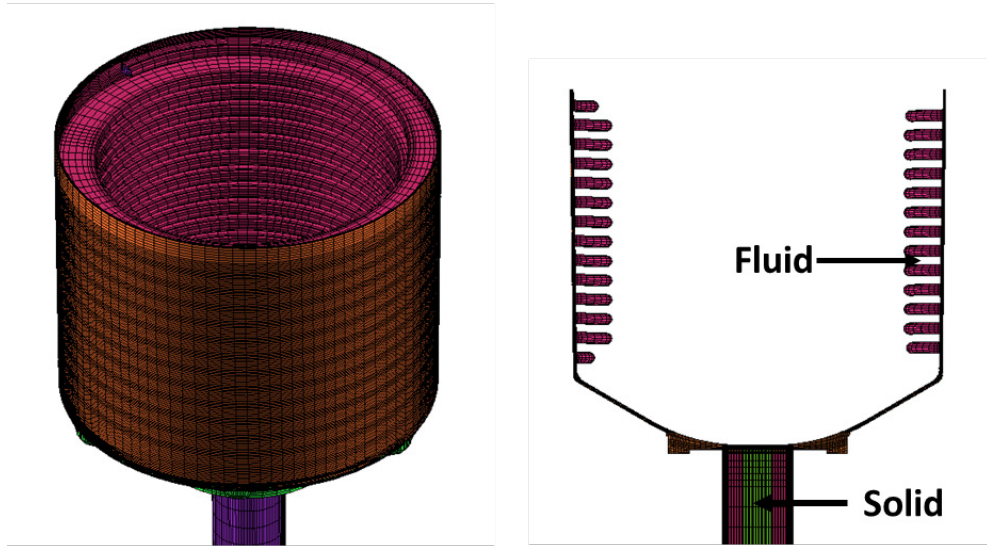
Figure 4.5 3D and Section view of Smart Heater Computational Grid
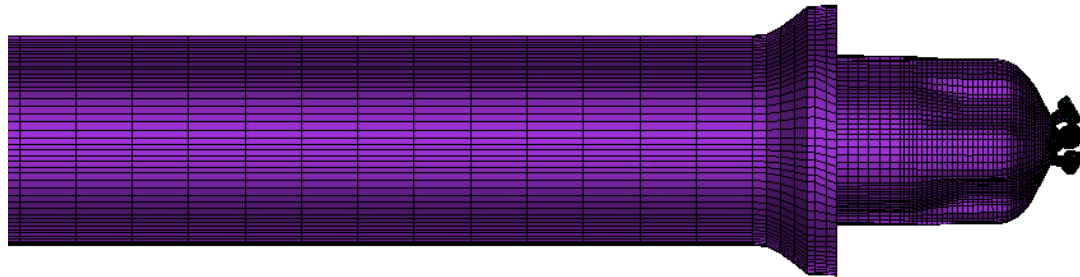
Figure 4.6 Injector Computational Grid
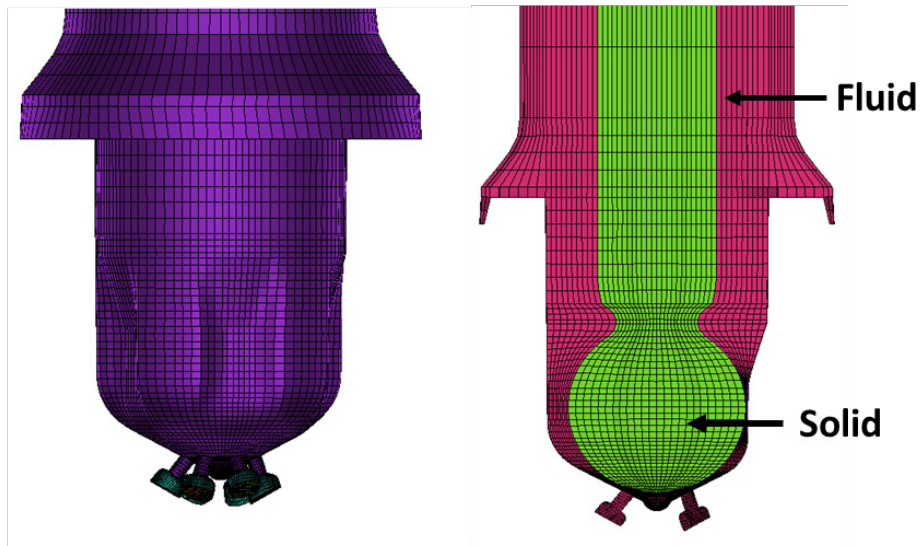
Figure 4.7 3D and Section view of Injector Computational Grid

Figure 4.5 shows the 3D and sectional view of the computational grid of the heater part. From the section view the solid region was also considered for calculations

Figure 4.6 shows the injector grid that was used for computation for all the cases.

Figure 4.7shows the near nozzle region. The section view shows that the injector is asymmetric. Hence 3D injector grid is considered to understand the effects of dimple on the nozzle exit condition.

Table 4.2 Number of cells in Heater and Injector grid

Part	Total Number of Cells
Heater	~470K
Injector	~400K

Table 4.2 describes the total number of cells used for the computation. As discussed earlier due to computation limitation the domain was broken into two parts.

4.3. Models and Approach

In a fluid flow the conservations are described with the governing equations. These governing equations should satisfy the principle of conservation of mass, momentum and energy. Since the fluid is considered as continuum its microscopic properties such as molecular motions and interactions are neglected and the macroscopic properties such as velocity, pressure, density and temperature are used to model the flow field.

27

ANYSYS Fluent CFD package was used to simulate the fuel flow through the heater and injector. The models used in Fluent are described in the Table 4.3.

Table 4.3 Models utilized for simulation

Code	Ansys Fluent
Time Dependency	Transient
Time stepping method	Fixed
Solver Type	Pressure-Based
Pressure-Velocity Scheme	SIMPLE
Models	Turbulence (RNG k-epsilon)

Transient simulation was performed using Ansys Fluent with the boundary conditions as described in Table 4.4. The reason for choosing 260K as initial fuel and outer wall temperature was because during cold conditions the ambient temperature would be equal to or less than the assumed temperature. The performance chart of heater indicated that the heater could go up to a maximum temperature of 250°C and hence the heater wall temperature was set to 523K. Initial velocity input condition was calculated based on the Bernoulli's equation.

Table 4.4 Initial and Boundary Conditions

Fuel	E10, E85 (Properties based on KIVA simulation)
Operating Pressure (bar)	100, 150, 200, 250
Outlet Pressure (bar)	1
Inlet Fuel Temperature	260K
Heater Temperature	530K
Wall Temperature	260-530K

The properties were based on Multicomponent fuel calculated from KIVA based Distillation code. A polynomial curve fit was generated as a function of temperature to describe the fuel properties such as density, specific heat, viscosity and surface tension. These relations were used as input to Fluent to represent the fuel properties. The properties equations are given in Table 4.5

28

Table 4.5 Polynomial equation representing the fuel property

Properties E10	Equation
Density	$807.1060 + 0.3044T - 0.0020T^2 - 3.3098e^{-7}T^3$
Specific Heat	$2591.5 - 10.2289T + 0.0375T^2 - 2.848e^{-5}T^3$
Viscosity	$0.0349 - 3.3342e^{-4}T + 1.1992e^{-6}T^2 - 1.910^{e-9}T^3 + 1.1335e^{-12}T^4$
Surface Tension	$0.0423 - 9.5839e^{-6}T - 3.369e^{-7}T^2 + 3.9248e^{-10}T^3$
Properties E85	**Equation**
Density	$1270 - 3.7013T + 0.0105T^2 - 1.2622e^{-5}T^3$
Specific Heat	$2267.0 - 4.4601T + 0.0083T^2 + 2.5591e^{-5}T^3$
Viscosity	$0.7627 - 0.0122T + 8.1878e^{-5}T^2 - 2.9052e^{-7}T^3 + 5.5794e^{-10}T^4$
Surface Tension	$0.0391 - 1.8453e^{-5}T - 1.7185e^{-7}T^2 + 1.1716e^{-10}T^3$

Unsteady fuel flow simulation was performed with the injector pintle wide open. The energy equation is also solved for the solid domain to study the effect on the fuel on heating injector needle. However, the simulation was performed in two domains i.e., the full model was broken into heater and injector domains.

Interestingly the total amount of fuel present in the entire system was estimated approximately to be around 1600 mg. During cold start condition at lower cranking speed the fuelling rate is between 150 to 200 mg/injection. The total amount of unheated fuel contained in the system is sufficient enough to be injected for the first few cycles. Thus to reduce the amount of unheated fuel, simulations were performed without fuel flow to understand efficiency of the fuel heater to heat up the stagnant fuel.

4.4. Results: Heater-GDI Injector and Nozzle Flow
With the above discussed models, fuel properties and boundary conditions transient simulation was performed on the Heater-GDI Injector for E10 and E85 and the results are discussed as follows.

4.4.1.With Fuel Flow

Fuel flow simulation was performed on the separated Smart heater domain to determine the exit condition. ANSYS Fluent was used to perform the CFD analysis with model and boundary conditions described in Table 4.3 and Table 4.4 and with fuel properties described in Table 4.5
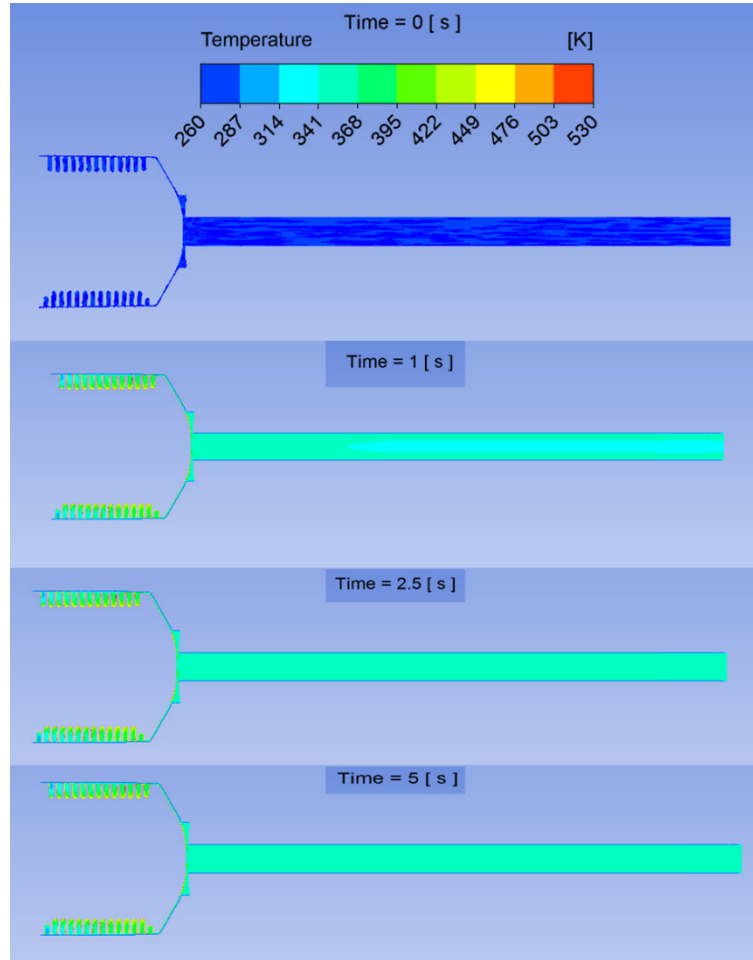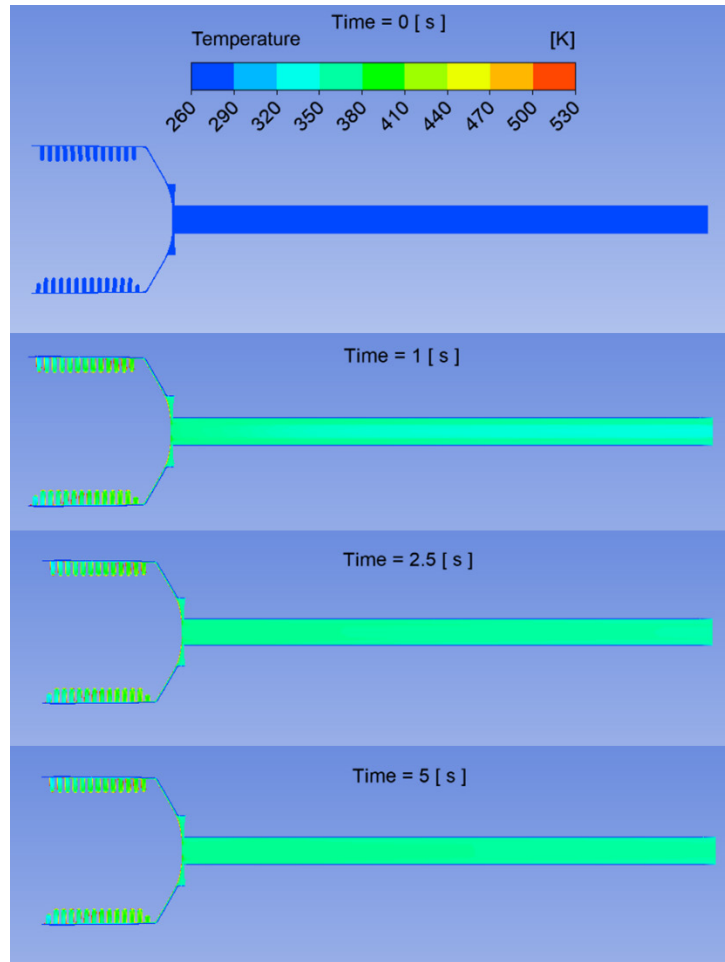

Figure 4.8 Temperature Contour for E10 fuel

Figure 4.8 shows the contour plot of temperature distribution in the Smart Heater at different times for the ethanol 10% fuel at 150 bar operating condition. It can be observed through the contour plot that the temperature of the fuel inside the heater is higher than the temperature near the exit condition.

30
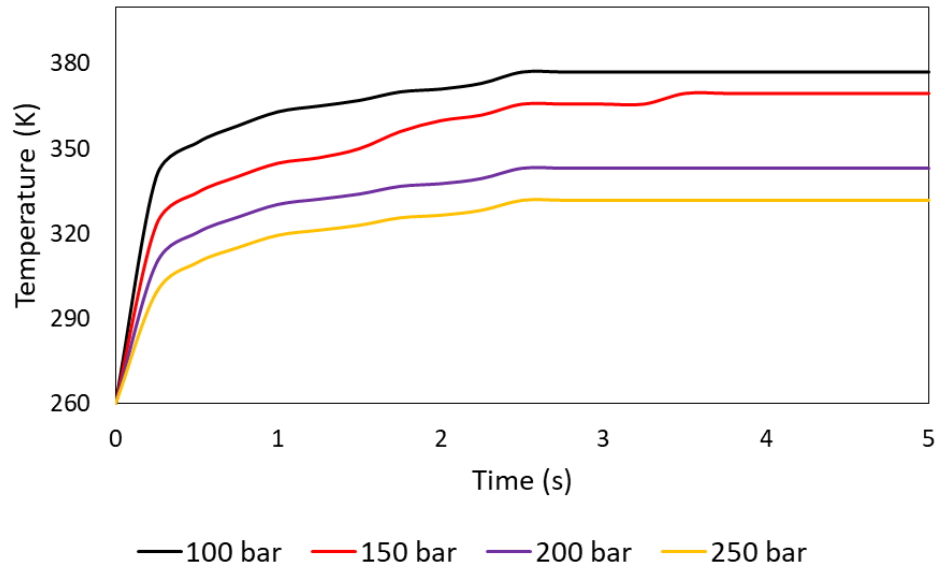
Figure 4.9 Temperature distribution at the exit - E10

Figure 4.9 shows the average temperature at the exit plane of the ethanol 10% fuel for different operating pressure conditions. The plot shows a similar trend for all operating conditions with a sudden increase in temperature at the exit and then flattens out to a constant temperature with the increase in time. From the boundary conditions provided it is observed that the heater surface is maintained at a constant temperature of 530K, which is the maximum temperature the heater can reach and the outer walls are provided with 260K considering cold condition temperature. A closer observation of the temperature contour shows that the heater reaches an average temperature in the range between 430K – 470 K in the heater rail region, but however due to the pintle heating effect and heat losses to the wall, the average temperature drops down. Thus the fuel experience heating and cooling in this process. The sudden rise in the temperature is due the purging of unheated fuel from the domain. As indicated the amount of unheated fuel in the domain is approximately around 1600 mg and for these injection pressure conditions at a wide open needle position, the mass flow rate achieved is high and thus the unheated fuel is purged out. Due to this the heated fuel reaches the outlet in a short period of time showing sudden increase in the exit temperature and later reaches a steady state.

31

Figure 4.10 Temperature Contour for E85 fuel

Figure 4.10 shows the contour plot of temperature distribution in the Smart Heater at different times for the ethanol 85% fuel at 150 bar operating condition. It can be observed through the contour plot that the temperature of the fuel inside the heater is higher than the temperature near the exit condition.

32
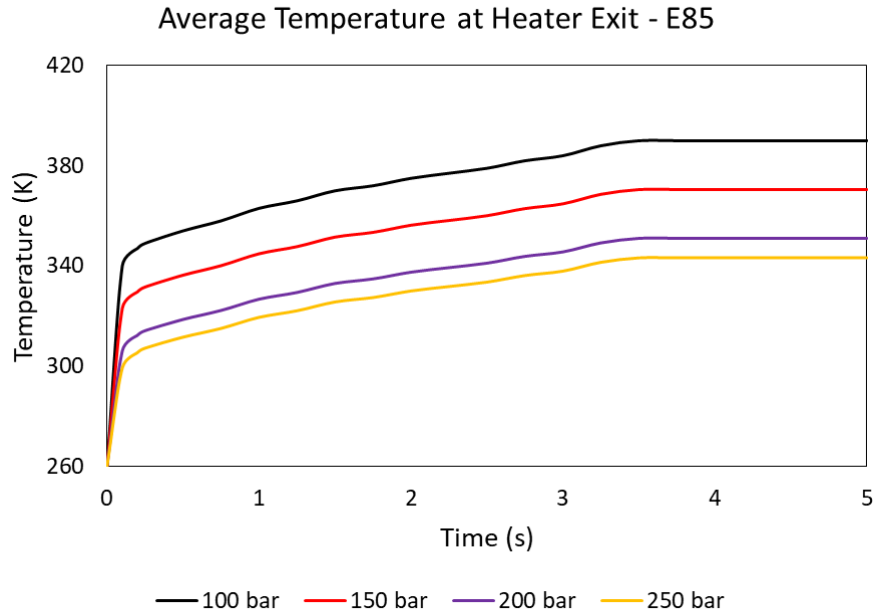
Figure 4.11 Temperature distribution at the exit - E85 fuel

Figure 4.11shows the average temperature at the exit plane of the ethanol 85% fuel for different operating pressure conditions. Even E85 fuel shows the similar trend that of E10. However the average temperature is little higher than E10. This is because the specific heat of E85 fuel as discussed in Figure 3.7 is higher than E10 fuel.

The exit condition of the heater is used as the input condition for the determining the exit condition properties at the injector nozzle outlet. ANSYS Fluent was used for this simulation. The models, boundary conditions and fuel properties used for the injector flow simulation is described in Table 4.3, Table 4.4 and Table 4.5.
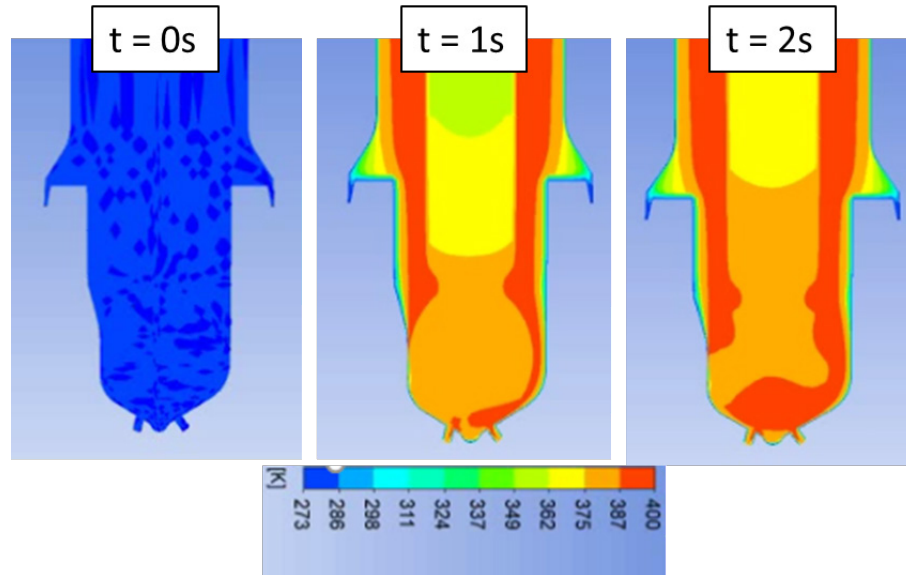
Figure 4.12 Temperature distribution through injector

Figure 4.12 shows the temperature contour for E10 fuel through the Y=0 plane of the injector. The injector flow is simulated with the input conditions from the heater. The contour shows, distribution of temperature at the nozzle exit. Along with the fluid domain, even the solid pintle was considered and conjugate heat transfer calculations were performed for the injector.

Figure 4.13 shows the normalized velocity variation from nozzle to nozzle at the exit condition of the fuel injector. As temperature of the fuel increases density decreases and in order to maintain the same mass flow rate velocity increases and this velocity increase is observed as a function of temperature. However the ratio of variation from nozzle to nozzle remained the same for all operating pressures and temperatures. The 6 nozzles of the injector are located asymmetrically with respect to the other nozzles. The nozzle angle of each nozzle with respect to the injector axis is different. The difference in exit velocity is due to the location of nozzles holes. Nozzle 2 and 6 shows less exit velocity than the other nozzles, this is because these nozzles are located below the dimple. This dent in the injector region affects the temperature by locally cooling down the fuel causing the drop in the average temperature. Similar trend is observed irrespective of the fuel variation.

34
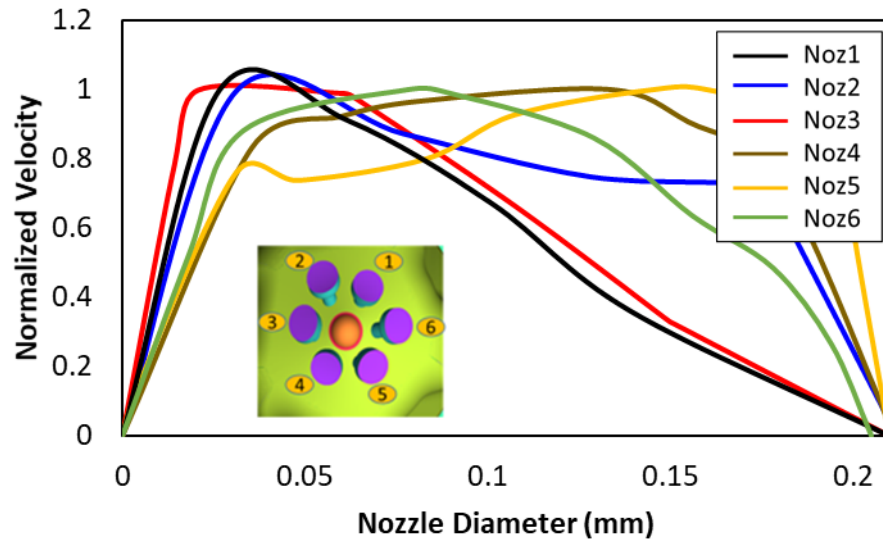
Figure 4.13 Normalized Velocity Profile at Nozzle exit

5. CVCC Spray

Advancement in engine technologies and developments in advanced combustion concepts has widened the scope of using fuel injectors in direct injection system for Gasoline engines. Fuel sprays issued from these injectors plays an important role in the spray development process as it governs the mixture formation, combustion efficiency, power output and emissions. Spray process involves atomization, droplet breakup, droplet interactions, collisions, coalescence, momentum and energy exchange. To simulate and understand the spray behaviour such as spray penetration, drop size distribution, spray angle, evaporation rate, wall impingement, mixture formation a well validated models that considers all the above mentioned processes should be used.

Thus, fuel spray studies plays a crucial role in developing new spray patterns, injection strategies, optimizing the combustion chamber design for efficient combustion. To understand the macroscopic spray properties such as penetration, drop size distribution simulation studies were carried out in a Constant Volume Combustion Chamber (CVCC).

Two kinds of computational initialization conditions were used. Method 1 is based on the uniform distribution among nozzles and the Method 2 is based on nozzle exit conditions calculated from ANSYS Fluent which considers the effect of nozzle to nozzle variation for the given mass flow rate. The numerical results were compared and validated with the available experimental data.

5.1. Computational Domain

The constant volume combustion chamber is a cube with the volume 10.6 X 10.6 X 10.6 cubic centimetre as shown in Figure 5.1. The fuel is sprayed from asymmetric 6-hole injector and hence full 3D geometry was considered. ICEM CFD was used to generate computational grids for simulation using in-house KIVA code.

36
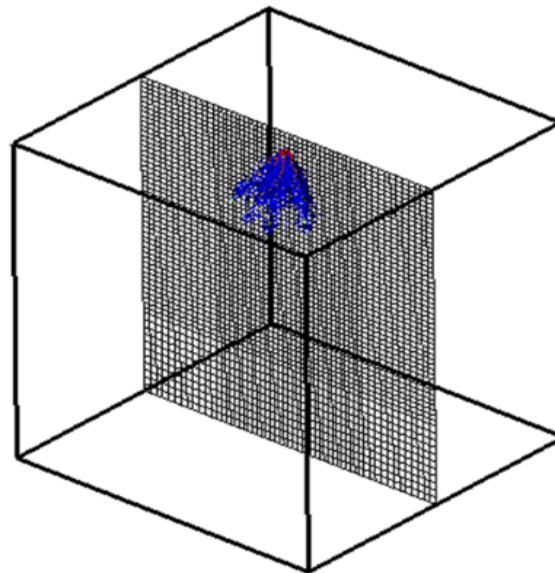
Figure 5.1 CVCC chamber with the Section View

The total number of cells used for the simulations were around 200K. Gradually increasing cell size with its minimum and maximum cells size being 1 mm and 2 mm were generated. Dense resolution was used in the near nozzle spray region and very far away from the nozzle less dense resolution were used.

5.2. Physical Models

Spray simulations were performed using in-house MTU-KIVA-Chemkin code. For simulating spray process and the fuel air mixing process various physical sub-models were incorporated in the in-house KIVA code. The sub-models includes models related to primary atomization, secondary atomization, drop collision, deformation, drop evaporation etc.

The physical numerical model is based on Eulerian-Lagrangian method of two-phase flow. The liquid droplets are described by stochastic system of discrete number of parcels which are tracked computationally by Lagrangian method. The gas phase is treated as continuous and Eulerian method is used to describe the flow field along with the RNG k-ε turbulence model. The two phases are coupled through the mass, momentum and energy exchange terms. For the primary atomization a hybrid primary spray model that considers that effects of aerodynamics of the drop, nozzle flows as well as computationally efficient was employed. In this model the liquid fuel is treated as a point source and the liquid fuel is injected as a fuel blobs whose diameter is equal to the effective diameter of the nozzle was tracked by Lagrangian method and the breakup of each blob is calculated based on the jet stability using Kelvin-Helmholotz (KH) instability theory. The model constants used for the simulations is described in Table 5.1

Table 5.1 KH-RT Model Constants

KH	Constant	RT	Constant
B_0	0.80	C_{3RT}	0.1
B_1	25	C_{2B}	1.0

The droplet collision model is based on the stochastic particle method in which the collision frequency is used to calculate the probability of drops in a parcel that collides with a drop in another parcel. The probability of coalescence is calculated based on the weber number which is a function of density and surface tension of the droplets.

Droplet deformation i.e., droplet distortion from its spherical shape was modelled is using forced, damped harmonic oscillator model where the surface tension and viscosity are the important properties used in restoring and damping terms. These distortions in the droplets

37

affect the momentum exchange between the drops and the ambient gas also the relative velocity that induces drop breakup and evaporation.

A Discrete Multi-Component (DMC) approach was used to model the vaporization of multicomponent fuels used in spray analysis. The vaporization model accounts for variable internal drop temperature and considers unsteady internal heat flux with internal circulation. The effective heat transfer coefficient calculated from the model is used to determine the amount of fuel to be treated as vapour when the drop temperature reaches the critical temperature [40,41,42,43,44,48].

The physical models described above are employed in the in house CFD code and were used for the CVCC spray calculations.

5.3. Computational Condition

Spray simulation was performed in a constant volume combustion chamber. The composition of E10 and E85 fuel described in Figure 3.4 and Figure 3.5 was considered. The fuel injector was located at 5 mm below the top face of the CVCC with its axis in the Z-direction. The location of each nozzle and its angle of inclination with the injector axis was given as input as shown in Figure 5.2. Spray analysis was performed for different injector pressure ranging from 100 bar to 250 bar by sweeping injected fuel temperature from -6°C to 250^{0}C. Two different chamber temperature was used to describe cold start condition and high in-cylinder temperature (considering port fuel and direct injection conditions). The simulation parameters are described in Table 5.1.
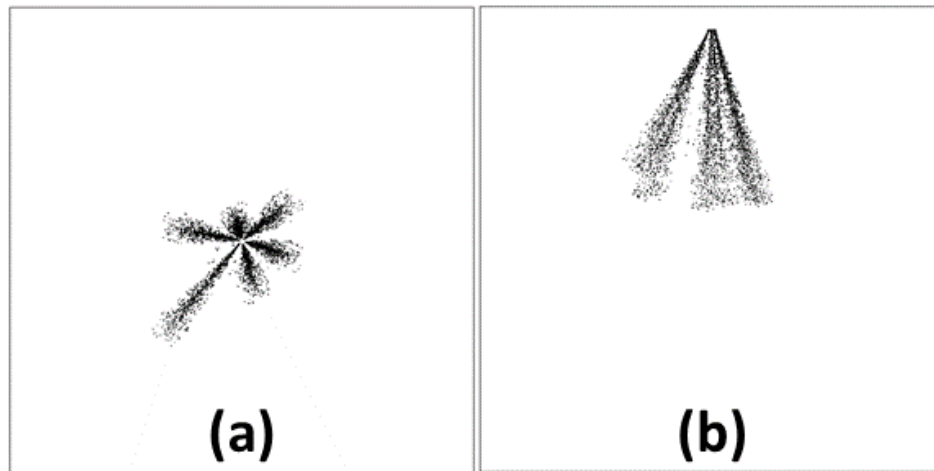
Figure 5.2 CVCC Spray location (a) Top View (b) Front View

Table 5.2 CVCC computational condition

Fuel	E0, E10, E85
Injection Pressure (bar)	100, 150, 200, 250
Fuel Temperature (°C)	-6, 25, 75, 100, 150, 200, 250
Chamber Temperature (°C)	45
Chamber Pressure (bar)	1
Nozzle Diameter (μm)	200
Solid Cone Angle	12°
Injection Duration (ms)	1.2

The experimentally measured injection rate shape was not available and hence the rate shape described in Table 5.2 was used for this simulation. Besides, Ra and et.al [40] showed that flat injection rate shape could accurately predict the spray behaviour.

5.4. Results: CVCC spray simulation

CVCC spray simulation was performed for the asymmetric six hole GDI Injector for E0, E10 and E85 with the models described in section 5.2 along with the fuel properties and computational conditions described in section 3 and section 5.3. The results are discussed as follows. The experiments were performed with different operating conditions such as injection pressure, fuel temperature, chamber pressure and temperature as shown in Table 5.2 for E10 and E85 fuel. However, the results of 150 bar injection pressure and 1 bar chamber pressure at 45°C chamber temperature for Ethanol 10% and 85% fuel is at all fuel temperatures is compared for validation.

The results of Mie Scattering is compared with the numerical data. In the Figure 5.5 the figure on the left hand side represents the Spray image captured through Mie Scattering. The yellow line represents the spray angle and the red colour represents the spray boundary and green dot indicates the maximum penetration.

5.4.1. Validation of Spray Morphology: E10 Fuel at 150 bar

The spray morphology is from the simulation is compared with the Mie Scattering imaging for Ethanol 10% fuel at 150 bar injection pressure at all fuel temperature as described in Table 5.1 at two different time 0.44 ms and 0.84 ms. 0.44 ms represents the early stages of spray formation and 0.84 ms indicates the later stage of spray development. In the following figures the a and a' represents Method 1 at t = 0.44 ms and 0.84 ms, b and b' of

39

the figure represents the Mie Scattering imaging from experiments at t = 0.44 ms and 0.84 ms and c and c' represents the spray morphology from Method 2 simulation. The viewing window of the Mie Scattering image is 75 mm in x direction and 60 mm in the y direction while the simulated result domain shows 100 X 100 mm viewing window. The 10 mm grid size in the Mie Scattering image is marked by converting the pixels and the simulated image is based on the computational grid.

Figure 5.3 shows the spray morphology of Ethanol 10% fuel with -6°C fuel temperature at 150 bar injection pressure. The qualitative comparison shpws that the simulation has captured the spray development accurately. The yellow line on the figure shows the spray angle. The spray angle qualitatively matched with the experiments.

Figure 5.4 and Figure 5.5 shows the spray morphology qualitative agreement of spray morphology at 25°C and 75°C fuel temperature.
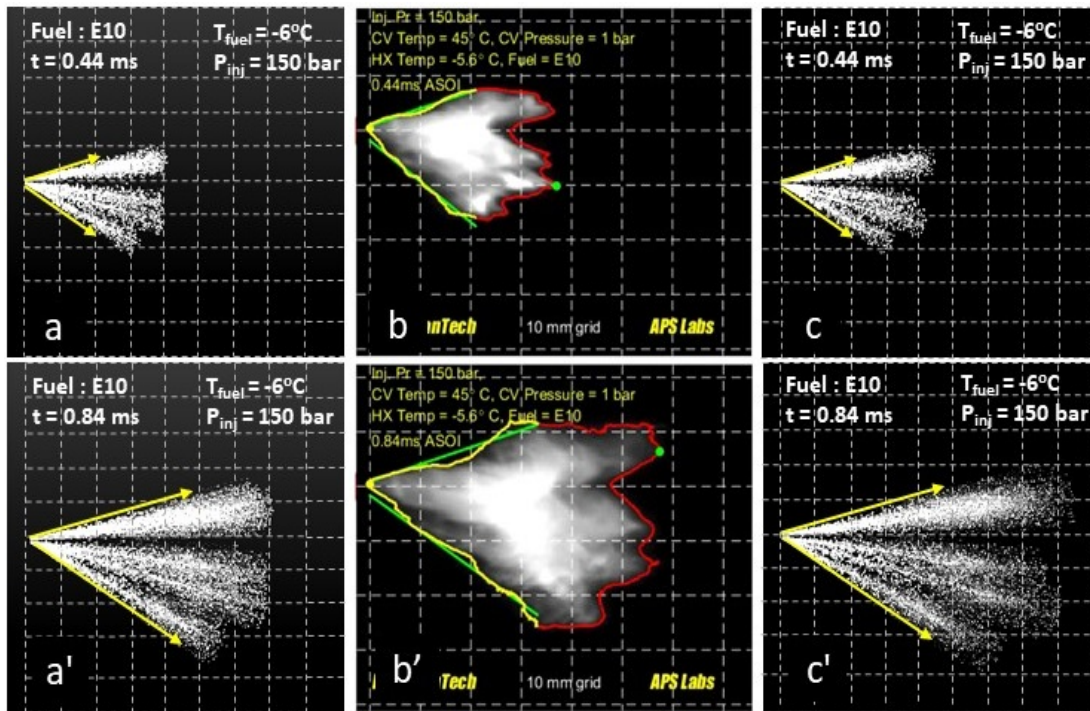
Figure 5.3 Spray Morphology of T_f = -6°C at t = 0.44 and 0.84 ms
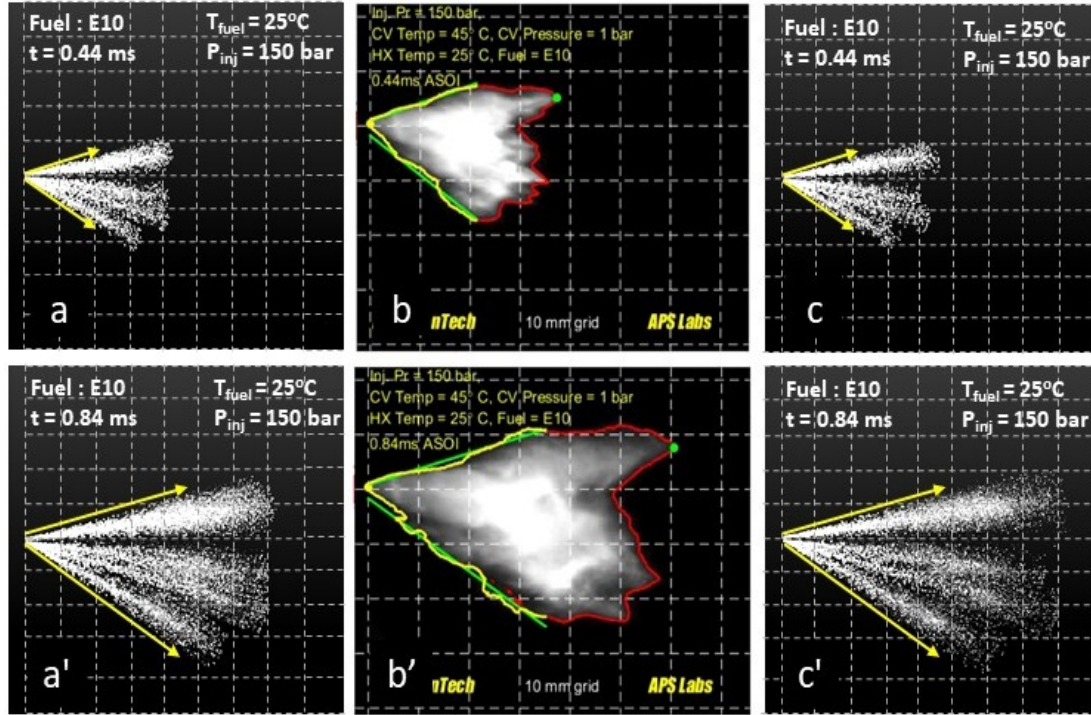
Figure 5.4 Spray Morphology of $T_f = 25^{\circ}C$ at t = 0.44 and 0.84 ms
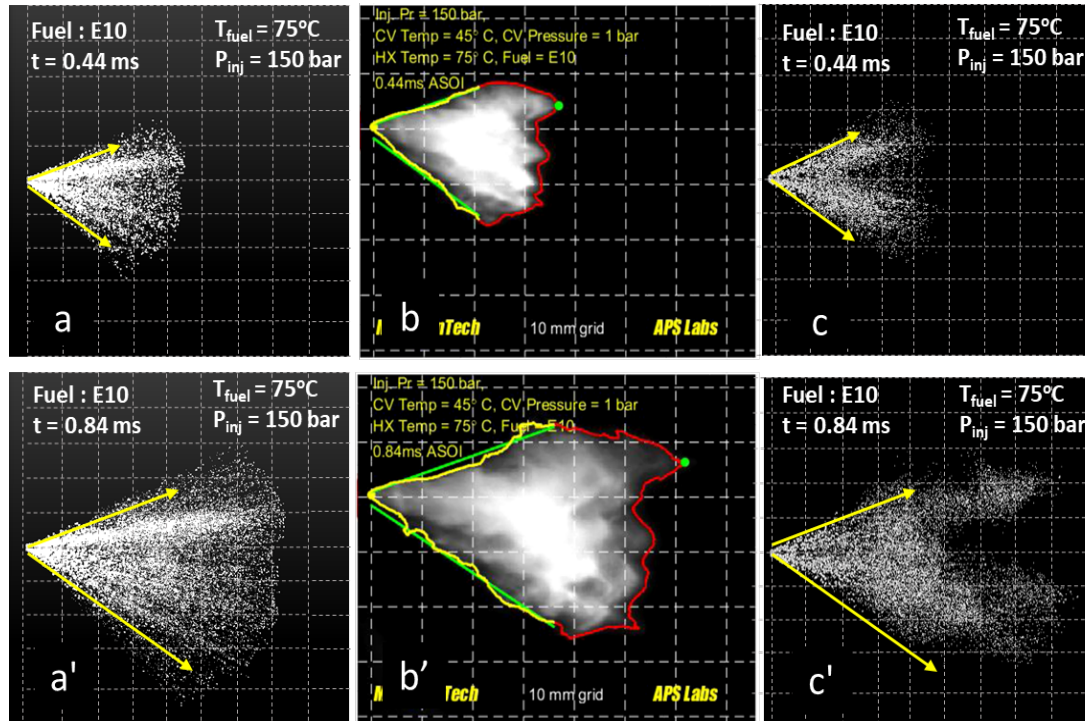
Figure 5.5 Spray Morphology of $T_f = 75^{\circ}C$ at t = 0.44 and 0.84 ms
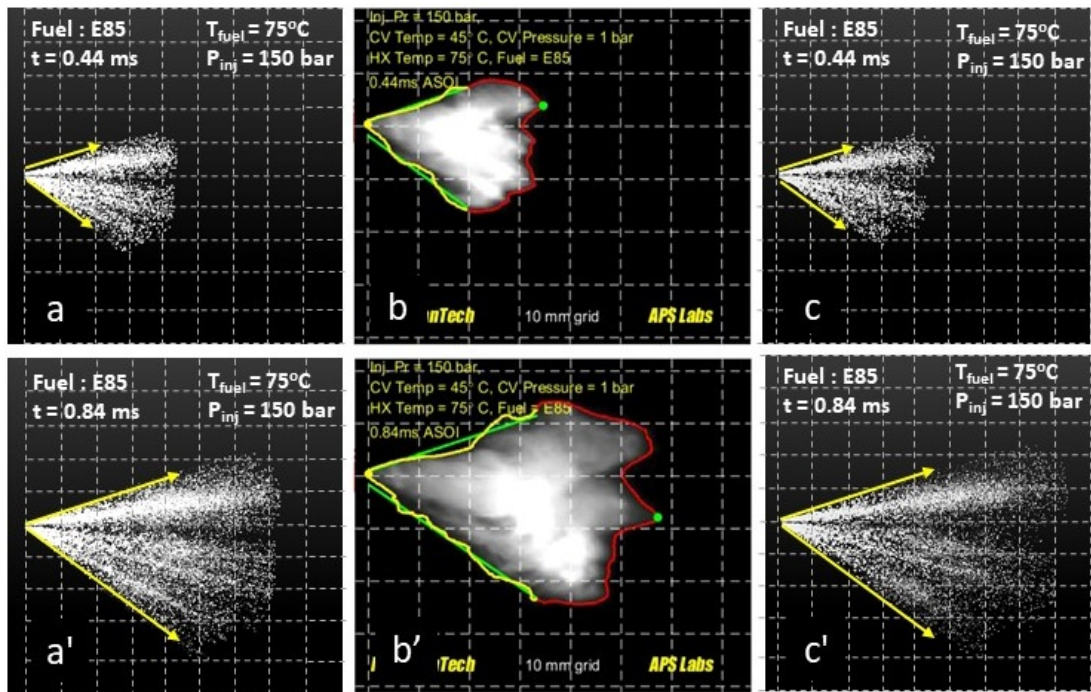
41
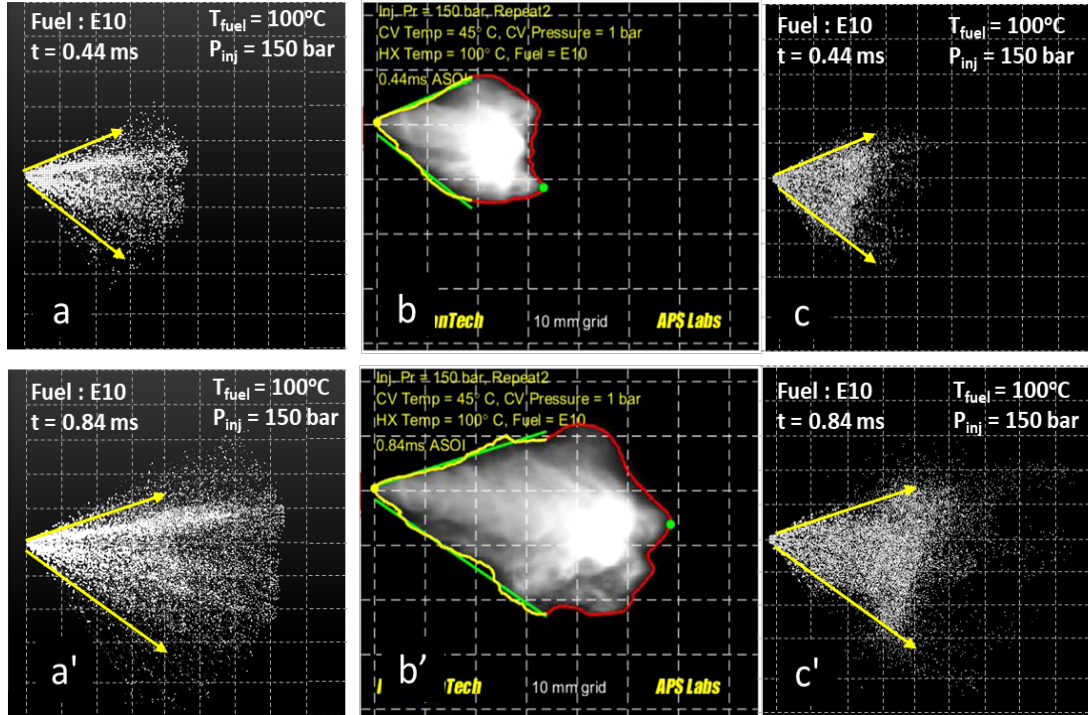
Figure 5.6 Spray Morphology of $T_f = 100$ºC at t = 0.44 and 0.84 ms
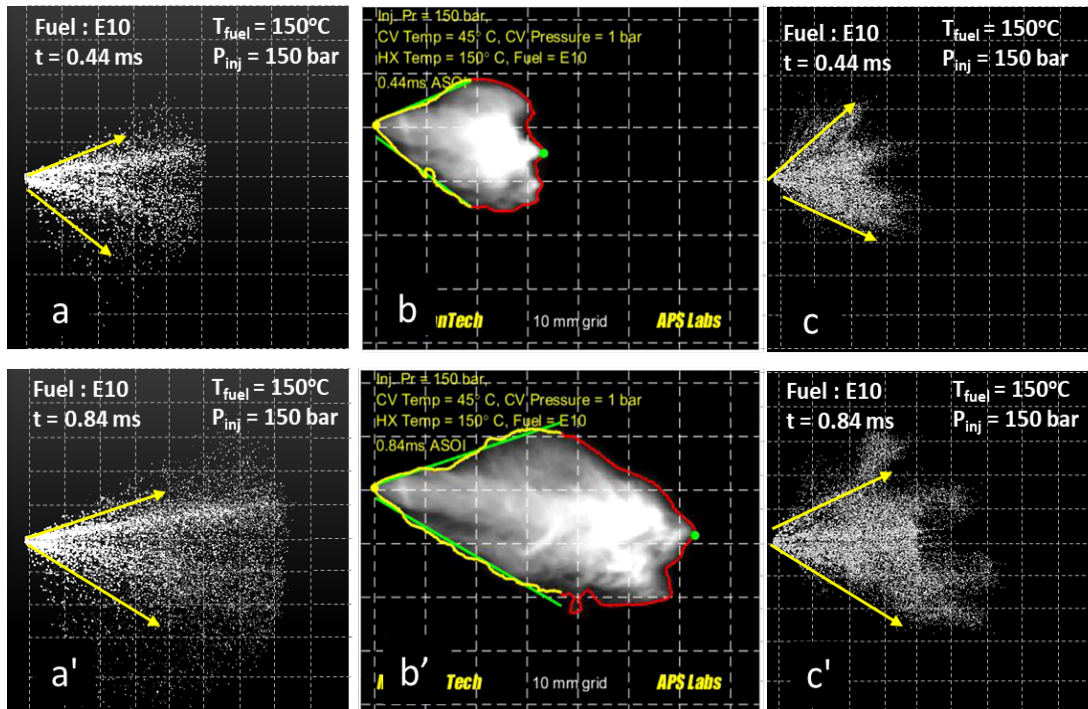
Figure 5.7 Spray Morphology of $T_f = 150$ºC at t = 0.44 and 0.84 ms
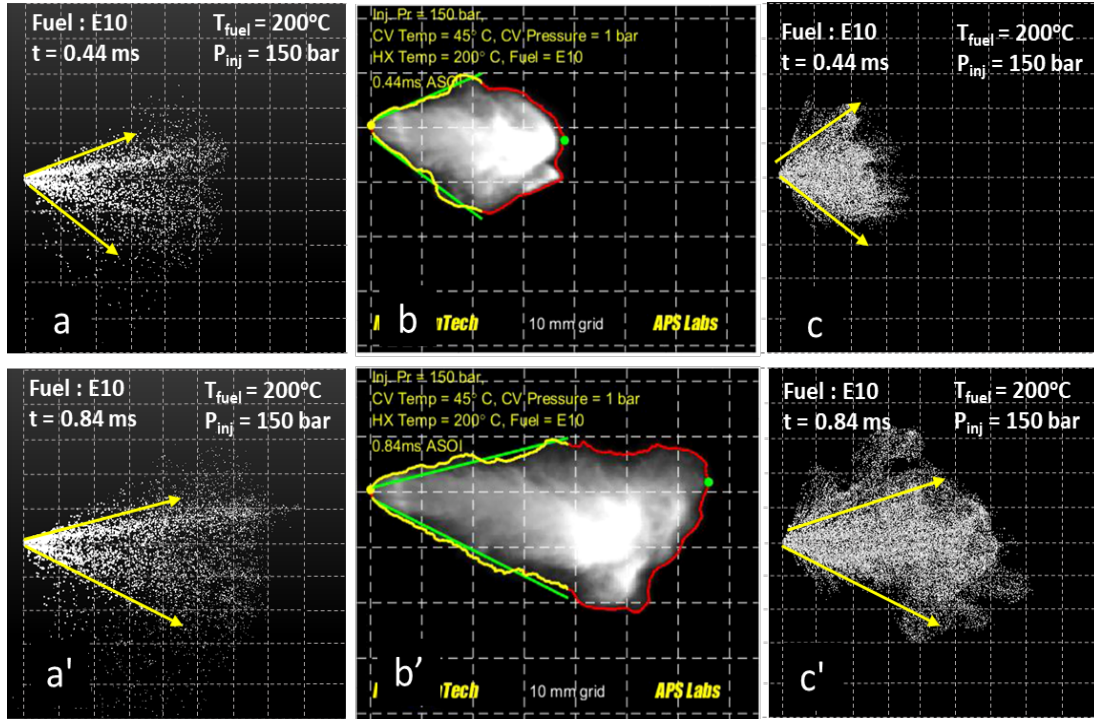
Figure 5.8 Spray Morphology of T_f = 200ºC at t = 0.44 and 0.84 ms
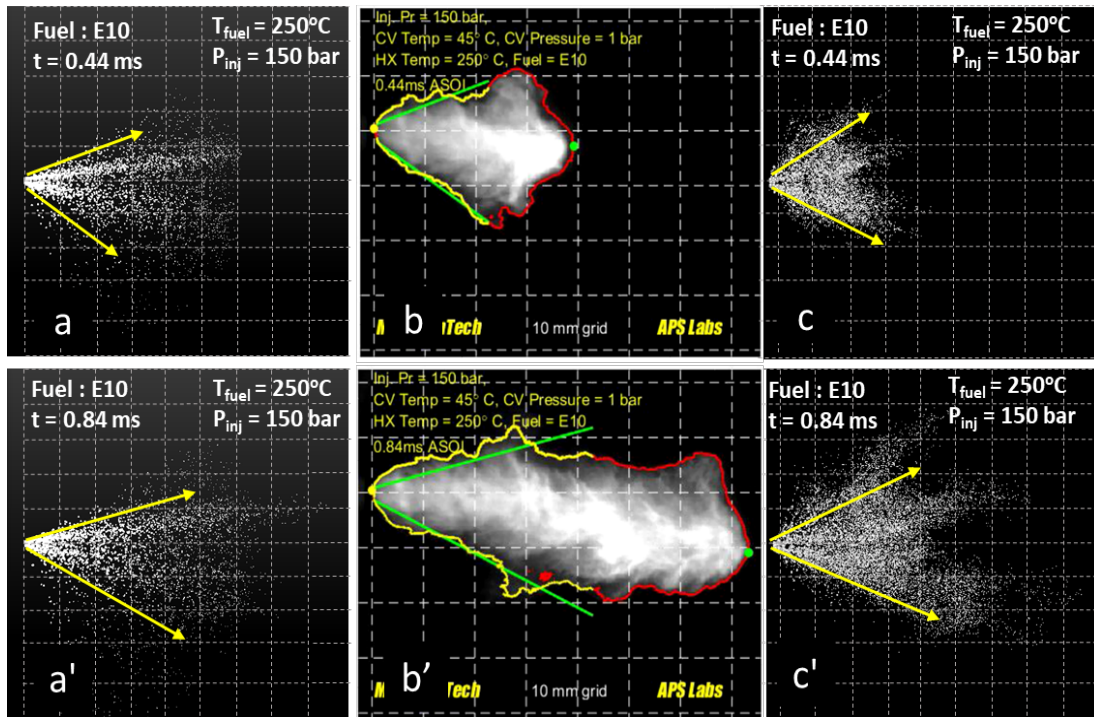
Figure 5.9 Spray Morphology of T_f = 250ºC at t = 0.44 and 0.84 ms

43

Figure 5.6, Figure 5.7, Figure 5.8 and Figure 5.9 shows the qualitative comparison of spray morphology at 0.44 ms and 0.84 ms ASOI for fuel temperatures 100°C, 150°C, 200°C and 250°C. It is observed through the simulation results that the early stages of the spray has been predicted good, however as the fuel temperature increases the prediction does not match well with the experiments using Method 1. This is clearly observed for the fuel temperatures 200°C and 250°C. However, using the Method 2 where instead of using the single velocity and temperature for the nozzle, distributed velocity and temperature calculated from fluid flow simulation was used. This was able to capture the spray developing into flash boiling mode. At temperatures greater than 100°C the spray tends to collapse forming a bell like structure at the tip. At 200°C, the spray completely collapses into a single plume as seen in the experiments.

From the fuel distillation shown in Figure 3.6, the maximum temperature the fuel exits in liquid and vapour phase is around 480 K which is the boiling point of the heaviest compound used to model this 14 component surrogate fuel to represent ethanol 10% fuel. Increasing the fuel temperature increases the vapour pressure of the fuel. Figure 3.9 represents the vapour pressure relation for Ethanol (E10) 10% fuel as a function of temperature. When the vapour pressure is higher than the momentary chamber pressure, the fuel becomes superheated and the degree of superheat is determined by the ratio of ambient pressure over saturation pressure. During this condition bubble formation in the near nozzle region promotes vaporization and in-cylinder charge preparation process.

However several research has proposed that during the superheated condition, this bubble formation for a multi-hole GDI injectors widens the spray angle in the near nozzle region and as the spray develops it collapses resulting in higher spray penetration [45,46,47].

The spray simulation is performed at 1 bar chamber pressure and from the vapour pressure relation for Ethanol 10% the vapour pressure becomes higher than the chamber pressure at a temperature in the range of 70-75°C. Thus, the flash boiling and spray collapse is observed beyond this fuel temperature.

In Figure 5.7, Figure 5.8 and Figure 5.9 the experimental image shows spray widening and collapsing characteristics at elevated fuel temperature while the simulated results using Method 1 does not show those behaviours and over predicting the spray behaviours while the Method 2 captures the spray shape at all temperatures, but the initial part of the spray is under predicted.
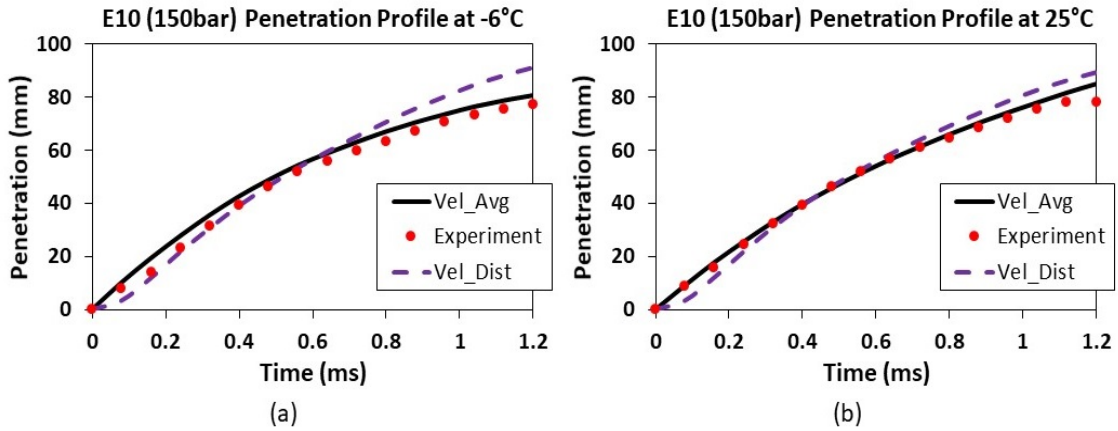
Figure 5.10 Comparison of Spray Penetration at (a) T_f = -6ºC (b) T_f = 25ºC
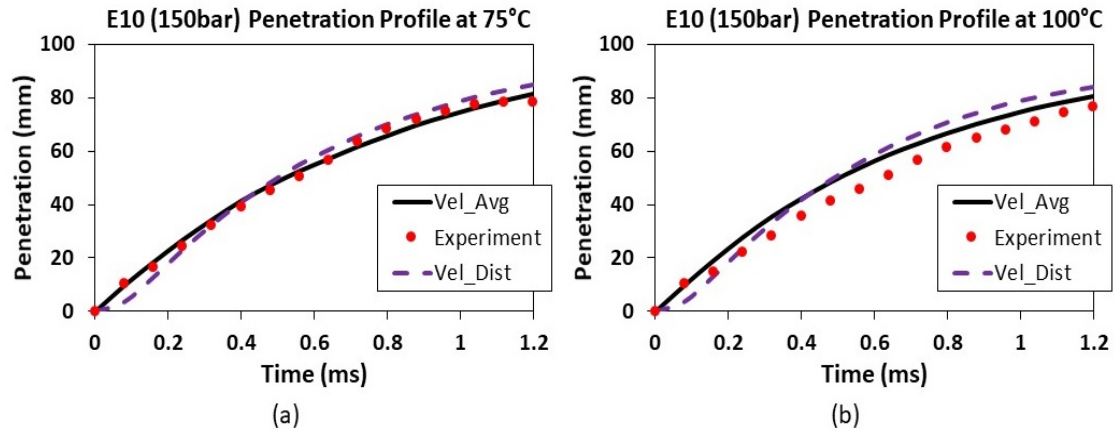
Figure 5.11 Comparison of Spray Penetration at T_f = 75ºC and 100ºC
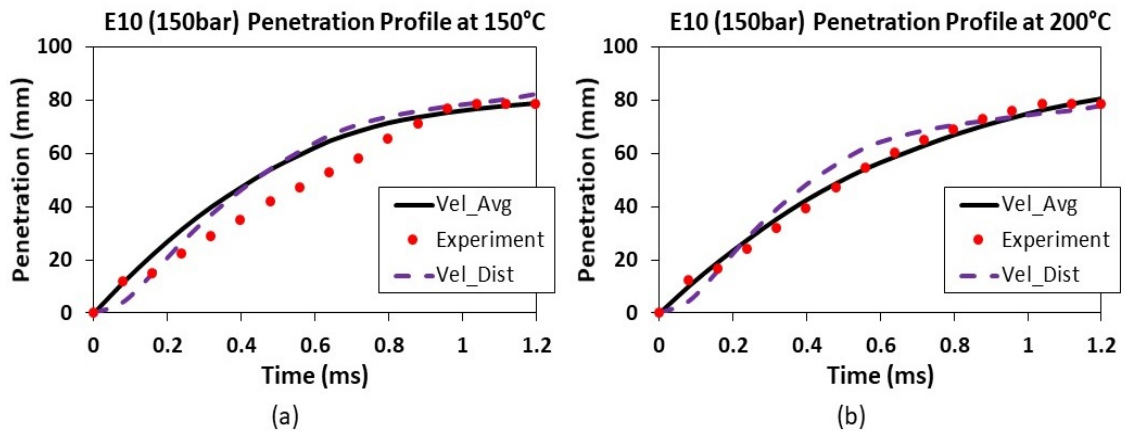
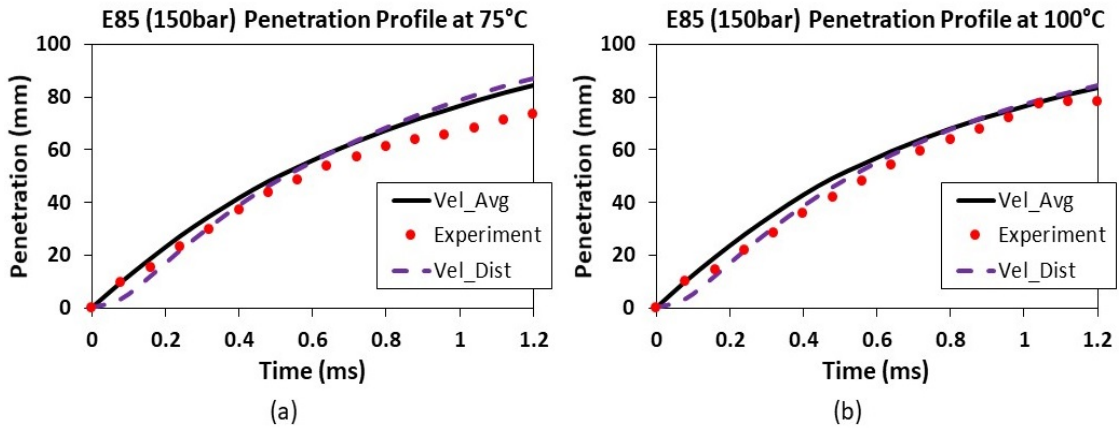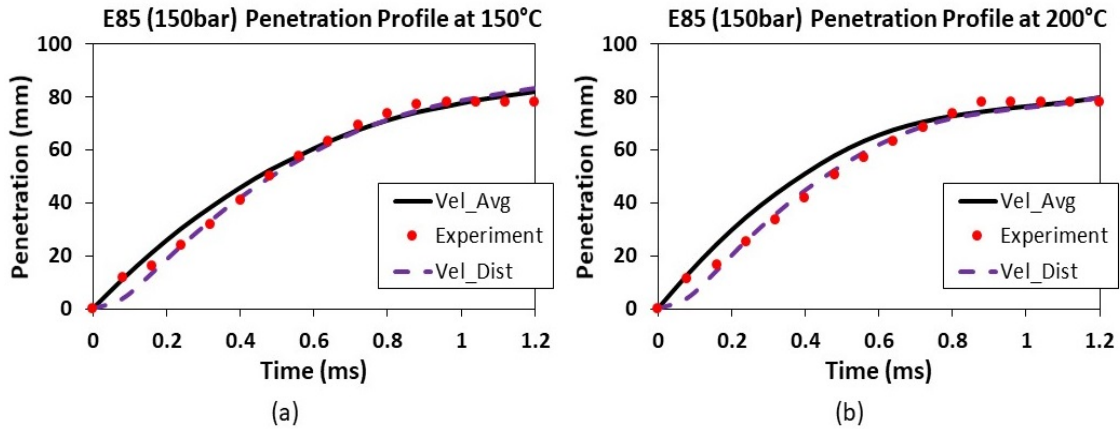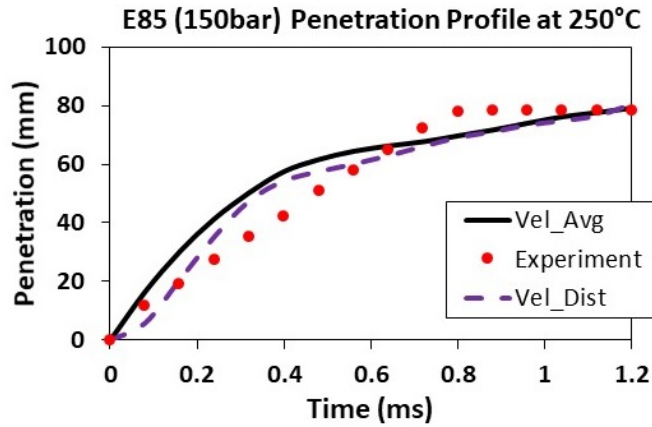Figure 5.12 Comparison of Spray Penetration at T_f = 150ºC and 200ºC

45
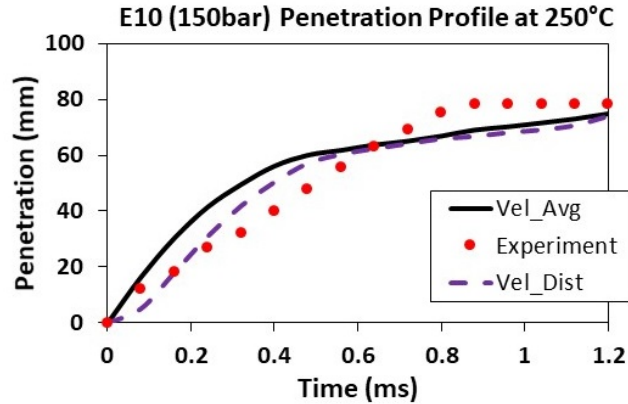
Figure 5.13 Comparison of Spray Penetration at $T_f = 250^{\circ}C$

Spray penetration is measured as the distance between injector nozzle tip and furthest axial point on the spray boundary. Figure 5.10, Figure 5.11, Figure 5.12 and Figure 5.13 shows the spray penetration comparison between experiments and simulated results of Ethanol 10% fuel at 150 bar injection pressure for different fuel temperatures.

A good agreement is achieved for injection cases whose vapour pressure is less than the ambient pressure. But however, for elevated temperature cases the penetration did not match well with the experiments, because at high temperatures the spray collapses and penetrates further resulting in higher penetration. Figure 5.16 shows the spray penetration profile at 250°C fuel temperature, it is observed that the penetration profile did not match with the experiments. As time develops the spray collapsing behaviour is observed numerically in Method 2, but there is not enough momentum to push the sprays in the forward direction. This could be due to poor drop collision in the later stages of the spray.
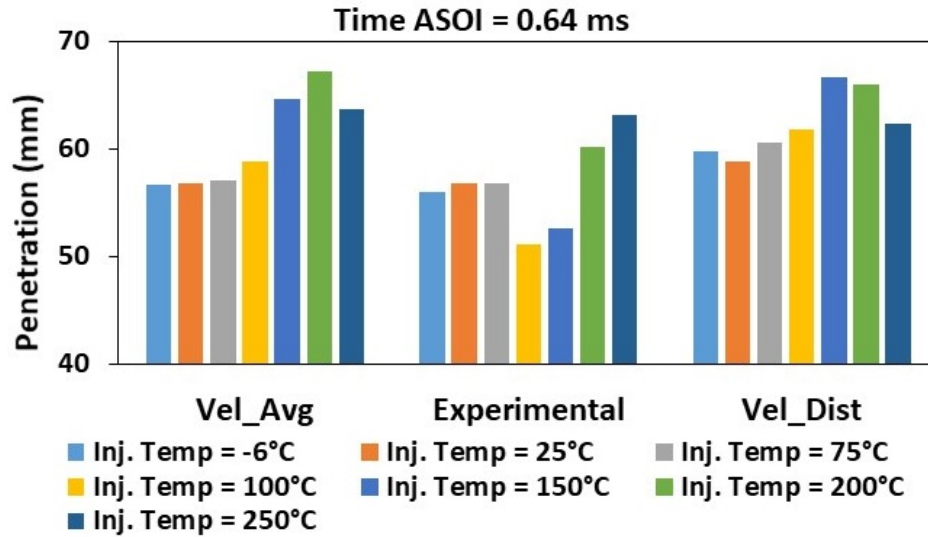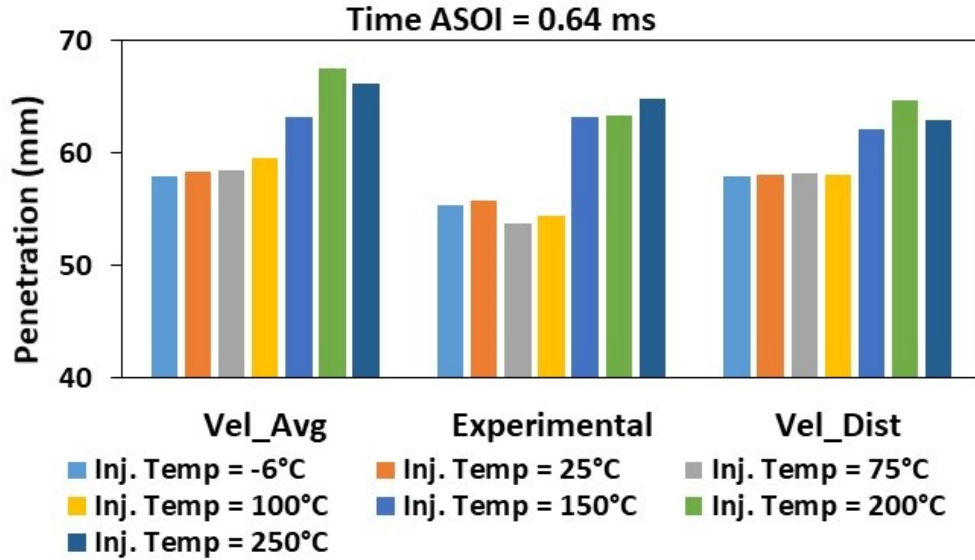
Figure 5.14 Comparison of Penetration at ASOI = 0.64 ms
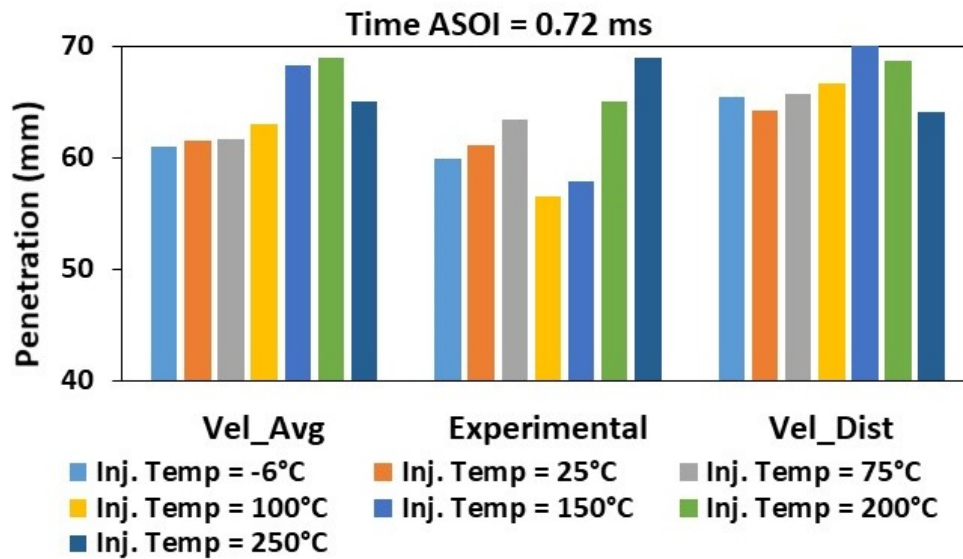
Figure 5.15 Comparison of Penetration of ASOI = 0.72 ms

Figure 5.14 and Figure 5.15 shows the trend between experimental and simulated penetration at ASOI 0.64 ms and 0.72 ms for E10 fuel at 150 bar injection pressure. Experimental measurements shows a reduced penetration value at 100°C and 150°C at 0.64 ms and 0.72 ms while the simulated results does not capture those trend due to the effect of spray collapsing.

47
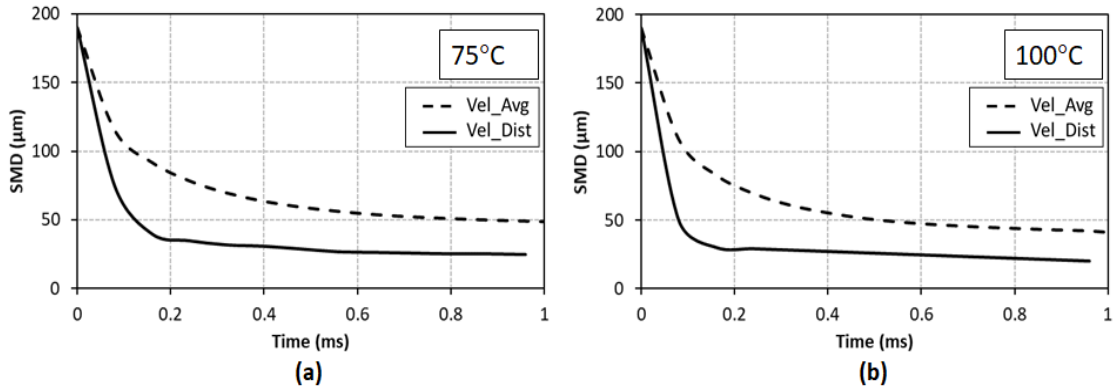
Figure 5.16 Average SMD distribution for 75ºC and 100ºC
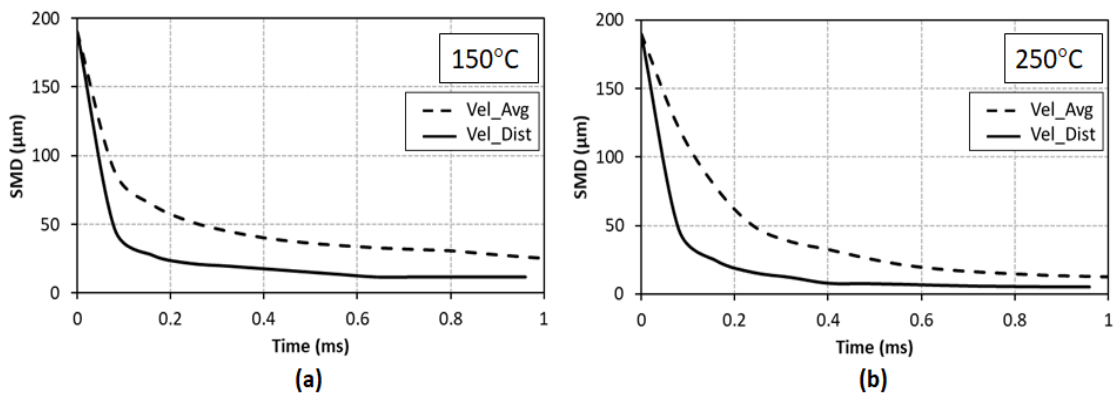
Figure 5.17 Average SMD distribution for 150ºC and 250ºC

Figure 5.16 (a) and (b), Figure 5.17 (a) and (b) shows the overall average SMD distribution at 75°C, 100°C, 150°C, 250°C between Method 1 and Method 2 which is indicated as Vel_Avg for Method 1 and Vel_Dist for Method 2. The SMD using the average velocity as input is higher than the distributed velocity and temperature as input condition. Also, for both the methods the breakup model constants were kept constant as shown in Table 5.1

In Figure 5.16 (a), the overall SMD drops to a smaller value in less than 1 ms, than the Method 1. This clearly indicates there is a faster breakup, that leads to the smaller droplets. Due to the smaller droplets generated, the surrounding gas is able to push these tiny droplets to the axis of the injector, instead of the injection direction leading to the collapse of the individual spray plumes to a single plume. Similar behaviour is observed for all other temperatures greater than 75°C. Table 5.3 shows the total number of particles present in the computational domain at time = 0.84 ms. This also indicates, the distributed input helps in improving the spray prediction.

Table 5.3 Total computational Particles at time, t = 0.84 ms

Temperature	Method1	Method2
100°C	~7500	~20000
150°C	~11000	~24000

5.4.2. Validation of Spray Morphology: E85 Fuel at 150 bar
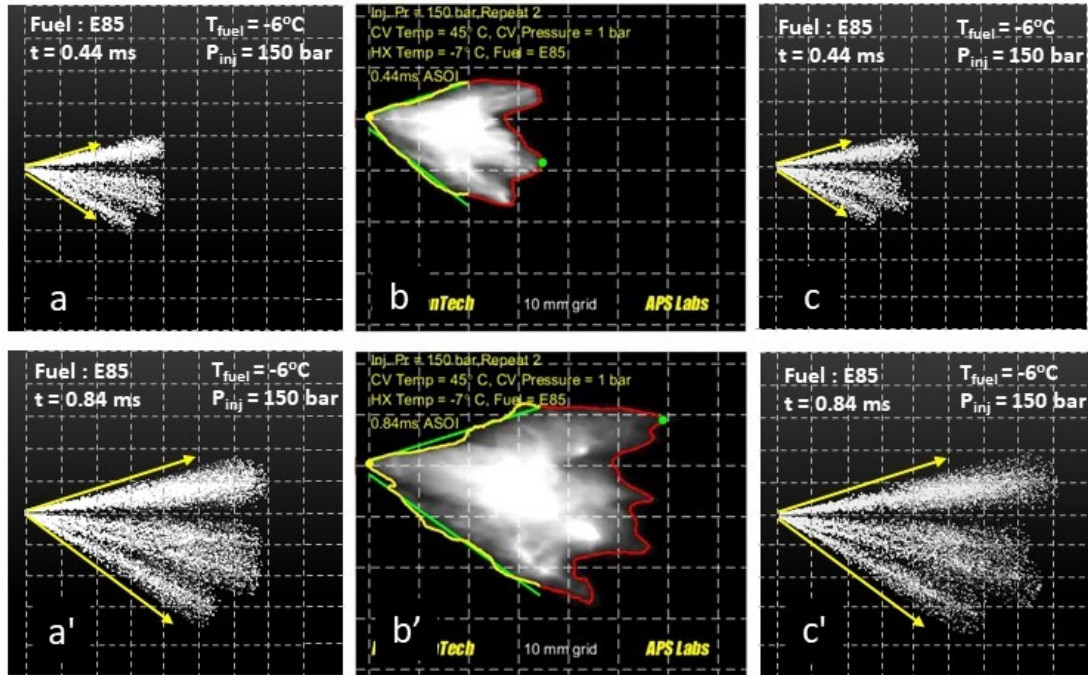
Figure 5.18 Spray Morphology of T_f = -6°C at t = 0.44 and 0.84 ms

The spray morphology is from the simulation is compared with the Mie Scattering imaging for Ethanol 85% fuel at 150 bar injection pressure at all fuel temperature as described in Table 5.1 at two different time 0.44 ms and 0.84 ms. The 14 component fuel model that is used to describe the physical properites of the E85 fuel is represented in Figure 3.5. 0.44 ms represents the early stages of spray formation and 0.84 ms indicates the later stage of spray development. In the following figures the a and a' represents Method 1 at t = 0.44 ms and 0.84 ms, b and b' of the figure represents the Mie Scattering imaging from experiments at t = 0.44 ms and 0.84 ms and c and c' represents the spray morphology from Method 2 simulation.

Figure 5.18 shows the spray development process of E85 fuel at -6°C. It is seen that both the method predicts the spray development process at early and later stages of the spray. Even the spray angle agrees well with the experiments.

49
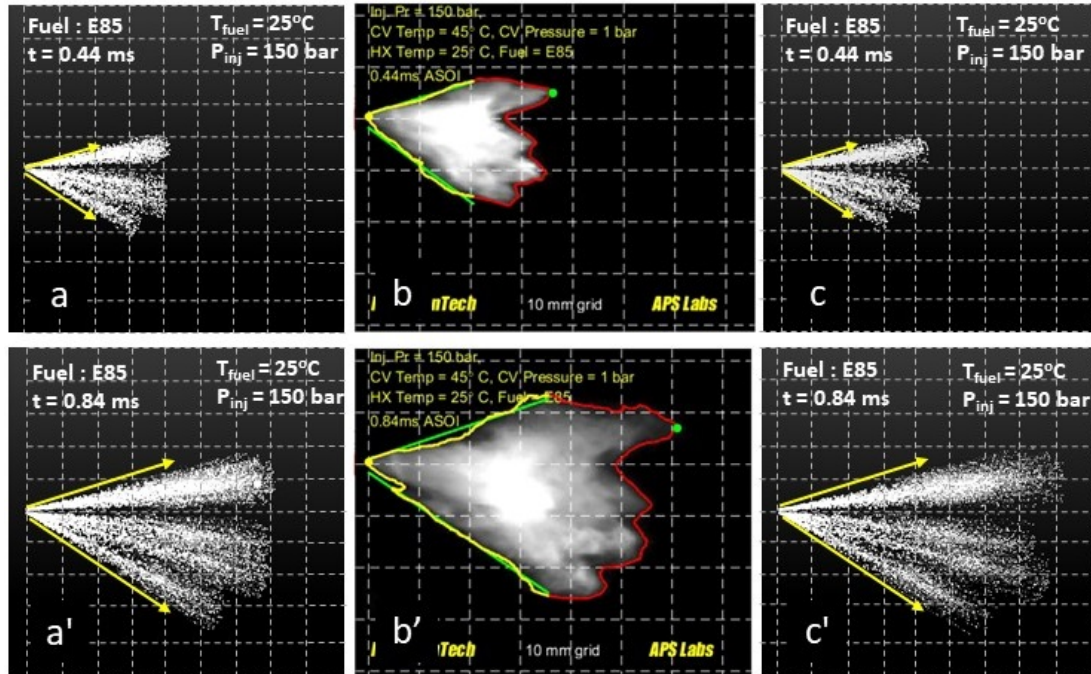
Figure 5.19 Spray Morphology of $T_f = 25^oC$ at t = 0.44 and 0.84 ms

Figure 5.20 Spray Morphology of $T_f = 75^oC$ at t = 0.44 and 0.84 ms
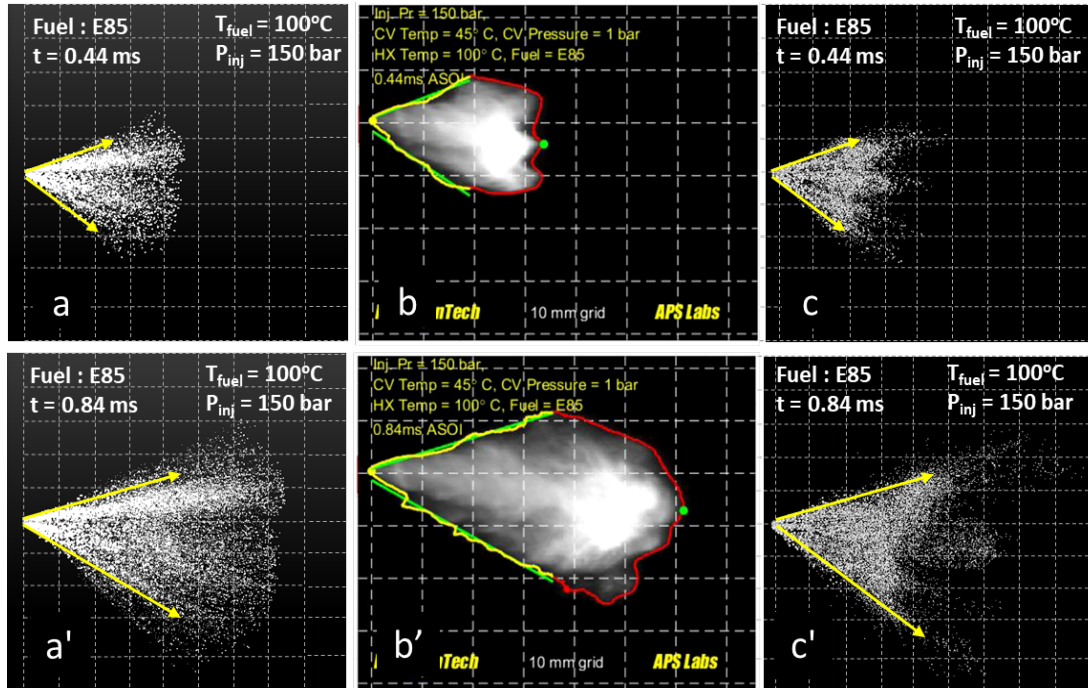
Figure 5.21 Spray Morphology of $T_f = 100°C$ at t = 0.44 and 0.84 ms
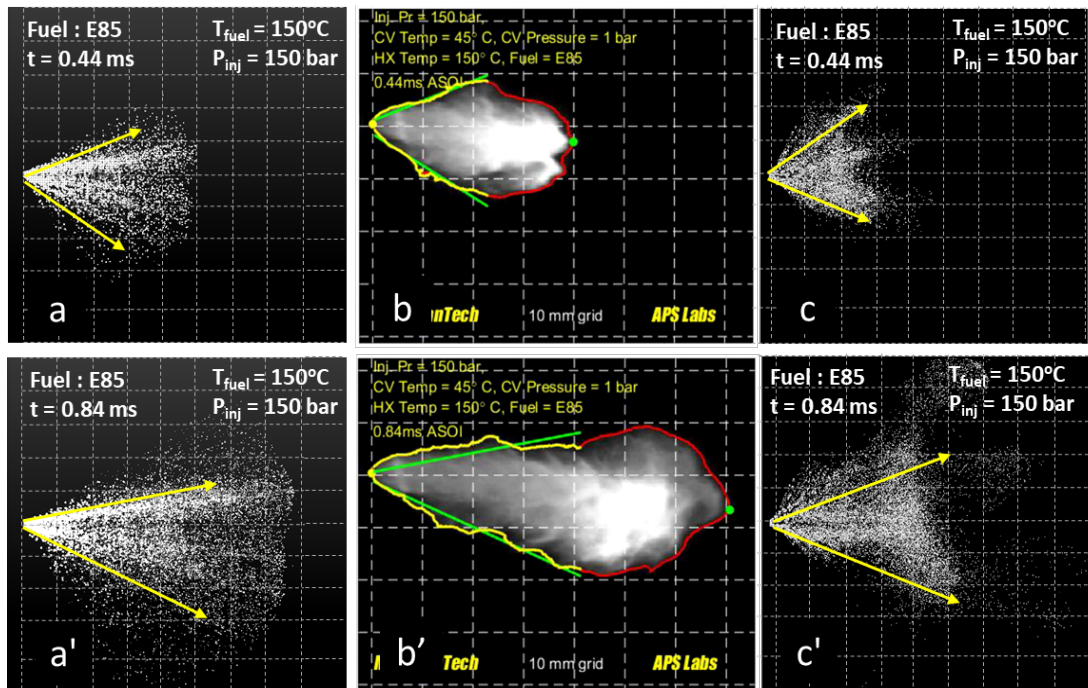
Figure 5.22 Spray Morphology of $T_f = 150°C$ at t = 0.44 and 0.84 ms

51
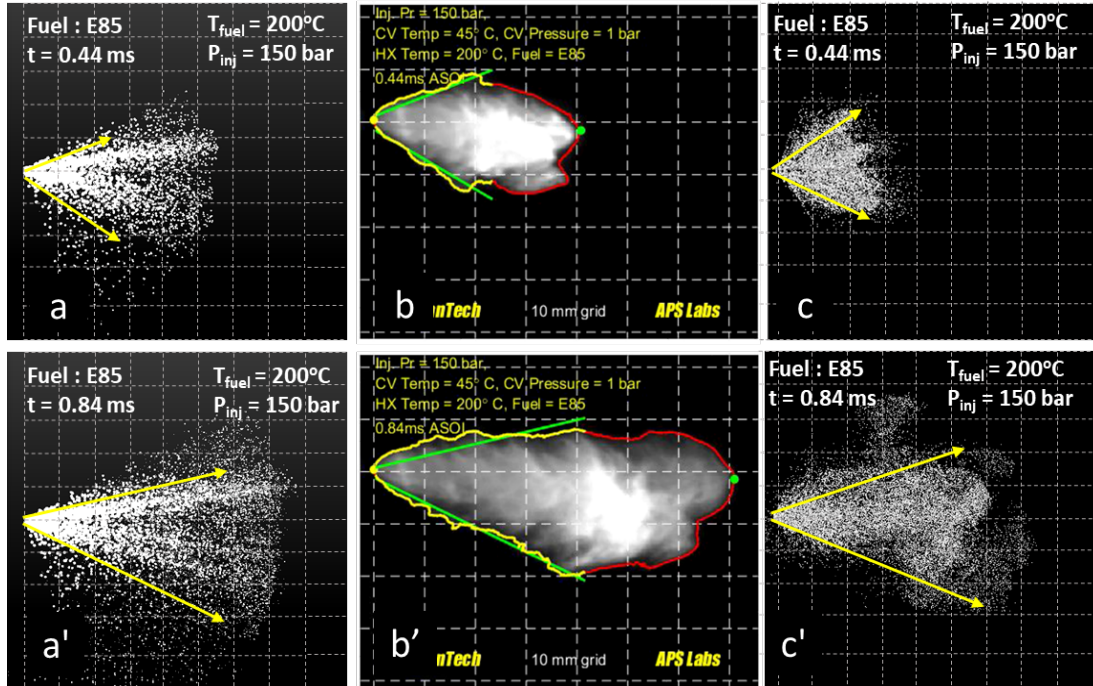
Figure 5.23 Spray Morphology of $T_f = 200^oC$ at t = 0.44 and 0.84 ms
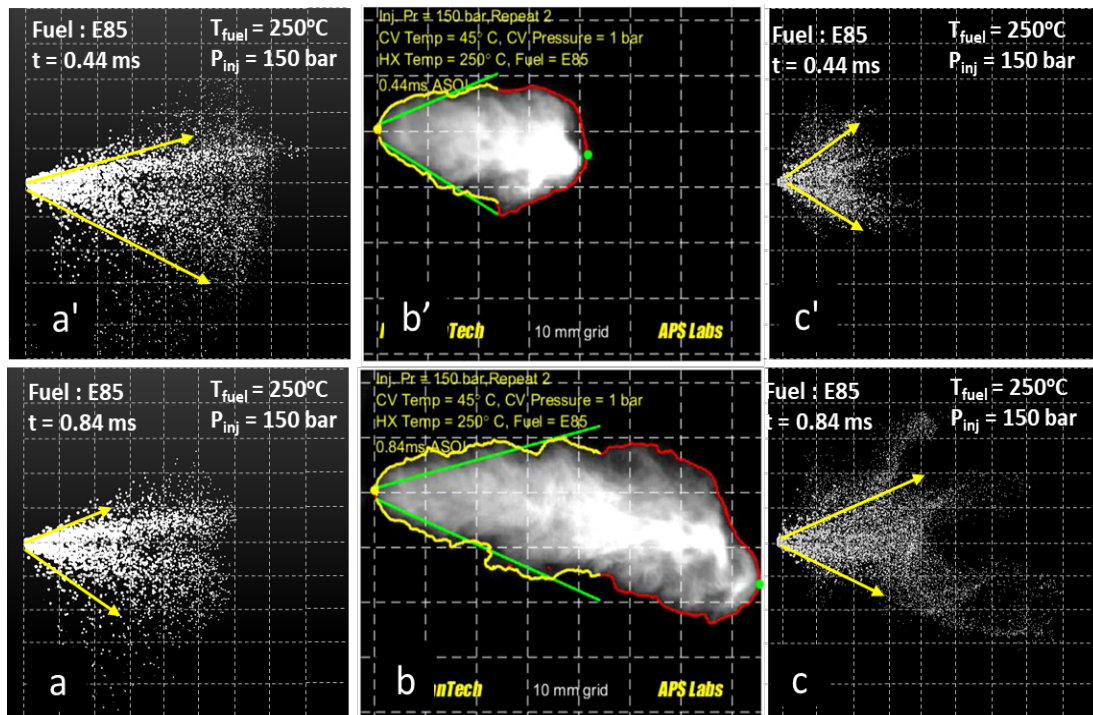
Figure 5.24 Spray Morphology of $T_f = 250^oC$ at t = 0.44 and 0.84 ms

Figure 5.19, Figure 5.20, Figure 5.21, Figure 5.22, Figure 5.23, Figure 5.24 and Figure 5.25 shows the spray morphology comparison for Ethanol 85% fuel at 150 bar injection pressure at different fuel temperatures. Similar to E10 case predictions does not match for elevated fuel temperature cases as the vapour pressure for high temperature cases are high than the ambient pressure leading to superheated fuel, during which shows spray collapse occurs commonly with GDI multi-hole injectors.
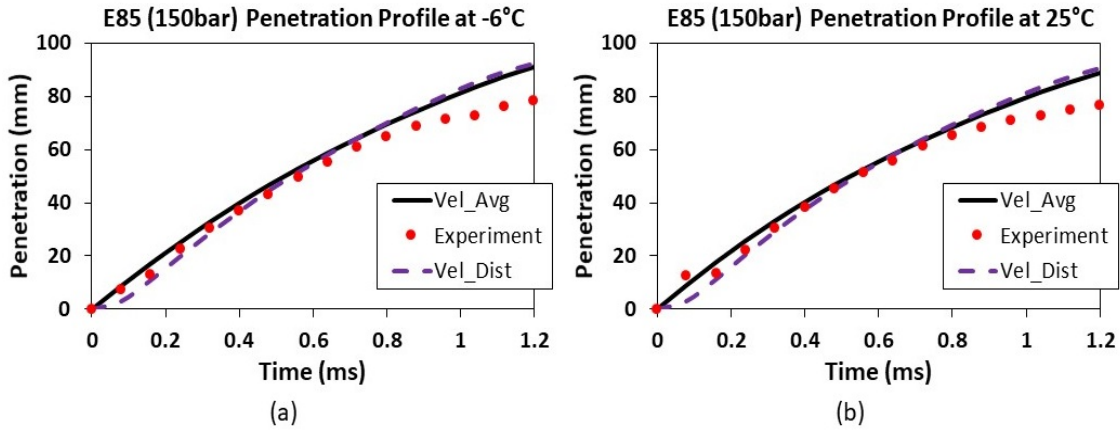
Figure 5.25 Comparison of Spray Penetration at T_f = -6°C and 25°C

Figure 5.26 Comparison of Spray Penetration at T_f = 75°C and 100°C

Figure 5.27 Comparison of Spray Penetration at T_f = 150ºC and 200ºC

Figure 5.28 Comparison of Spray Penetration at T_f = 250ºC

Figure 5.26, Figure 5.27, Figure 5.28 and Figure 5.29shows the spray penetration comparison between experiments and simulated results of Ethanol 85% fuel at 150 bar injection pressure for different fuel temperatures. A similar behaviour to that of E10 is observed for E85 fuel.

Figure 5.29 Comparison of Penetration at ASOI = 0.64 ms
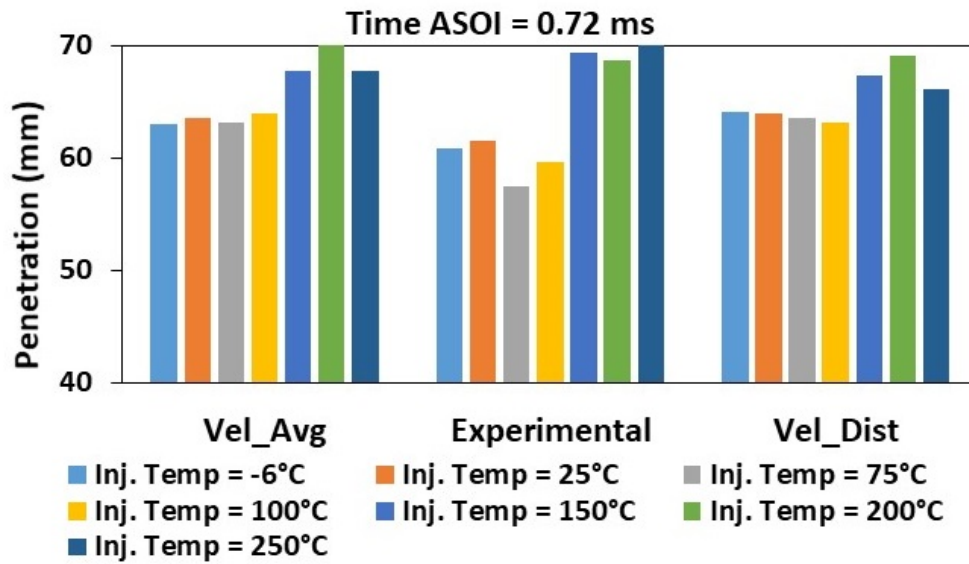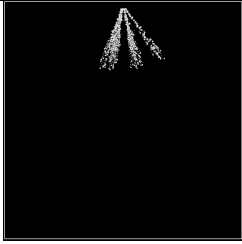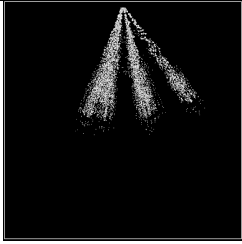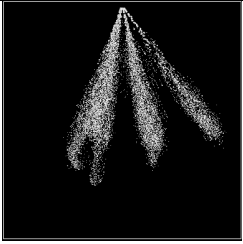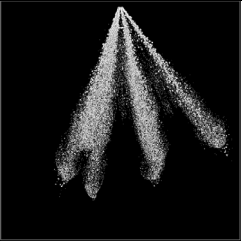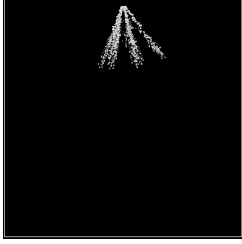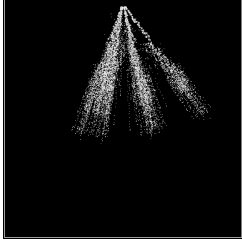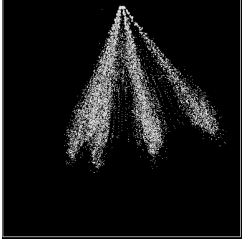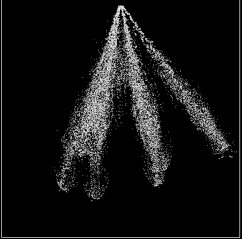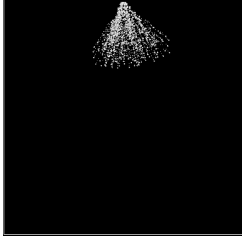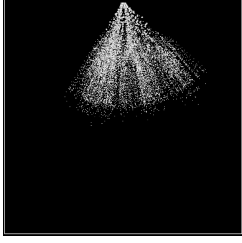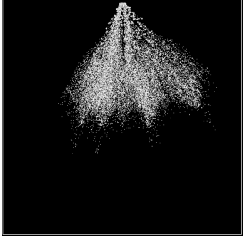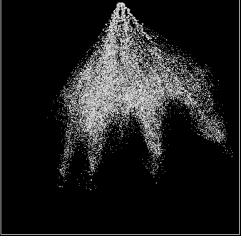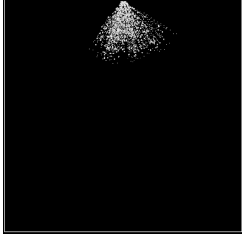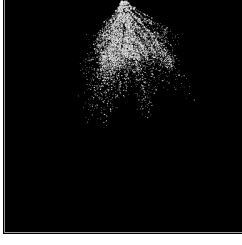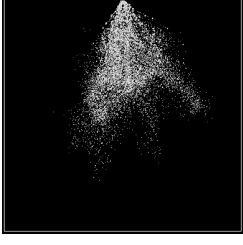
Figure 5.30 Comparison of Penetration at ASOI = 0.72 ms

Figure 5.30 and Figure 5.31 shows the trend between experimental and simulated penetration at ASOI 0.64 ms and 0.72 ms for E85 fuel at 150 bar injection pressure. Experimental measurements shows a reduced penetration value at 75°C and 100°C at 0.64 ms and 0.72 ms while the simulated results does not capture those trend. However, for E85 fuel minimum penetration both experimental measurement and simulation shows at 75°C for both 0.64 ms and 0.72 ms ASOI.

55

5.4.3. Transition to Flash boiling

From the previous results, Method 2 gives good agreement for spray morphology. The results from the spray studies are discussed to understand how the spray transforms its shape under flash boiling condition. The spray morphology discussed below is shown in XZ plane (Front view)

Temp /ASOI	0.16 ms	0.4 ms	0.64 ms	0.84 ms
-6°C				
25°C				
75°C				
100°C				

150° C			
200° C			
250° C			

Figure 5.31 Spray Morphology for E0 fuel

Temp /ASOI	0.16 ms	0.4 ms	0.64 ms	0.84 ms
-6°C				
25°C				

57

75°C				
100°C				
150°C				
200°C				
250°C				
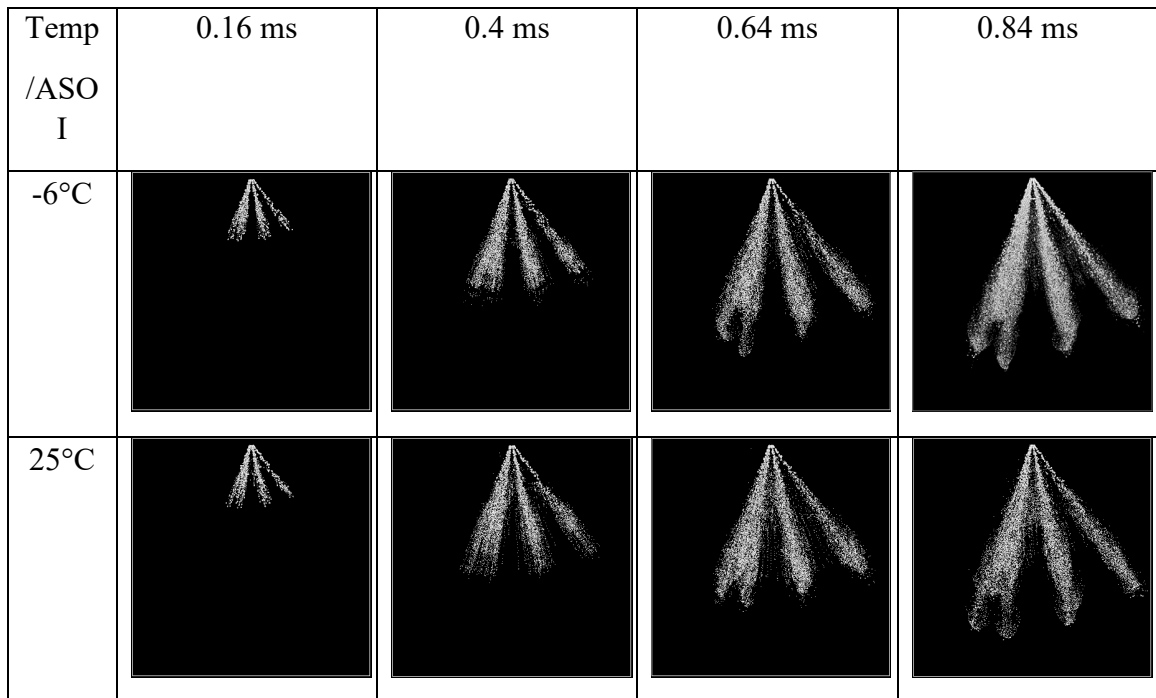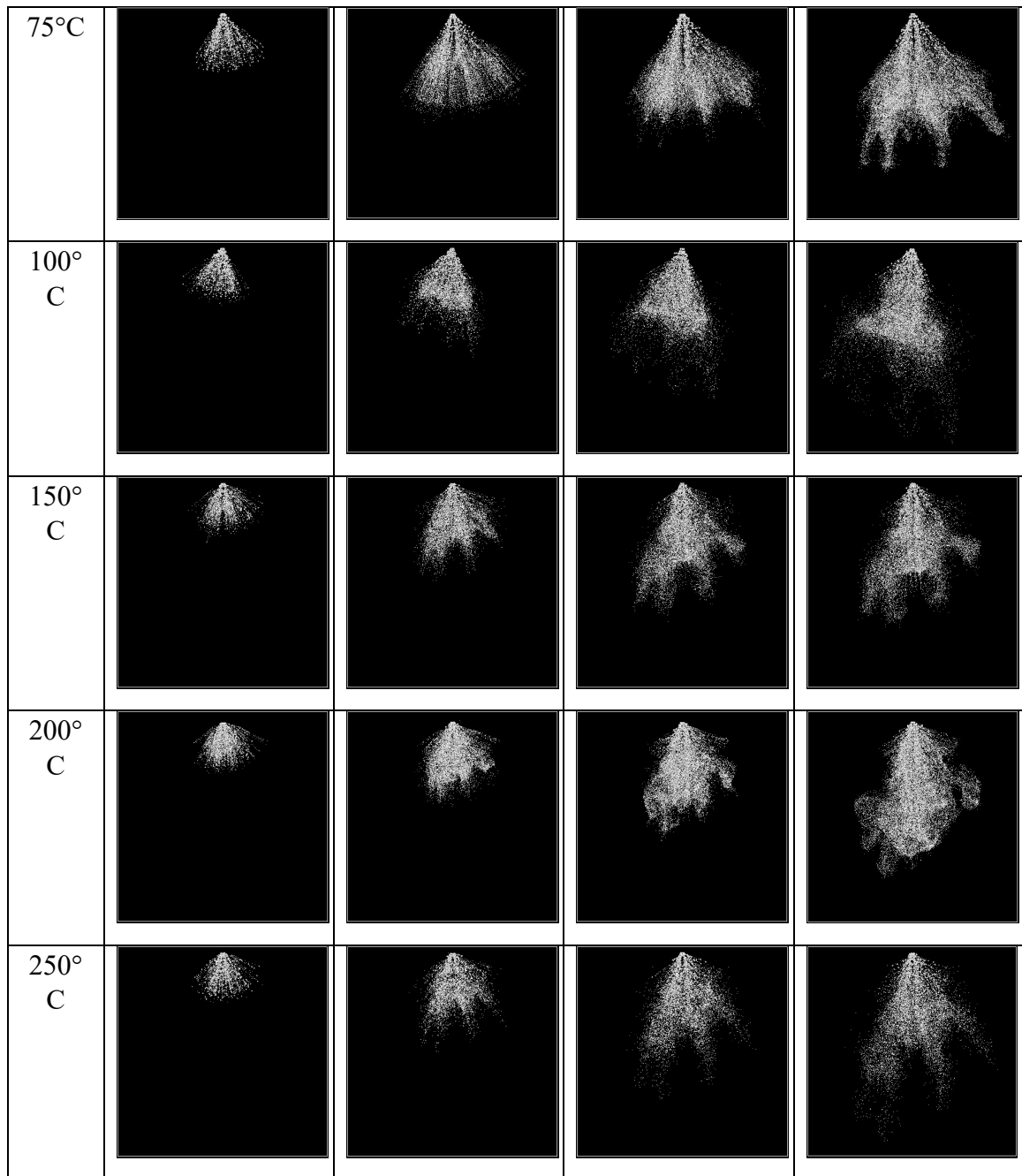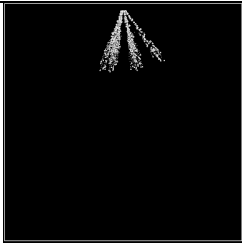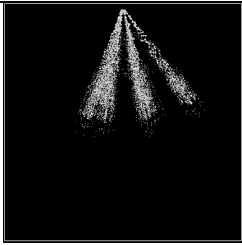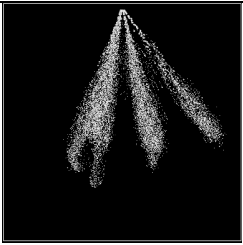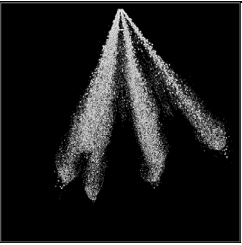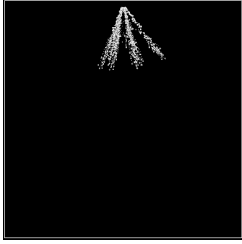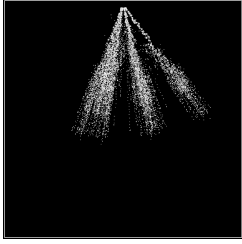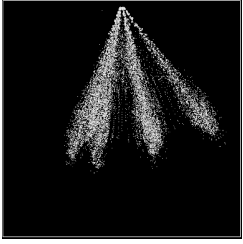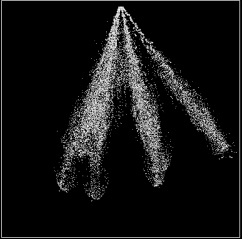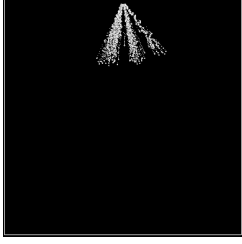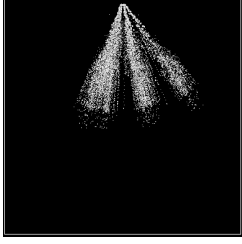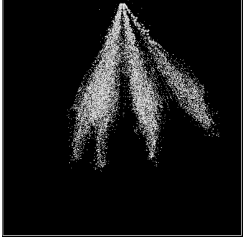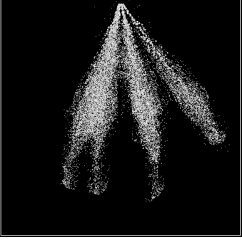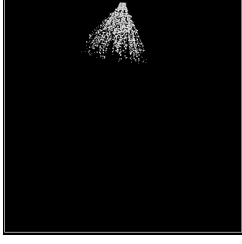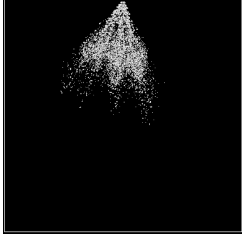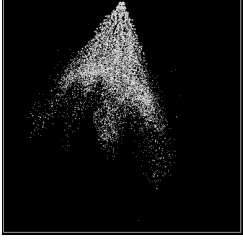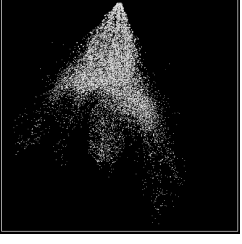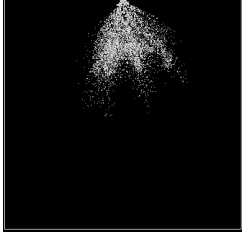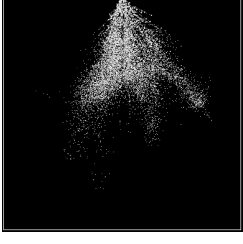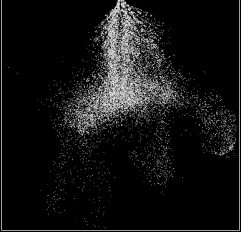
Figure 5.32 Spray Morphology for E10 fuel
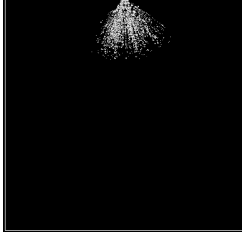
Temp /ASOI	0.16 ms	0.4 ms	0.64 ms	0.84 ms
-6°C				
25°C				
75°C				
100°C				
150°C				

Figure 5.33 Spray Morphology for E85 fuel

Figure 5.31 Figure 5.32 and Figure 5.33 shows the spray development for different start of injection time at different fuel temperature from -6°C to 250°C at chamber pressure 1 bar and chamber temperature 45°C with injection pressure at 150 bar. At 0.16 ms individual spray plumes are clearly observed for -6°C upto 150°C, however at higher temperatures there is no clear individual spray plume is observed at 0.16 ms.

Figure 5.34 Overall SMD profile E10 fuel

Figure 5.35 Overall SMD profile E85 fuel

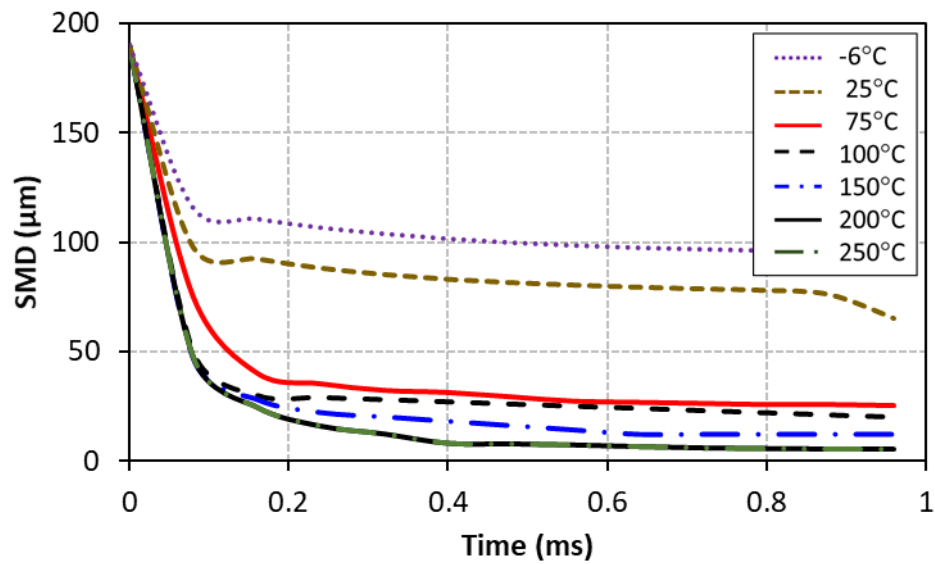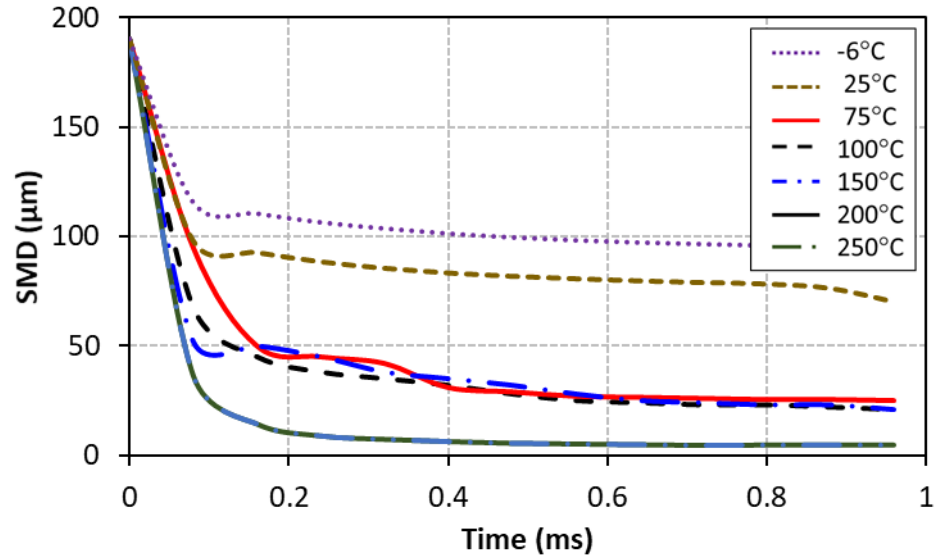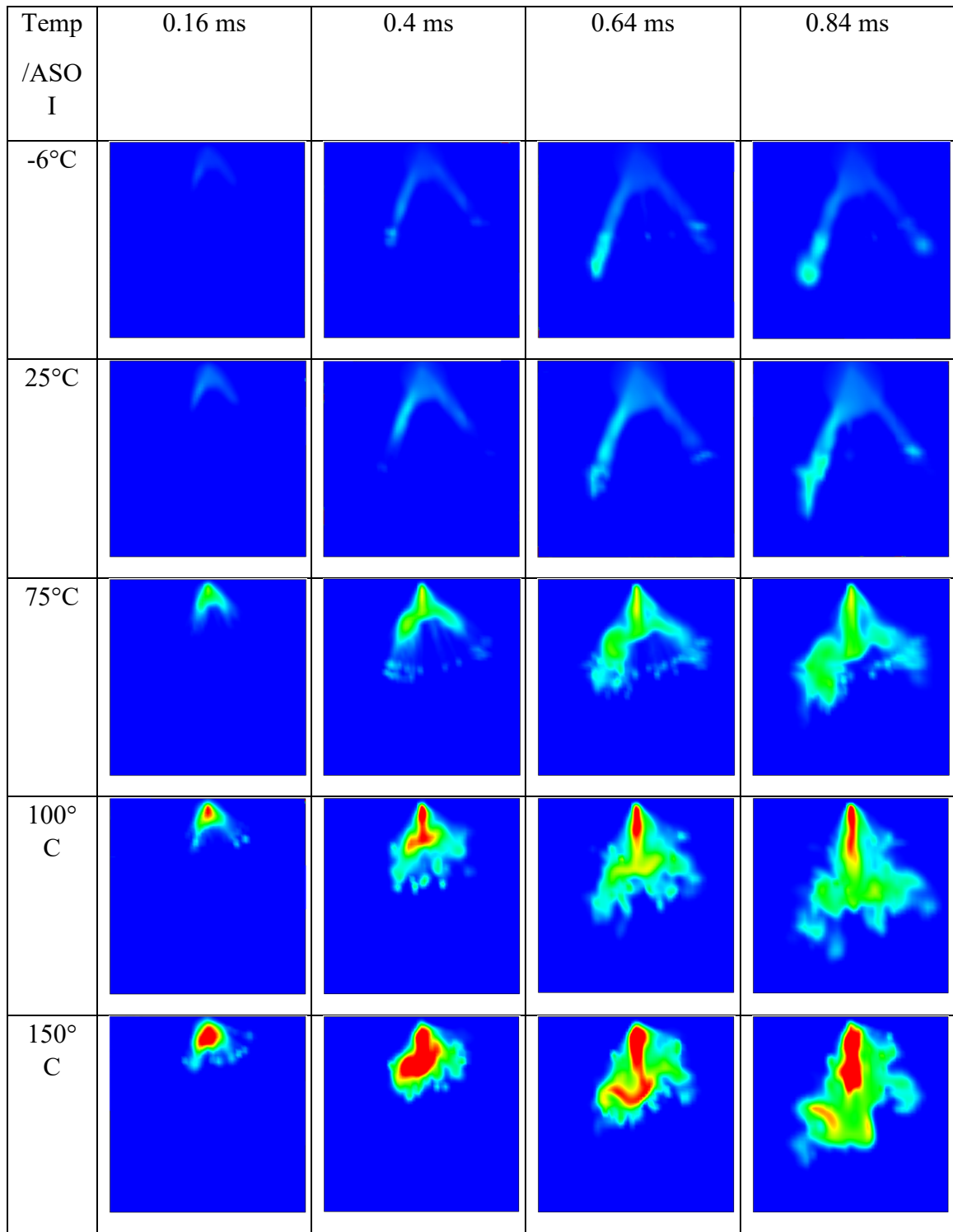At 0.4 ms the spray plume tends to collapse starting from 150°C to 250°C. At this time individual plumes are observed for temperatures less that 100°C. However, at the later stages temperature less that 75°C did not show any spray collapse as they are under non-flashing condition. However at temperatures greater than 75°C, there is clear collapsing of spray, indicating for the given injector for the mentioned operating condition, flashing occurs from 75°C for all three fuel ethanol 0%, 10% and 85%. This is because at flash boiling condition the drops explode forming tiny droplets. These droplets tends to collapse forming these structures. At 0.84 ms for 100°C, the spray tends to form a bell like structure at the tip. Upon increasing the temperature, the bell like structure tends to disappear, forming a corn like structure at the spray tip for all the fuels.

Figure 5.34 and Figure 5.35 shows the overall SMD profile for E10 and E85 fuel. The SMD profile for E0 was on top of E10 fuel and hence not shown. In the Figure 5.34 the initial drop injected into the chamber is of the effective nozzle diameter and irrespective of the temperature, the initial drop diameter is constant. The overall SMD profile decreases initially and almost becomes constant as the time increases. The overall SMD is larger for low temperature (-6°C) and decreases as temperature increases, this is due to the reduction of drop diameter due to evaporation at higher temperatures. Similar behaviour is observed for E85 fuel. For the flash boiling conditions with temperature range greater than 75°C, the overall SMD is of the order of 10-30 microns. This tiny droplets generated along with the flow field converge towards the axis of the injector, instead of travelling along the direction of the nozzle axis.

61

Temp /ASOI	0.16 ms	0.4 ms	0.64 ms	0.84 ms
-6°C				
25°C				
75°C				
100°C				
150°C				

200° C			
250° C			

fuel mass fraction

0   0.0625   0.125   0.1875   0.25
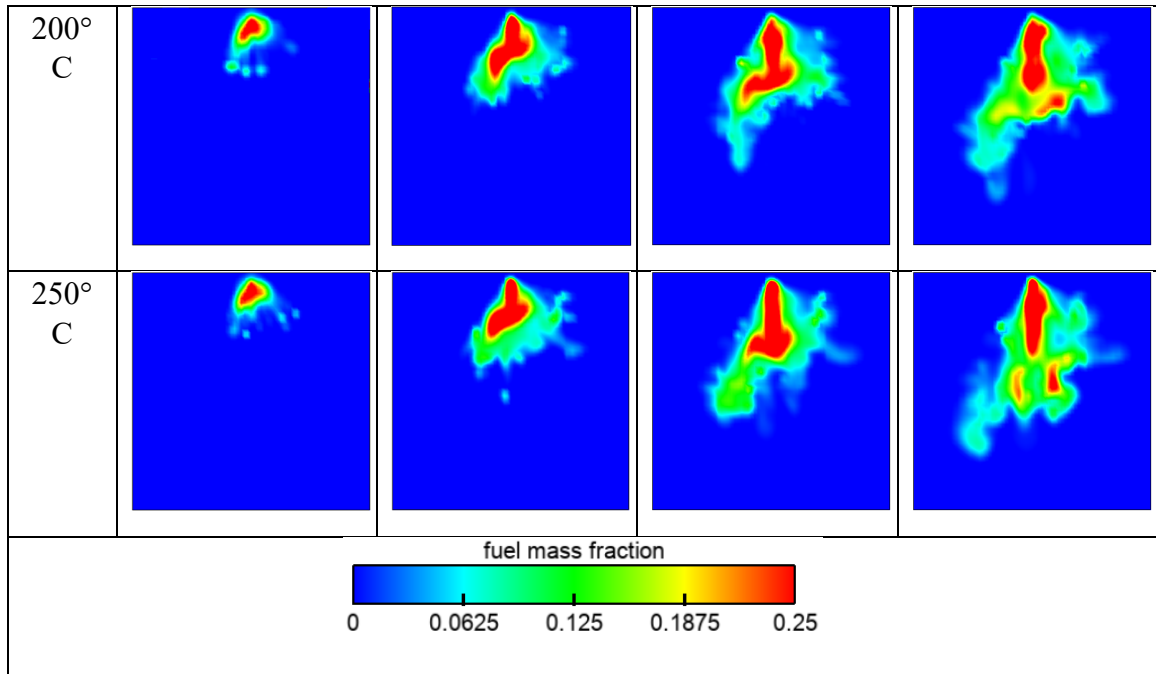
Figure 5.36 Fuel Vaporization Contour E0 fuel

Temp /ASOI	0.16 ms	0.4 ms	0.64 ms	0.84 ms
-6°C				
25°C				
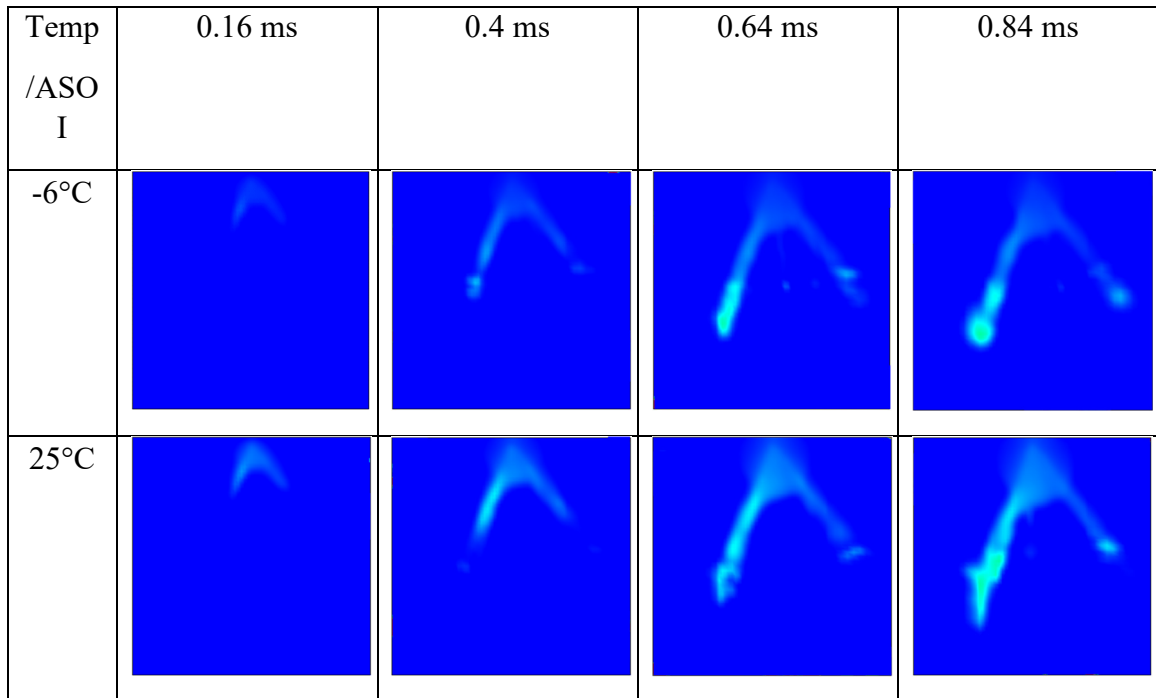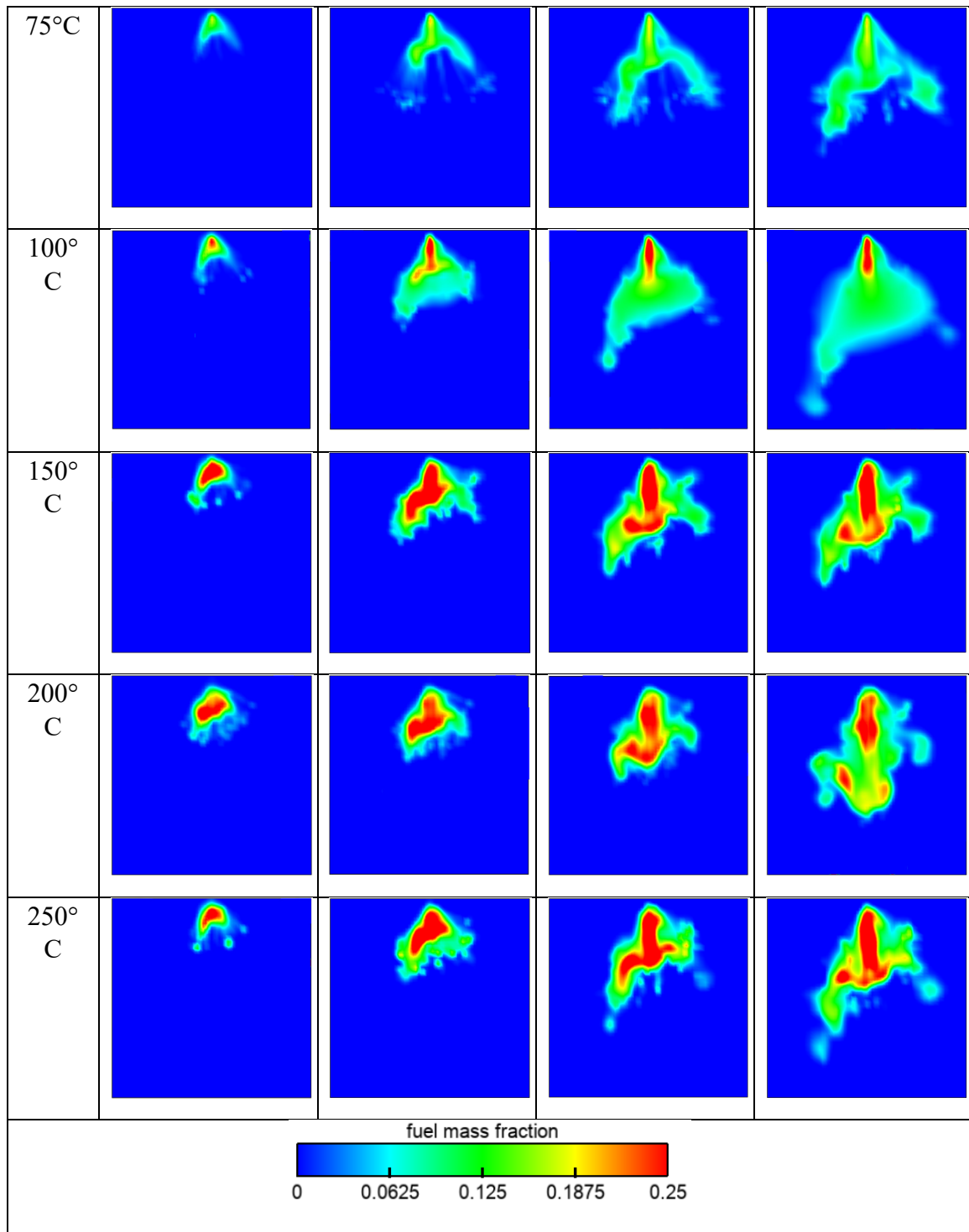
Figure 5.37 Fuel Vaporization Contour E10 fuel

Temp /ASOI	0.16 ms	0.4 ms	0.64 ms	0.84 ms
-6°C				
25°C				
75°C				
100°C				
150°C				

65
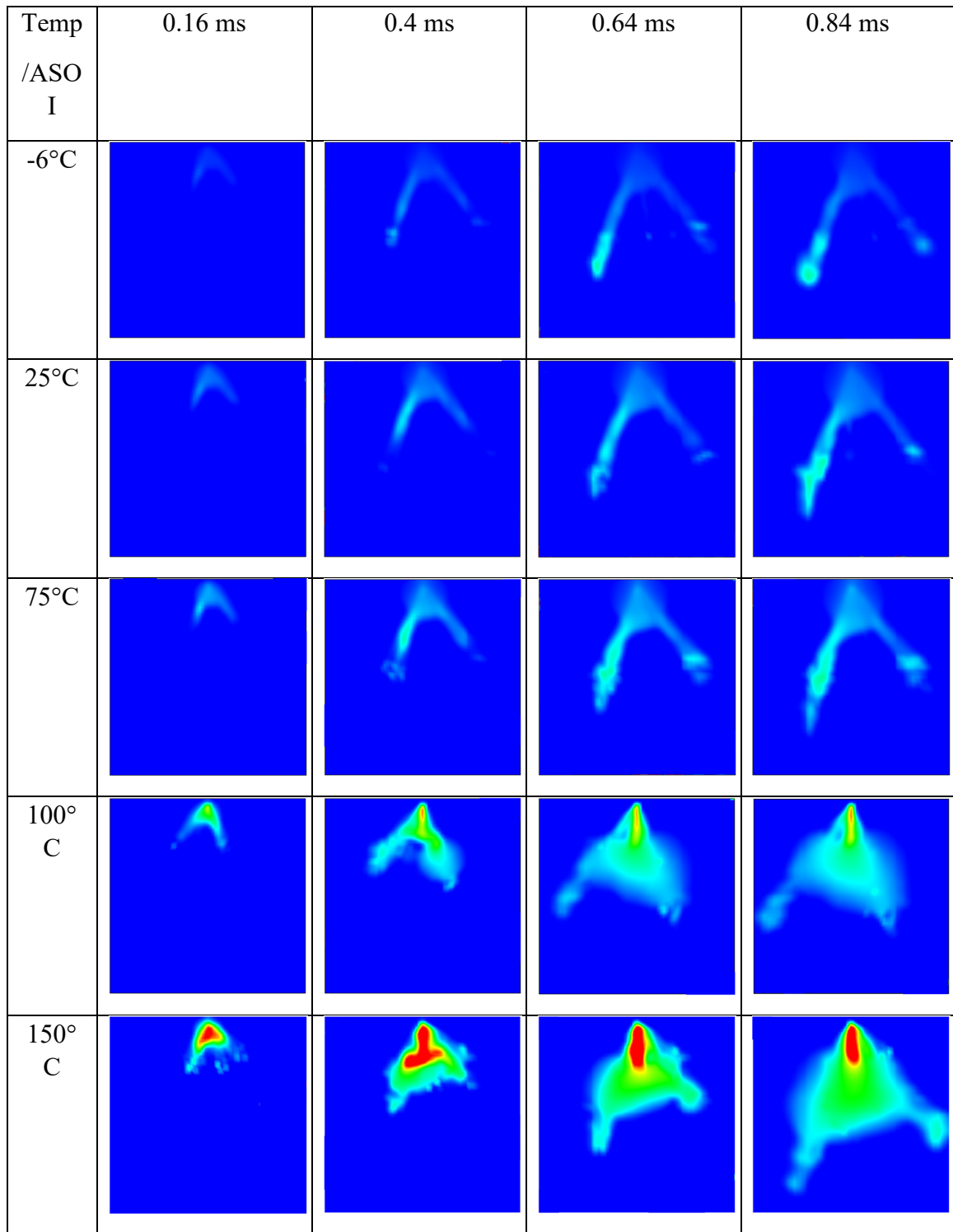
Figure 5.38 Fuel Vaporization Contour E85 fuel
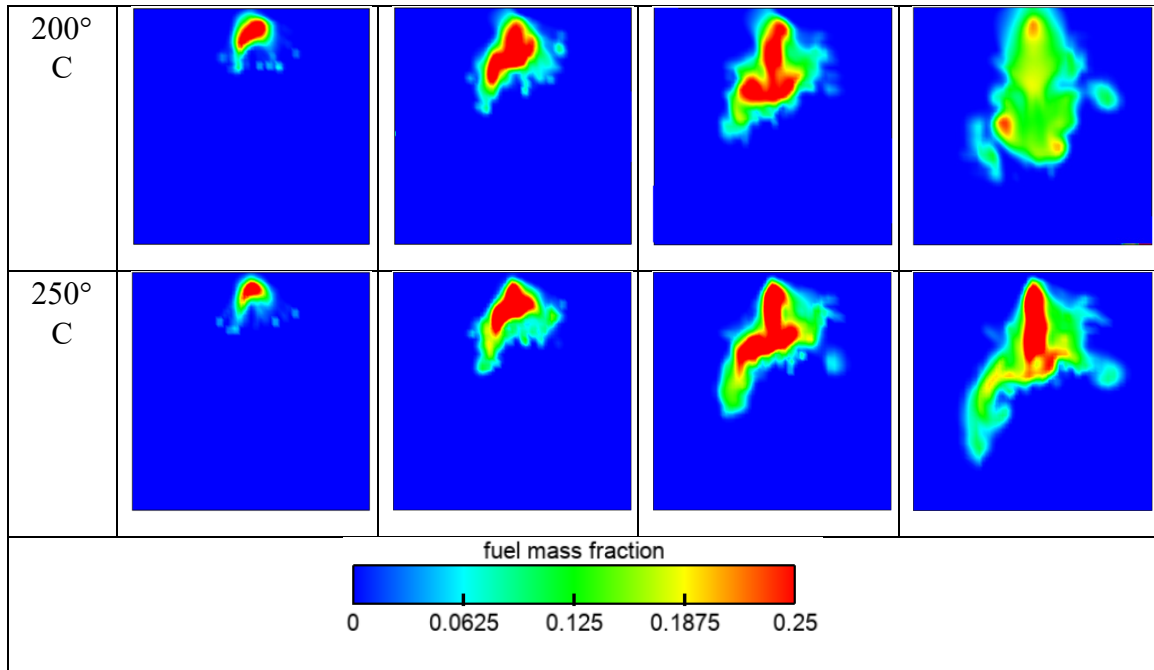
When a heated fuel is injected into an environment at lower pressures than that corresponding to its saturation pressure flash boiling occurs. During this process, the plumes interact and form a region of dense spray clouds trapping the fuel vapor within the region included by the spray plumes. Thus, fuel vapor distributions are substantially altered by the temperature of the injected fuel. Figure 5.36 Figure 5.37 and Figure 5.38 shows the fuel vaporization contours at different start of injection time for different fuel temperature

from -6°C to 250°C at chamber pressure 1 bar and chamber temperature 45°C with injection pressure at 150 bar. The contour plane is at Y=0 location (XZ-plane).
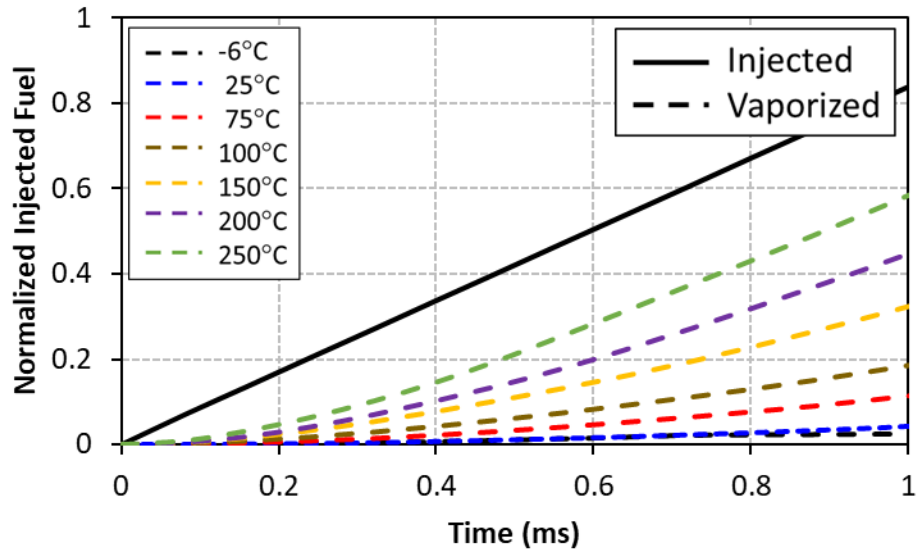

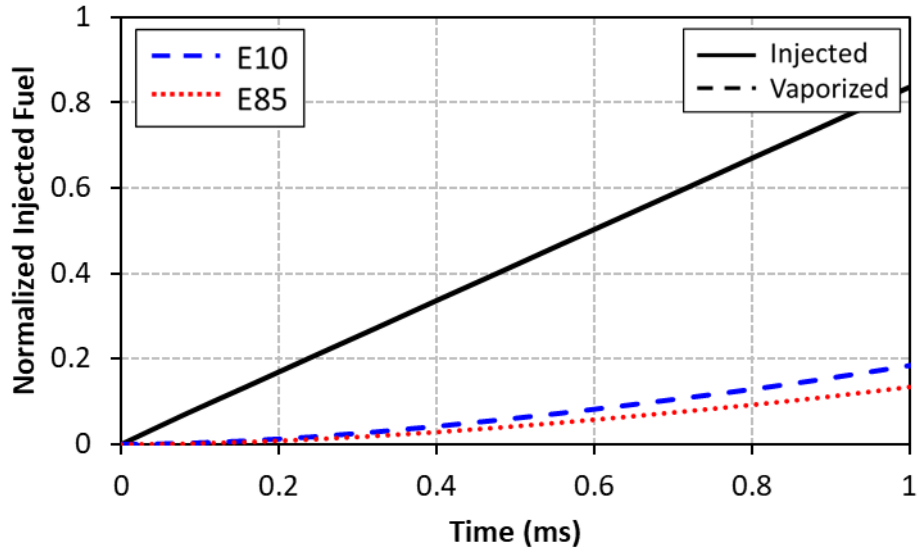Figure 5.39 Injected Fuel vs Vaporized Fuel E10 Fuel

Figure 5.40 Normalized fuel vaporization profile E10 and E85 at 100°C
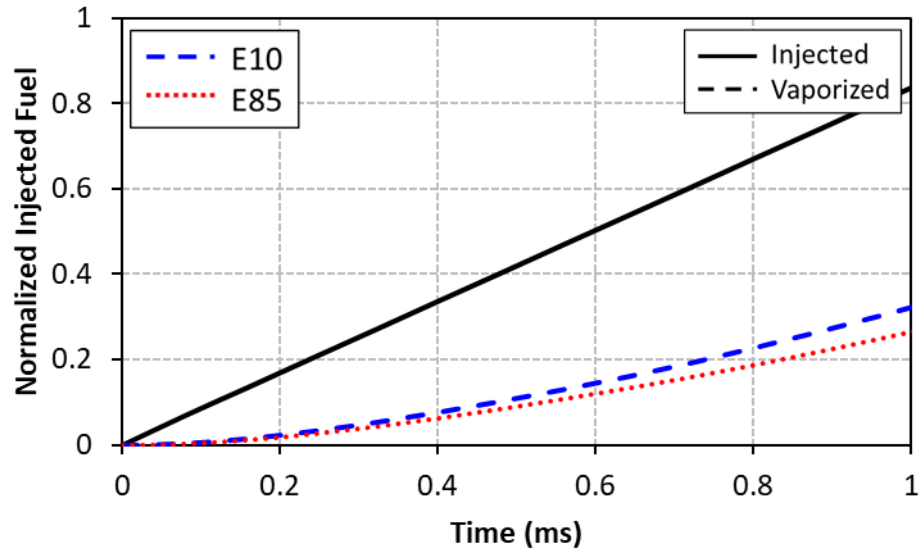
67

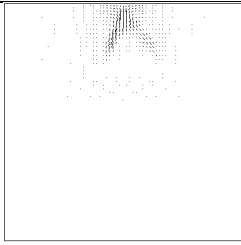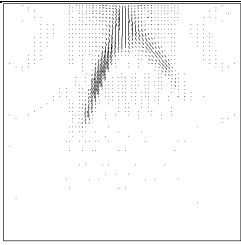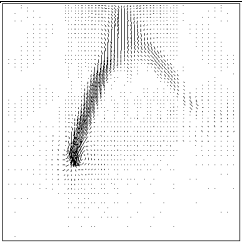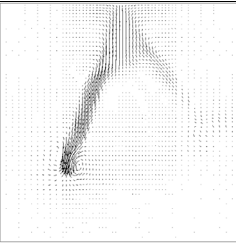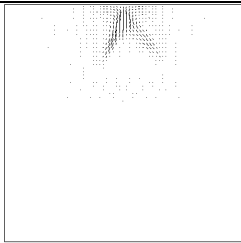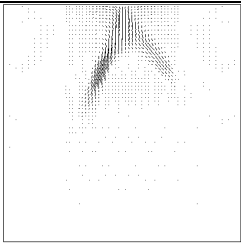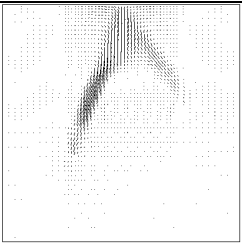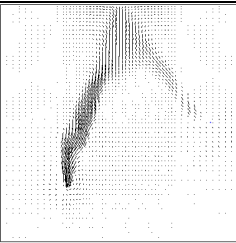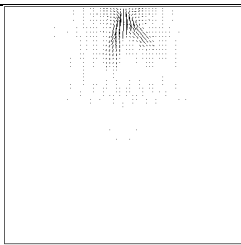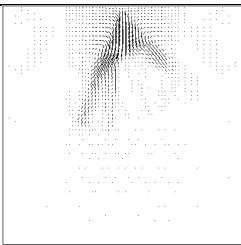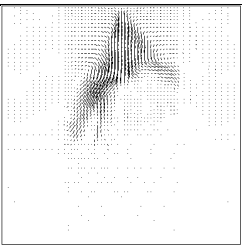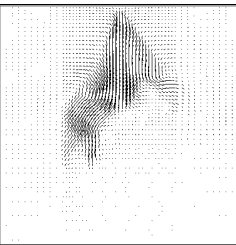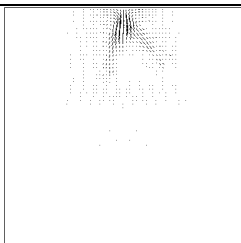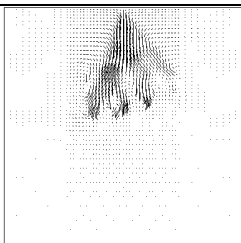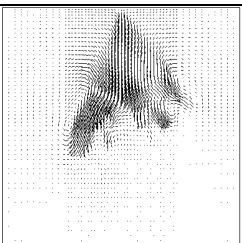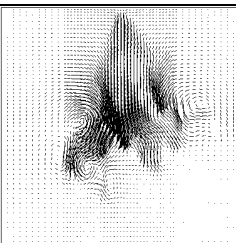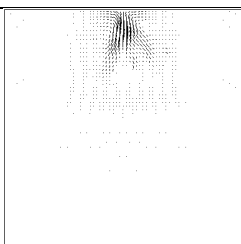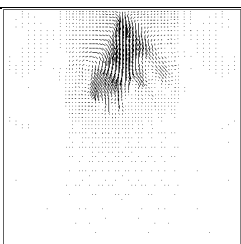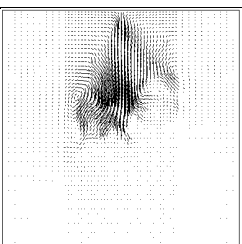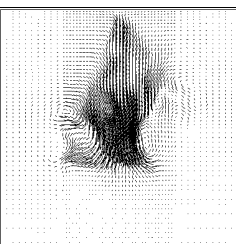Figure 5.41 Normalized fuel vaporization profile E10 and E85 at 150°C

At 0.16 ms ASOI the fuel vapor concentration reaches the highest for 250°C and the least for -6°C. This is because the evaporation at the early stage of spray is mainly governed by the fuel injection temperature. Figure 5.39 shows the vaporization rate profile for E10 fuel for different fuel temperatures. Figure 5.39 vaporization is low for -6°C and higher for 250°C. The vaporization rate increases as a function of temperature. Similar trend is observed for E0 and E85 fuel. Figure 5.40 and Figure 5.41 shows the vaporization behaviour between E10 and E85 fuel at 100°C and 150°C, irrespective of the temperature similar behaviour is observed between E10 and E85 fuel. In Figure 5.36, as the spray develops, it is clearly seen that the fuel vapor is redirected into the direction of the injector axis with increasing injection fuel temperature. Fuel-rich regions are seen in the center core regions in the flash-boiling cases (75 and 250°C). The extension of these rich regions into the injector axis direction is consistent with the increased penetration of spray droplets and reduced divergence angle of the spray plumes, as shown above (see Figure 5.36 Figure 5.37 and Figure 5.38). On the contrary, fuel vapor distributions governed by the separate spray plumes are seen for the -6°C and 25°C cases.

www.manaraa.com

Temp /ASOI	0.16 ms	0.4 ms	0.64 ms	0.84 ms
-6°C				
25°C				
75°C				
100°C				
150°C				

200°C			
250°C			

Figure 5.42 Air Entrainment characteristics E0 fuel

Temp /ASOI	0.16 ms	0.4 ms	0.64 ms	0.84 ms
-6°C				
25°C				
75°C				
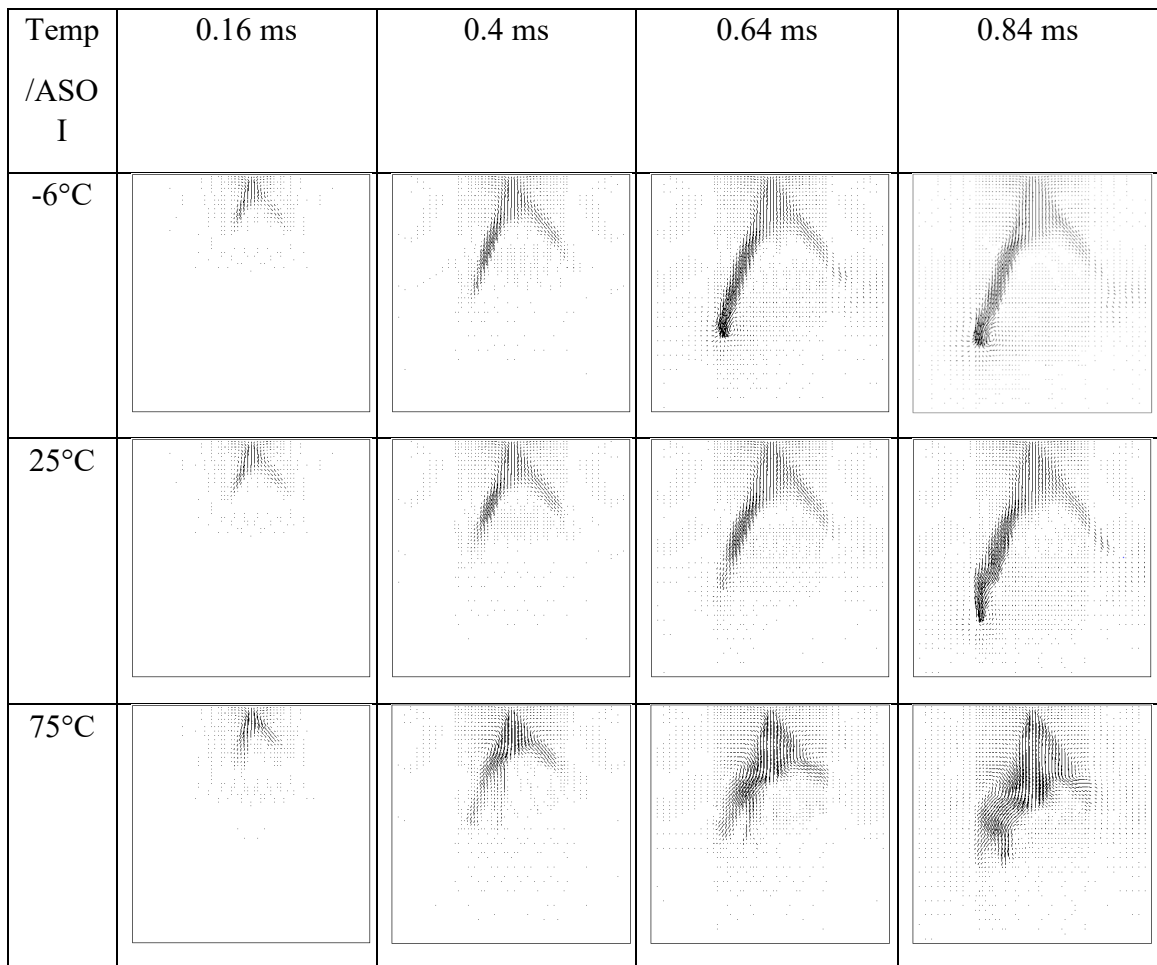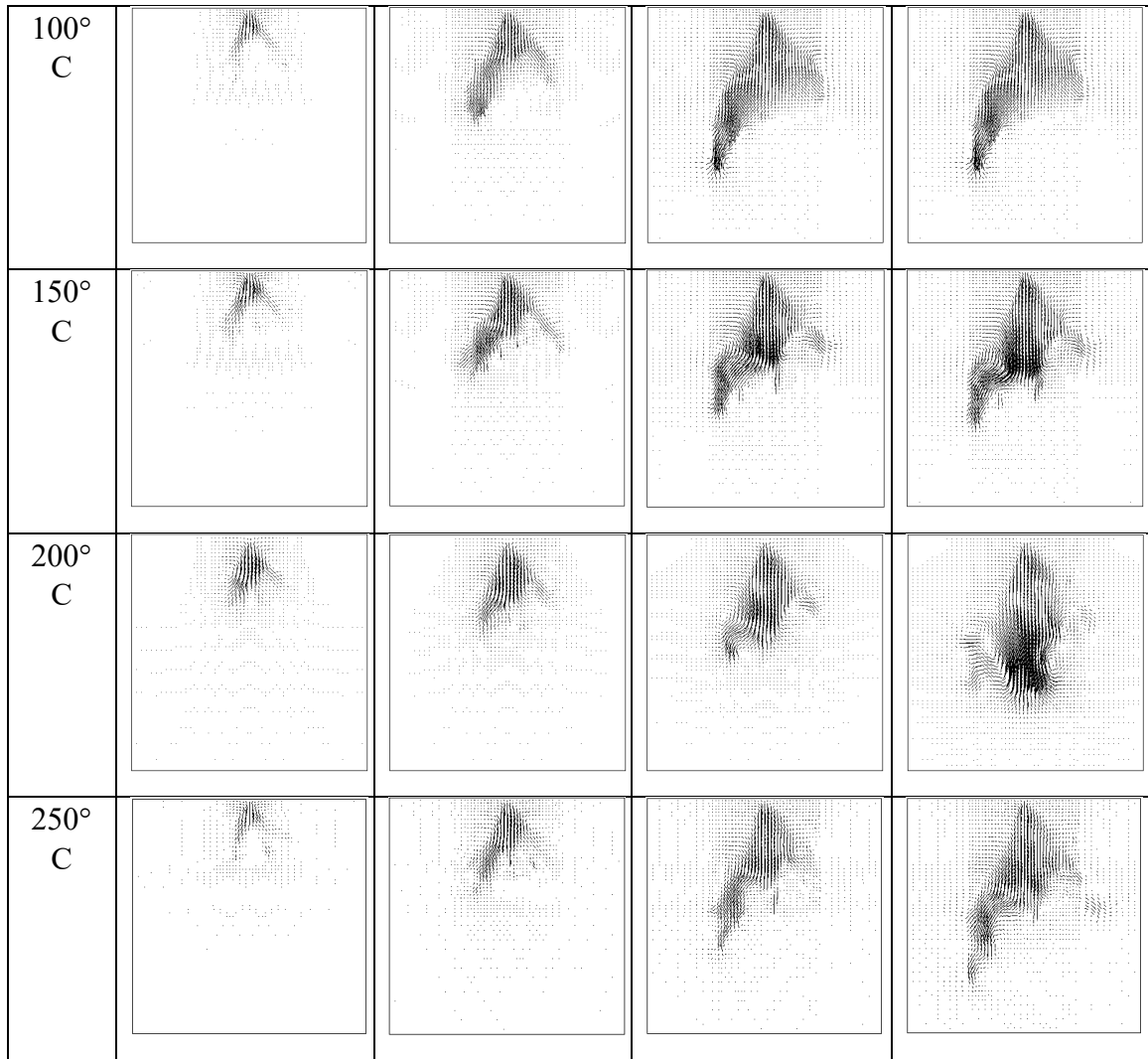
100° C			
150° C			
200° C			
250° C			

Figure 5.43 Air Entrainment characteristics E10 fuel

71

Temp /ASOI	0.16 ms	0.4 ms	0.64 ms	0.84 ms
-6°C				
25°C				
75°C				
100°C				
150°C				

200° C				
250° C				
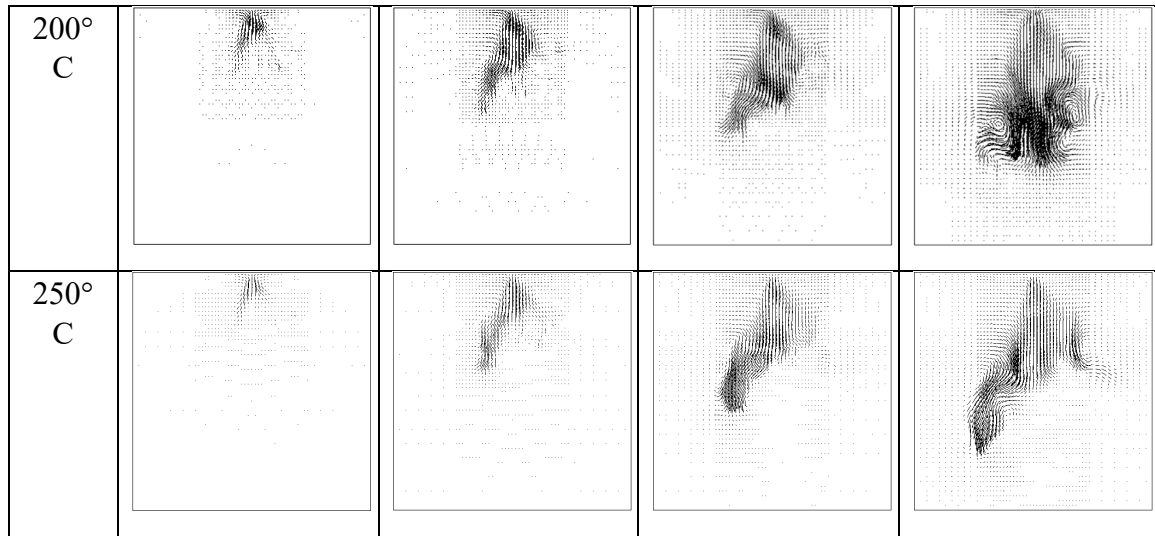
Figure 5.44 Air Entrainment characteristics E85 fuel

Figure 5.42 Figure 5.43 and Figure 5.44 shows the air entrainment behaviour at different ASOI for different fuel temperature between -6°C and 250°C at chamber pressure 1 bar and chamber temperature 45°C with injection pressure at 150 bar. The vector arrows are plotted at Y=0 plane (XZ-plane). For low temperature, -6°C and 25°C cases as the spray enters the chamber, air is dragged in from the bottom and as well as the sides of the spray, thus helping the spray to develop in the direction of the injection. However, for the flashing condition at temperatures greater than 75°C, as seen in Vapor contour figures, thick regions of vapor is formed in the center region of the spray and hence air cannot enter from the bottom of the spray and hence air is dragged in from the sides thus helping the spray to elongate axially. This is clearly seen in Figure 5.31. Hence ambient air is entrained from both outer and inclusion regions of the spray for low fuel temperatures while air is entrained from the outer region only when fuel temperatures are in the flash boiling range.

5.4.4. Effect of Fuel Temperature
5.4.4.1   E10

Figure 5.45 describes the effect of temperature on spray penetration for E10 fuel. Figure 5.45 (a) shows the experimentally measured profile while the Figure 5.45 (b) indicates the simulated profile. It can be seen that in experimental result two different trends in penetration is observed. In the initial part of the spray the from lower to higher is seen to be from -6°C, 25°C, 75°C, 100°C, 150°C, 200°C and 250°C and in the later part of the spray the trend is seen to be from increasing to decreasing order of 250°C, 200°C, 75°C, 25°C, -6°C, 150°C and 100°C. This is because the initial part of the spray is governed by the injection velocity. As temperature increases density decreases to conserve mass the initial injected velocity is higher for high temperature case. In the later part of the spray at higher temperature spray collapsing behaviour is observed which increases the spray penetration at elevated temperatures. However minimum penetration is observed for

73

100°C. The simulated results shows the similar trend in the initial stage of the spray development as that of experiments, however in the later stage of the spray penetration is over-predicted compared to experiments.
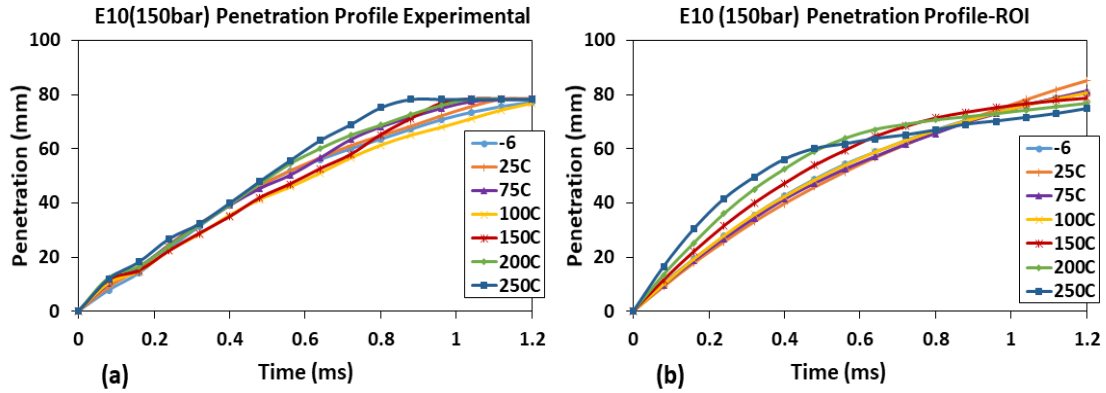
Figure 5.45 Effect of Temperature on Spray Penetration at P_{inj} = 150 bar (a) Experimental (b) ROI
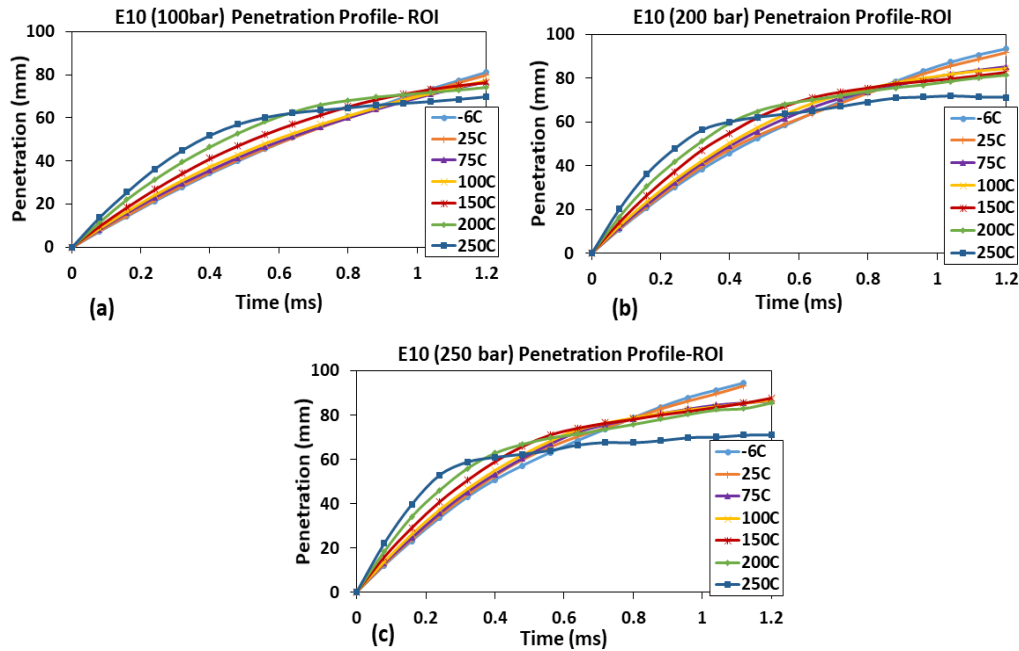
Figure 5.46 Effect of Temperature on Spray Penetration at P_{inj} = (a) 100, (b) 200, (c) 250bar

Figure 5.46 shows the effect of temperature on Spray penetration at different injection pressures. The trend for the other injection pressure cases remains the same as that of the 150-bar injection pressure case.
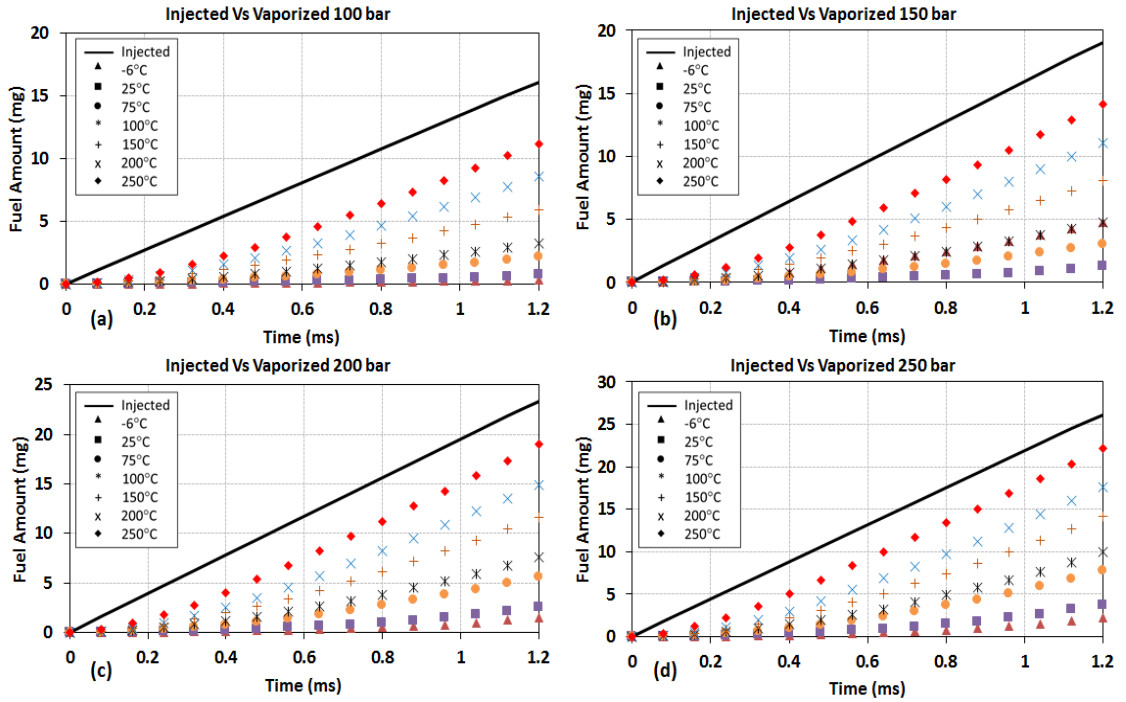
Figure 5.47 Injected fuel vs Vaporized fuel-E10 fuel

Figure 5.47 represents the injected fuel versus vaporised fuel profile for E10 fuel at different pressures. The vaporization rate is higher for 250°C case and it reduces with decrease in pressure. The trend is similar for all pressures.

5.4.4.2   E85
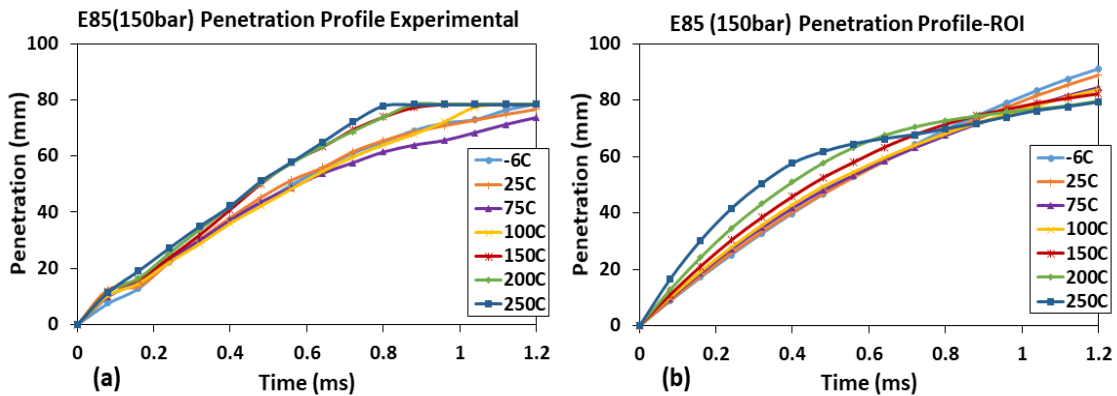
Figure 5.48 Effect of Temperature on Spray Penetration at P_{inj} = 150 bar (a) Experimental (b) ROI

Figure 5.48 describes the effect of temperature on spray penetration for E85 fuel. The image on the left hand side shows the simulated profile while the right indicates the experimentally measured profile. It can be seen that in experimental result two different trends in penetration is observed. As discussed for E10 fuel the minimum penetration profile is observed at 75°C while simulation shows 250°C as minimum profile at the end of injection.
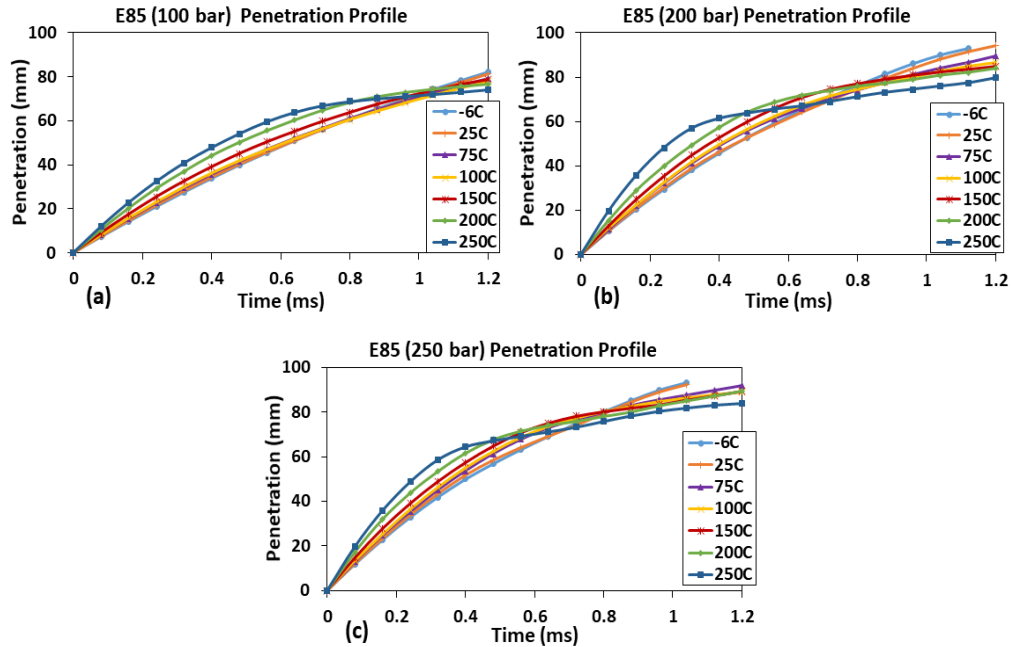
Figure 5.49 Effect of Temperature on Spray Penetration at P$_{inj}$ = (a) 100, (b) 200, (c) 250 bar

Figure 5.49 shows the effect of temperature on Spray penetration at different injection pressures (100, 200 and 250 bar). The trend for the other injection pressure cases remains the same as that of the 150 bar injection pressure case.
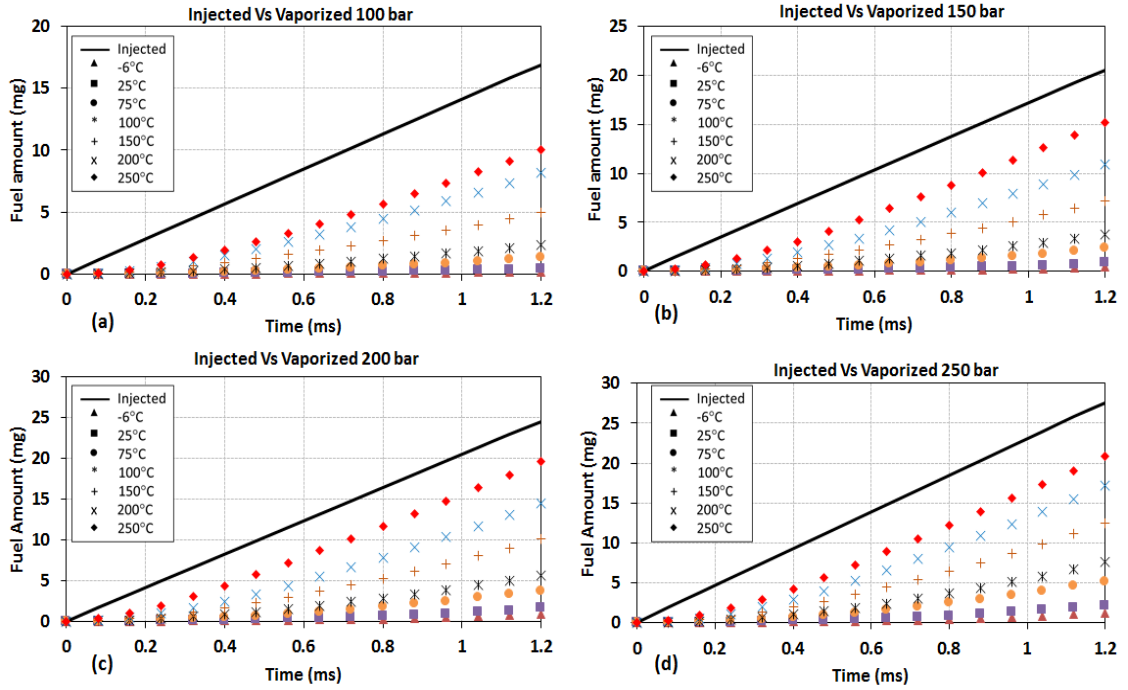
Figure 5.50 Injected fuel vs Vaporized fuel-E85 fuel

Figure 5.50 represents the injected fuel versus vaporised fuel profile for E10 fuel at different pressures. The vaporization rate is higher for 250°C case and it reduces with decrease in pressure. -6°C case has the lowest fuel vapor formed at chamber pressure 1 bar and 45°C. The trend is similar for all pressures.

5.4.5. Effect of Injection Pressure
5.4.5.1   E10
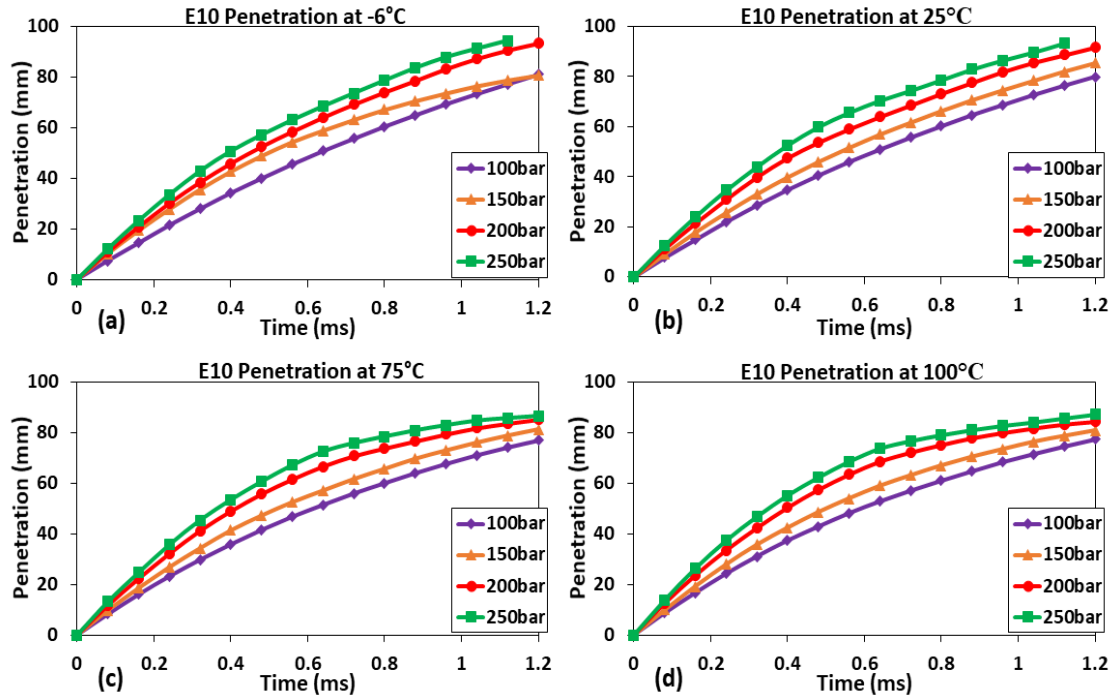
Figure 5.51 Effect of Pressure on Spray Penetration at (a) -6ºC, (b) 25°C (c) 75ºC (d) 100°C
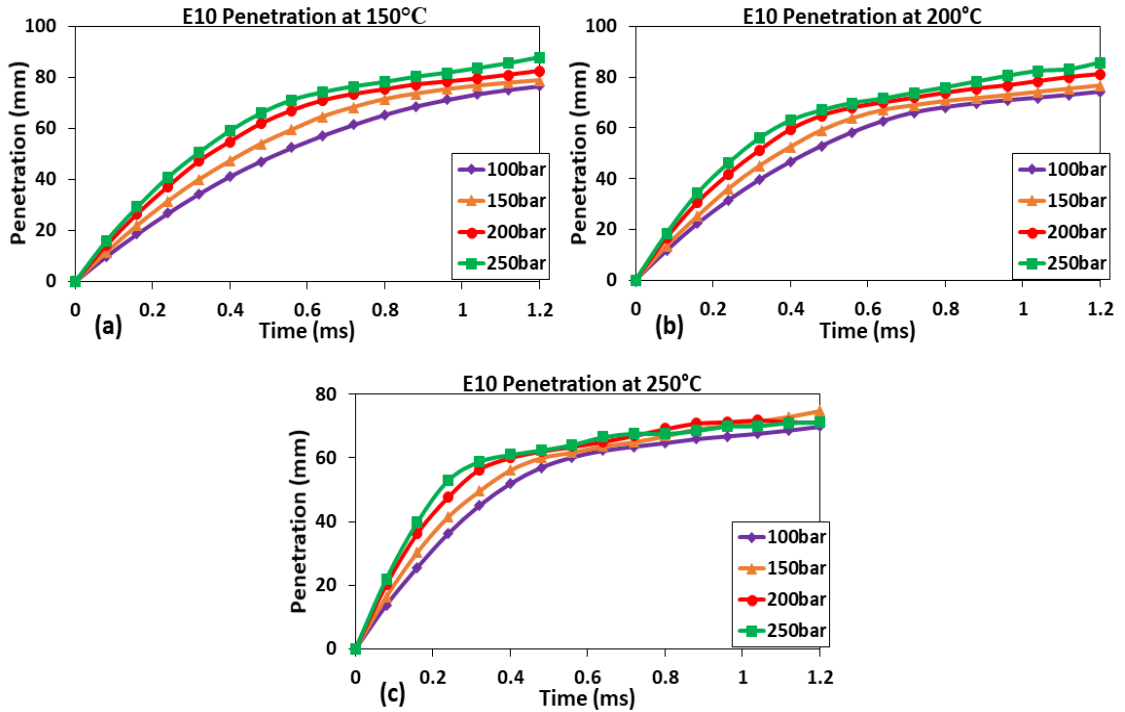
Figure 5.52 Effect of Pressure on Spray Penetration at (a) 150°C, (b) 200ºC, (c) 250ºC

Figure 5.51 and Figure 5.52 shows the effect of Injection Pressure on spray penetration. For this case the injection duration and other input parameters like spray angle, rate shape was kept constant however the injected amount is varied for achieve different injection pressure. With the higher injection pressure penetration observed is higher this is because higher injection pressure results in higher outlet velocity and higher spray momentum at the nozzle exit. Same trend was observed for other fuel temperatures at different injection pressures however at 250°C higher injection pressure produced lower penetration. The vaporization profile in Figure 5.50 shows higher evaporation at 250°C. At this temperature, the evaporation predicted by the droplet is higher as the overall SMD is smaller of the order of 10-15 micron. Thus the drop lifetime is short and hence, the liquid does not penetrate as seen in the experiments.

5.4.5.2   E85
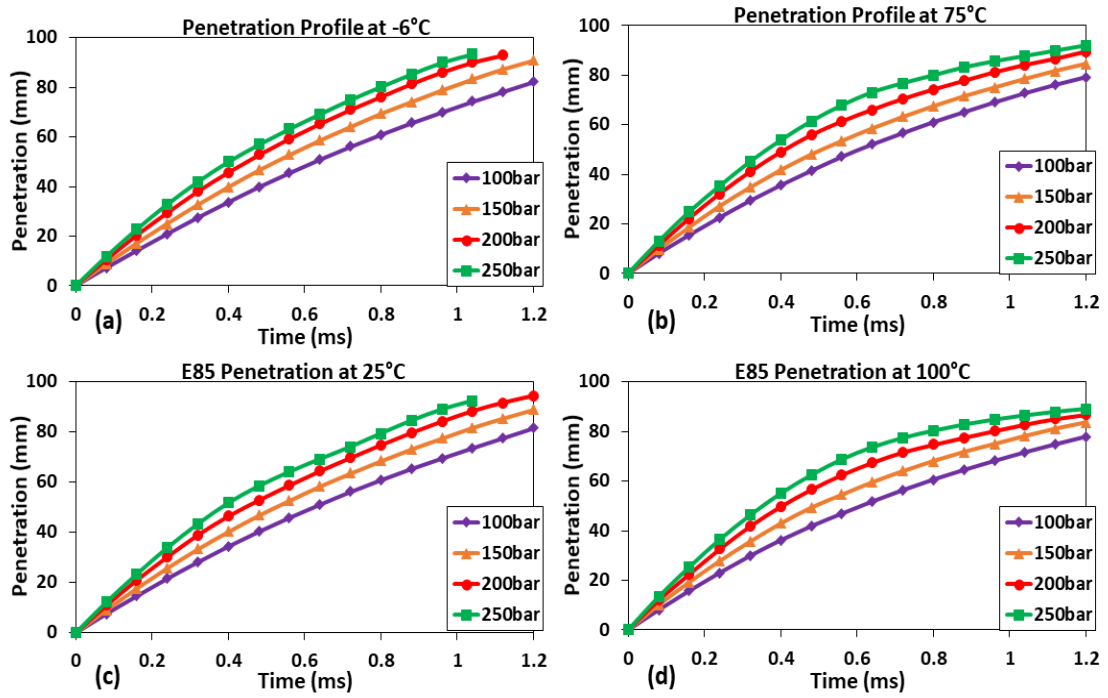
Figure 5.53 Effect of Pressure on Spray Penetration at (a) -6ºC, (b) 25°C (c) 75ºC (d) 100°C

Figure 5.53 and Figure 5.54 shows the effect of Injection Pressure on spray penetration. It shows the same trend observed for E10 fuel. Increasing injection pressure increases the spray penetration.
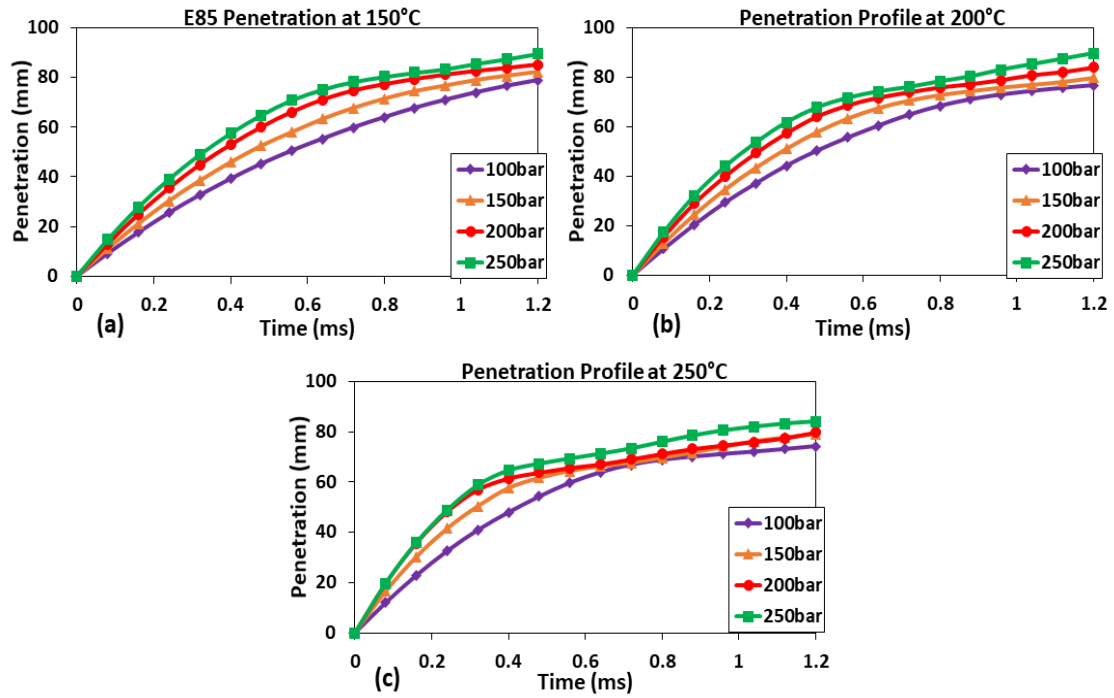
Figure 5.54 Effect of Pressure on Spray Penetration at (a) 150°C, (b) 200°C, (c) 250°C

6. Conclusion

The gasoline fuels blended with ethanol were modelled with 14-component surrogate models. The modelled physical properties and distillation behaviour were in good agreement with measurements.

The performance of the Heater-GDI injector and Spray studies in a Constant Volume Combustion Chamber has been successfully in investigated for different operating pressures and temperatures. The heater coupled with GDI injector increases the fuel temperature at the nozzle exit. This improves the spray vaporization during the cold start conditions. The nozzle exit conditions were used as input for the spray studies to improve the initial and boundary conditions.

Two kinds of spray initialization methodologies were utilized. Method 1 based on the uniform distribution of injection velocity and temperature among the fuel injection nozzle location. Method 2 considers the effect of nozzle to nozzle variation of the modelled fuel injector. The spray characteristics of gasoline blend with ethanol 10% and 85% were predicted and compared with the experimental data for the same operating conditions ranging from non-boiling conditions to flash boiling conditions. The model predicts the collapsing behaviour of the sprays subjected to superheating. However, the liquid penetration of the spray is under predicted for the high temperature flash boiling condition 250°C. This is due to the model over predicting the atomization, which leads to the generation of smaller droplets that vaporizes quickly leading to under prediction of liquid penetration. At flash boiling conditions, the individual spray plumes converge to form a single plume towards the axis of the injection and trapping the evaporated fuel in the center core region. This leads to poor mixture formation in the chamber. Though, flash boiling helps in rapid vaporization however, for this specific injector design, it forms poor mixture. Under controlled conditions better spray characteristics and mixture formation could be achieved with flash boiling operations.

7. Future Work

The Heater-GDI injector simulation was performed with two domains to determine the fuel exit temperature and velocity. Future work will consider the single full domain. The heater is operated at a higher temperature which is beyond the boiling point of the fuel used and phase change could be observed in the near nozzle region which could provide the insight on the cavitation phenomenon, however the current simulation considered only liquid phase for the injector simulation. Besides the dynamic pintle action was not considered. Future work will include the effect of needle motion which could provide the accurate rate shape for spray studies. The future work will also include the performance of this injector in on-board engine to understand the emission formation for cold start conditions.

8. References

[1] Malaguti, Simone, Giuseppe Bagli, Alessandro Montanaro, Stefano Piccinini, and Luigi Allocca. "Experimental and Numerical Characterization of Gasoline-Ethanol Blends from a GDI Multi-Hole Injector by Means of Multi-Component Approach." *SAE Technical Paper Series*, 2013. doi:10.4271/2013-24-0002.

[2] Bao, Yongming, Qing Nian Chan, Sanghoon Kook, and Evatt Hawkes. "A Comparative Analysis on the Spray Penetration of Ethanol, Gasoline and Iso-Octane Fuel in a Spark-Ignition Direct-Injection Engine." *SAE Technical Paper Series*, 2014. doi:10.4271/2014-01-1413.

[3] Tang, Meng, Jiongxun Zhang, Xiucheng Zhu, Kyle Yeakle, Henry Schmidt, Seong-Young Lee, Jeffrey Naber, and Cody Squibb. "Comparison of Direct-Injection Spray Development of E10 Gasoline to a Single and Multi-Component E10 Gasoline Surrogate." *SAE International Journal of Fuels and Lubricants*10, no. 2 (2017). doi:10.4271/2017-01-0833.

[4] Kabasin, Daniel Francis, Youssef Joseph, William Fedor, Scott Geiger, and Tobias Hurter. "Emission Reduction with Heated Injectors." *SAE International Journal of Engines*3, no. 1 (2010): 982-95. doi:10.4271/2010-01-1265.

[5] Li, Hu, Gordon E. Andrews, Grant Zhu, Basil Daham, Margaret Bell, James Tate, and Karl Ropkins. "Impact of Ambient Temperatures on Exhaust Thermal Characteristics during Cold Start for Real World SI Car Urban Driving Tests." *SAE Technical Paper Series*, 2005. doi:10.4271/2005-01-3896.

[6] Ku, Jason, Yiqun Huang, Brian Hollowell, Stephen Belle, Ronald D. Matthews, and Matt Hall. "Conversion of a 1999 Silverado to Dedicated E85 with Emphasis on Cold Start and Cold Driveability." *SAE Technical Paper Series*, 2000. doi:10.4271/2000-01-0590.

[7] Xu, Zheng, Jianwen Yi, Steven Wooldridge, David Reiche, Eric W. Curtis, and George Papaioannou. "Modeling the Cold Start of the Ford 3.5L V6 EcoBoost Engine." *SAE International Journal of Engines*2, no. 1 (2009): 1367-387. doi:10.4271/2009-01-1493.

[8] Das, Sudhakar, Shi-Ing Chang, and John Kirwan. "Spray Pattern Recognition for Multi-Hole Gasoline Direct Injectors Using CFD Modeling." *SAE Technical Paper Series*, 2009. doi:10.4271/2009-01-1488.

[9] Befrui, Bizhan, Giovanni Corbinelli, Mario Donofrio, and Daniel Varble. "GDI Multi-Hole Injector Internal Flow and Spray Analysis." *SAE Technical Paper Series*, 2011. doi:10.4271/2011-01-1211.

[10] Malaguti, Simone, Stefano Fontanesi, and Elena Severi. "Numerical Analysis of GDI Engine Cold-Start at Low Ambient Temperatures." *SAE Technical Paper Series*, 2010. doi:10.4271/2010-01-2123.

[11] Jiao, Qi, Youngchul Ra, and Rolf D. Reitz. "Modeling the Influence of Molecular Interactions on the Vaporization of Multi-component Fuel Sprays." *SAE Technical Paper Series*, 2011. doi:10.4271/2011-01-0387.

[12] Badshah, Huzeifa, David Kittelson, and William Northrop. "Particle Emissions from Light-Duty Vehicles during Cold-Cold Start." *SAE International Journal of Engines*9, no. 3 (2016). doi:10.4271/2016-01-0997.

[13] Epa, "EPA and NHTSA Set Standards to Reduce Greenhouse Gases and Improve Fuel Economy for Model Years 2017-2025 Cars and Light Trucks," 2012.

[14] California Air Resources Board, "Advanced Clean Cars Summary," 2012.

[15] Grünefeld, Gerd, Michael Knapp, Volker Beushausen, and Peter Andresen. "Direct Air Injection for Substantial Improvement of SI Engine Cold Start Performance." *SAE Technical Paper Series*, 1997. doi:10.4271/971069.

[16] Using On-board Fuel Reforming by Partial Oxidation to Improve SI Engine Cold-Start Performance and Emissions Kristine Drobot Isherwood, Jan-Roger Linna and Peter J. Loftus Arthur D. Little, Inc.

[17] Pihl, Josh, John Thomas, Sreshtha Sinha Majumdar, Shean Huff, Brian West, and Todd Toops. "Development of a Cold Start Fuel Penalty Metric for Evaluating the Impact of Fuel Composition Changes on SI Engine Emissions Control." *SAE Technical Paper Series*, 2018. doi:10.4271/2018-01-1264.

[18] Kabasin, Daniel, Kevin Hoyer, Joseph Kazour, Rudolf Lamers, and Tobias Hurter. "Heated Injectors for Ethanol Cold Starts." *SAE International Journal of Fuels and Lubricants*2, no. 1 (2009): 172-79. doi:10.4271/2009-01-0615.

[19] Sales, Luis Carlos, Matheus Guilherme Carvalho, Frederico Oliveira, and Jose Ricardo Sodre. "Improving Cold Start Emissions from an Ethanol-Fuelled Engine through an Electronic Gasoline Injector." *SAE Technical Paper Series*, 2010. doi:10.4271/2010-01-2131.

[20] Fedor, William, Joseph Kazour, James Haller, Kenneth Dauer, and Daniel Kabasin. "GDi Cold Start Emission Reduction with Heated Fuel." *SAE Technical Paper Series*, 2016. doi:10.4271/2016-01-0825.

[21] Adomeit, Philipp, Rolf Weinowski, Jens Ewald, Andre Brunn, Henning Kleeberg, Dean Tomazic, Stefan Pischinger, and Markus Jakob. "A New Approach for Optimization of Mixture Formation on Gasoline DI Engines." *SAE Technical Paper Series*, 2010. doi:10.4271/2010-01-0591.

[22] Moulai, Maryam, Ronald Grover, Scott Parrish, and David Schmidt. "Internal and Near-Nozzle Flow in a Multi-Hole Gasoline Injector Under Flashing and Non-Flashing Conditions." *SAE Technical Paper Series*, 2015. doi:10.4271/2015-01-0944.

[23] Saha, Kaushik, Shaoping Quan, Michele Battistoni, Sibendu Som, P. K. Senecal, and Eric Pomraning. "Coupled Eulerian Internal Nozzle Flow and Lagrangian Spray Simulations for GDI Systems." *SAE Technical Paper Series*, 2017. doi:10.4271/2017-01-0834.

[24] Schmidt, D. P., and M. L. Corradini. "The Internal Flow of Diesel Fuel Injector Nozzles: A Review." *International Journal of Engine Research*2, no. 1 (2001): 1-22. doi:10.1243/1468087011545316.

[25] Experimental and Numerical Studies of Fuel Spray By Daliang Jing A thesis submitted to The University of Birmingham for the degree of DOCTOR OF PHILOSOPHY

[26] Reitz, R.D., Modeling atomization processes in high-pressure vaporizing sprays. Atomisation Spray Technology, p. 309-337, 1987.

[27] Reitz, R.; Diwakar, R. Structure of High-Pressure Fuel Sprays. SAE Int.J.Engines 870598, 1987

[28] Rayleigh, On the instability of jets, University Press, Scientific Papers Vol. 3: 1887-1892, 1902.

[29] Beale, J.C. and R.D. Reitz, Modeling spray atomization with the Kelvin-Helmholtz/Rayleigh-Taylor hybrid model. Atomization and sprays, 1999.

[30] Saha, Kaushik, Sibendu Som, Michele Battistoni, Yanheng Li, Eric Pomraning, and P. K. Senecal. "Numerical Investigation of Two-Phase Flow Evolution of In- and Near-Nozzle Regions of a Gasoline Direct Injection Engine During Needle Transients." *SAE International Journal of Engines*9, no. 2 (2016). doi:10.4271/2016-01-0870.

[31] T. Ménard, S. Tanguy and A. Berlemont, "Coupling level set/VOF/ghost fluid methods: Validation and application to 3D simulation of the primary break-up of a liquid jet," International Journal of Multiphase Flow, vol. 33, pp. 510-524, 2007.

[32] M. Herrmann, "On Simulating Primary Atomization Using the Refined Level Set Grid Method," Atomization and Sprays, vol. 21, no. 4, pp. 283-301, 2011.

[33] M. Battistoni, C. Grimaldi and F. Mariani, "Coupled Simulation of Nozzle Flow and Spray Formation Using Diesel and Biodiesel for CI Engine," SAE World Congress 2012-01-1267, 2012.

[34] S. Som, D. Longman, A. I. Ramirez and S. K. Aggarwal, "A comparison of injector flow and spray characteristics of biodiesel with petrodiesel," Fuel, vol. 89, no. 12, p. 4014–4024, 2010.

[35] F. Wang, Z. He, J. Liu and Q. Wang, "Diesel nozzle geometries on spray characteristics with a spray model coupled with nozzle cavitating flow," International Journal of Automotive Technology, vol. 16, no. 4, p. 539−549, 2015.

[36] S. Quan, P. K. Senecal, E. Pomraning, Q. Xue, B. Hu, D. Rajamohan, J. Deur and S. Som, "A one-way coupled volume of fluid and Eulerian-Lagrangian method for simulating sprays," in ASME Internal Combustion Engine Fall Technical Conference ICEF2016-9390, Greenville, 2016.

[37] Malaguti, Simone, Giuseppe Bagli, Stefano Piccinini, and Giuseppe Cantore. "Development of a Multi-component Based Methodology for the Simulation of Reacting High Injection Pressure Diesel Sprays." *Energy Procedia*45 (2014): 879-88. doi:10.1016/j.egypro.2014.01.093.

[38] Su, Xingyuan, Youngchul Ra, and Rolf D. Reitz. "A Surrogate Fuel Formulation Approach for Real Transportation Fuels with Application to Multi-Dimensional Engine Simulations." *SAE International Journal of Fuels and Lubricants*7, no. 1 (2014): 236-49. doi:10.4271/2014-01-1464.

[39] Jiao, Qi, Youngchul Ra, and Rolf D. Reitz. "Modeling the Influence of Molecular Interactions on the Vaporization of Multi-component Fuel Sprays." *SAE Technical Paper Series*, 2011. doi:10.4271/2011-01-0387.

[40] Ra, Y., and Rolf D. Reitz. "The Use of Variable Geometry Sprays With Low Pressure Injection for Optimization of Diesel HCCI Engine Combustion." *SAE Technical Paper Series*, 2005. doi:10.4271/2005-01-0148.

[41] Ra, Youngchul, Paul Loeper, Michael Andrie, Roger Krieger, David E. Foster, Rolf D. Reitz, and Russ Durrett. "Gasoline DICI Engine Operation in the LTC Regime Using Triple- Pulse Injection." *SAE International Journal of Engines* 5, no. 3 (2012): 1109-132. doi:10.4271/2012-01-1131.

[42] Adhikary, Bishwadipa Das, Youngchul Ra, Rolf D. Reitz, and Stephen Ciatti. "Numerical Optimization of a Light-Duty Compression Ignition Engine Fuelled With Low-Octane Gasoline." *SAE Technical Paper Series*, 2012. doi:10.4271/2012-01-1336.

[43] Loeper, Paul, Youngchul Ra, David E. Foster, and Jaal Ghandhi. "Experimental and Computational Assessment of Inlet Swirl Effects on a Gasoline Compression Ignition (GCI) Light-Duty Diesel Engine." *SAE Technical Paper Series*, 2014. doi:10.4271/2014-01-1299.

[44] Jamali, Arash, Youngchul Ra, Wonah Park, and Gyubaek Cho. "A Combustion Model for Multi-Component Fuels Based on Reactivity Concept and Single-Surrogate Chemistry Representation." *SAE Technical Paper Series*, 2018. doi:10.4271/2018-01-0260.

[45] Jing, Daliang, Hongxue Zhao, Yanfei Li, Hengjie Guo, Jianhua Xiao, and Shi-Jin Shuai. "Numerical Investigation on the Effect of Fuel Temperature on Spray Collapse and Mixture Formation Characteristics in GDI Engines." *SAE Technical Paper Series*, 2018. doi:10.4271/2018-01-0311.

[46] Li, Yanfei, Hengjie Guo, Shubo Fei, Xiao Ma, Zhou Zhang, Longfei Chen, Liuyang Feng, and Zhi Wang. "An Exploration on Collapse Mechanism of Multi-jet Flash-boiling Sprays." *Applied Thermal Engineering*134 (2018): 20-28. doi:10.1016/j.applthermaleng.2018.01.102.

[47] Guo, Hengjie, Xiao Ma, Yanfei Li, Shuai Liang, Zhi Wang, Hongming Xu, and Jianxin Wang. "Effect of Flash Boiling on Microscopic and Macroscopic Spray Characteristics in Optical GDI Engine." *Fuel*190 (2017): 79-89. doi:10.1016/j.fuel.2016.11.043.

[48] Rajput, Oudumbar, Ra, Youngchul, Ha, Kyoung-Pyo, and Son, You-sang. "Numerical Analysis of a Six-Stroke Gasoline Compression Ignition (GCI) Engine Combustion With Continuously Variable Valve Duration (CVVD) Control." *Proceedings of the ASME 2018 Internal Combustion Engine Division Fall Technical Conference. Volume 1: Large Bore Engines; Fuels; Advanced Combustion*. San Diego, California, USA. November 4–7, 2018. V001T03A008. ASME. https://doi.org/10.1115/ICEF2018-9590